

# The Infrared Universe

Jonathan Holland

December 18, 2025

## Abstract

We develop a mesoscopic framework for semiclassical gravity in which the cosmological exterior is treated as an open quantum subsystem coupled to a horizon reservoir and described by a non-Riemannian Carnot–Carathéodory (CC) tangent geometry. In this setting, conservation laws hold locally as expectation-value identities,  $\nabla_\mu \langle J^\mu \rangle = 0$ , while the global charge content of the exterior evolves through irreversible horizon fluxes. When matter degrees of freedom cross a causal horizon, their conserved quantum numbers are sequestered into inaccessible modes, producing an apparent depletion in the exterior sector. Global unitarity then requires compensating source terms in the exterior continuity equations. This repopulation is not baryogenesis but a generic open-system effect arising from tracing over horizon and ultrasoft infrared degrees of freedom.

Black holes act as irreversible entropy converters, while the cosmological horizon functions as an effectively infinite entropy sink. The resulting entropy throughput drives an increase in exterior free energy that must be dissipated through accessible channels. Causality strongly constrains these channels: ultraviolet excitations propagate within the same light cones as the infalling matter and cannot enforce the required causal separation. Entropy and conserved charges must therefore return predominantly through long-wavelength geometric modes. The infrared geometric sector emerges as the dominant entropy-acceptance channel in any horizon-coupled nonequilibrium steady state, with matter and radiation production appearing as secondary, thermodynamically constrained processes.

The CC tangent geometry provides the complementary kinematical structure. Its intrinsic mesoscopic scale  $\sigma$  governs both particle kinematics and the excitation of infrared geometric modes. In the photon sector, CC mixing acts as an effective cavity whose stationary state is Planckian, with the photon temperature determined dynamically by the entropy-acceptance capacity of the infrared sector rather than imposed as an external boundary condition. In the matter sector, the same geometric structure yields asymptotically flat or rising rotation curves through horizontal CC geodesics. These phenomena arise from a single dynamically selected mesoscopic scale rather than independent assumptions.

Horizon thermodynamics, mesoscopic continuity, and infrared geometry together lock this scale to the cosmological expansion rate,  $H \sim \sigma$ ,

yielding a steady-state Universe in which expansion, entropy export, photon equilibration, and large-scale kinematics are controlled by a single underlying frequency. Throughout, the emphasis is on structural consistency between open-system thermodynamics, causal geometry, and conservation laws; observational agreements are presented as necessary consistency conditions rather than phenomenological inputs.

## Contents

<b>1</b>	<b>Introduction</b>	<b>5</b>
1.1	MOND as an Implicit Sub-Riemannian Theory	7
1.2	The $\Lambda$ CDM framework and its conceptual fragmentation	8
<b>2</b>	<b>Heisenberg Kinematics and Radial Potentials</b>	<b>9</b>
2.1	Canonical one-form and horizontal momenta	9
2.2	Free Hamiltonian in polar coordinates	10
2.3	Adding a radial potential	10
2.4	Circular orbits and rotational velocity	11
2.5	Virial theorem	12
<b>3</b>	<b>Bulk Carnot Geometry and the Origin of <math>\sigma</math></b>	<b>13</b>
3.1	A (3, 3) nilpotent model	13
3.2	Planar motions and the Heisenberg limit	14
3.3	Embedding in a sub-Lorentzian bulk	14
3.4	Geometric interpretation of the mesoscopic scale	15
<b>4</b>	<b>Mesoscopic Continuity Equations</b>	<b>16</b>
4.1	Observer-Dependence and Causal Partitioning	17
4.2	Coarse-grained currents and null boundaries	17
4.3	Entropy biases and compensating source terms	17
4.4	Baryon continuity equation	18
4.5	Scaling, dimensional analysis, and the role of $\sigma$	19
<b>5</b>	<b>The Cosmic Microwave Background as a Steady-State Radiative Equilibrium</b>	<b>19</b>
5.1	Why a stationary 2.7 K bath is thermodynamically natural	20
5.2	Why the photon bath does not cool under expansion	21
5.3	Conceptual summary	21
<b>6</b>	<b>Horizon-Coupled Thermodynamics</b>	<b>22</b>
6.1	Entropy production and horizon export	25
6.2	IR entropy from cosmic expansion	25
6.3	Grand-canonical constraints for the reduced exterior state	26
6.4	Stationarity and coupled balance laws	27
6.5	Entropy Balance, Horizon Charges, and the Necessity of Baryon Creation	27

6.6	Baryon number continuity . . . . .	29
6.7	Why Entropy Returns in the Infrared . . . . .	30
6.8	Free Energy and Internal Dissipation . . . . .	32
6.9	Feedback and Relaxation Toward $\sigma_*$ . . . . .	32
6.10	Infrared Universality . . . . .	33
6.11	Summary . . . . .	33
6.12	High- $\sigma$ Regime: Hot, Inefficient Structure Formation and Suppressed Black-Hole Sequestration . . . . .	34
6.13	Why Free Energy Is Not Exhaustively Dissipated into Infrared Gravitational Modes . . . . .	35
<b>7</b>	<b>Entropy–Acceptance Temperature and the Horizon as a Cold Sink</b>	<b>36</b>
7.1	Entropy–Acceptance Temperature . . . . .	36
7.2	Black Holes as Cold Entropy Amplifiers . . . . .	36
7.3	The Cosmological Horizon as an Effective Zero–Temperature Sink	36
7.4	Entropy Cascade . . . . .	37
<b>8</b>	<b>Minimal Thermodynamic Structure: Cold Entropy Export and Free–Energy Balance</b>	<b>37</b>
8.1	Cold Entropy Export . . . . .	37
8.2	Fixed Radiative Temperature of the Exterior . . . . .	38
8.3	Free–Energy Increase . . . . .	38
8.4	Chemical–Potential Imbalance . . . . .	38
8.5	Restoration of Equilibrium . . . . .	38
8.6	Summary . . . . .	39
<b>9</b>	<b>Minimum Exterior Temperature and Entropy–Sink Selection</b>	<b>39</b>
9.1	Free-energy balance and minimum temperature . . . . .	39
9.2	Why photons are <i>not</i> the dominant entropy sink . . . . .	40
<b>10</b>	<b>Stationary Solutions and Cosmological Implications</b>	<b>42</b>
10.1	The stationary system . . . . .	42
10.2	Determination of the expansion rate . . . . .	42
10.3	Baryon equilibrium . . . . .	43
10.4	Stationary radiation density . . . . .	43
10.5	Rotation curves and macroscopic geometry . . . . .	44
10.6	Global consistency and observational tests . . . . .	44
<b>11</b>	<b>Photon Confinement, Carnot Mixing, and Blackbody Equilibrium</b>	<b>45</b>
11.1	Effective confinement in Carnot–Carathéodory geometry . . . . .	45
11.2	Sub-Laplacian mixing and ergodicity . . . . .	46
11.3	A plausible origin of the CMB angular power spectrum from horizon mixing . . . . .	46

11.4	Photon Heating, Geometric Thermalization, and the Absence of Radiative Runaway . . . . .	48
11.5	Structural relation between entropy–acceptance and KMS temperatures . . . . .	49
<b>12</b>	<b>Entropy Throughput and the Origin of Apparent Expansion</b>	<b>51</b>
12.1	The exterior as an open thermodynamic system . . . . .	51
12.2	Free energy stored in resolved degrees of freedom . . . . .	51
12.3	Steady-state entropy balance . . . . .	52
12.4	Stationary CC geometry and timescale separation . . . . .	52
12.5	Resolved degrees of freedom, “tiles,” and apparent expansion . .	52
12.6	Free–Energy Throughput and Entropy Export: Quantitative Closure . . . . .	53
12.7	Sanity check on the entropy–export engine: required $T_{\text{ext}}$ . . . .	56
<b>13</b>	<b>Emergent Carnot–Carathéodory Geometry and the Horizon Fixed Point</b>	<b>58</b>
13.1	The horizon as a thermodynamic boundary condition . . . . .	58
13.2	Cold entropy, collapse timescales, and geometric response . . . .	59
13.3	Why purely Riemannian tangent geometries are disfavored . . . .	59
13.4	CC geometry as a thermodynamic fixed point . . . . .	59
13.5	Fixed-point interpretation . . . . .	60
13.6	Relaxation of the Geometric Relaxation Rate $\sigma$ . . . . .	60
13.6.1	Definition of $\sigma$ . . . . .	60
13.6.2	Entropy Export and the Throughput Functional . . . . .	61
<b>14</b>	<b>A Geometric Viewpoint on Luminosity Decay</b>	<b>61</b>
14.1	Wavefronts and angular accessibility . . . . .	61
14.2	The Heisenberg group as a geometric toy model . . . . .	62
14.3	Distance and effective luminosity . . . . .	63
14.4	Interpretation . . . . .	63
14.5	Local Phase Inheritance and Coarse–Grained Continuity . . . .	63
14.6	Single–packet CC phase drift and effective luminosity decay . .	64
14.7	Vertical Mixing, Fat–Tailed Phase Occupation, and the Stability of the Photon Bath . . . . .	67
14.8	Radiation and detection in the (3, 3) Carnot geometry . . . .	68
<b>15</b>	<b>Late-Time Cosmology, Chemical Steady State, and the Origin of Quasars</b>	<b>70</b>
15.1	Quasars as Terminal Galactic Attractors . . . . .	70
15.2	Nucleosynthesis Beyond the Primordial Paradigm . . . . .	70
15.3	Preferential Metal Sequestration . . . . .	71
15.4	Chemical Equilibrium and the Helium Fixed Point . . . . .	71
15.5	Summary . . . . .	72

<b>16 The Cosmic Helium Budget</b>	<b>72</b>
16.1 Helium as a Mesoscopic Observable . . . . .	72
16.2 Equilibrium Condition . . . . .	73
16.3 Microphysical Origin of the Helium Fixed Point . . . . .	73
16.4 Role of Metal Sequestration . . . . .	73
16.5 Thermodynamic consumption of metals as an exterior principle .	74
16.6 Interpretation . . . . .	75
<b>17 Concluding Remarks: Open-System Conservation, Entropy Production, and the Mesoscopic Universe</b>	<b>75</b>
<b>A Curved model geometries</b>	<b>83</b>
A.1 $SU(2)$ . . . . .	84
A.1.1 Clifford tori . . . . .	87
A.2 $N = 0$ . . . . .	87
A.2.1 The Cayley transform . . . . .	87
A.3 $SL_2(\mathbb{R})$ . . . . .	89
A.4 Case $\lambda_1 - \lambda_2 \in \mathbb{R}$ . . . . .	90
A.5 Case $\lambda_1 - \lambda_2 \in i\mathbb{R}$ . . . . .	92
A.6 $Sp(2)$ . . . . .	94
A.7 $Sp(1, 1)$ . . . . .	95

## 1 Introduction

Cosmological observations reveal a striking conjunction of late-time regularities: galaxies exhibit flattened or rising rotation curves, the cosmic radiation field maintains an almost perfect blackbody spectrum, and the cosmic baryon density remains nearly constant despite ongoing expansion [55, 60, 28, 1]. In the standard  $\Lambda$ CDM interpretation these features arise from distinct physical mechanisms—dark matter, primordial radiation, and a tuned early-universe baryogenesis episode—linked only indirectly through a shared Friedmann background. In this work we explore a different possibility: that *all three phenomena reflect a single mesoscopic structure of spacetime*, governed by a distinguished infrared frequency scale.

Our starting point is the observation that the coarse-grained, late-time Universe does not behave as a closed system. Any comoving worldtube loses degrees of freedom across its cosmological horizon at a steady rate, while black holes act as powerful localized sinks that absorb entropy and sequester conserved charges into exponentially redshifted interior states [31, 5, 37, 22]. The exterior region is therefore an *open thermodynamic subsystem*, and its macroscopic evolution must be described by balance laws that include horizon exchange [15, 66, 39]. These laws take a simple and universal form: for any conserved or effectively conserved quantity, one obtains continuity equations of the type

$$\partial_t n_X + 3Hn_X = -\Phi_X + \Gamma_X,$$

where the flux term  $\Phi_X$  encodes loss to horizon degrees of freedom and the source term  $\Gamma_X$  arises from the horizon-induced chemical potential in the reduced exterior density matrix.

A consistent late-time cosmology must therefore supplement local conservation with a global entropy budget. Matter accreting into black holes produces an enormous entropy increase in their horizons, while cosmological expansion continuously exports entropy to the cosmological horizon. To maintain stationarity, this outward flow must be compensated by an entropy-production channel in the exterior region.

The principal result of this paper is that entropy export from the exterior region is accommodated through a hierarchy of channels. The dominant entropy-acceptance channel consists of long-wavelength geometric (gravitational) modes, which provide efficient, causally separated transport of entropy to the horizon. Within this background flow, a much smaller but structurally essential fraction of the free-energy budget is diverted into the regeneration of baryons in the exterior sector, followed by their eventual accretion into black holes. Baryons are uniquely suited to this subsidiary role: they carry conserved charges, remain dynamically stable over cosmological timescales, and release large amounts of horizon entropy when accreted. In this sense, the *baryon-accretion cycle* supplies the “work-like” component of a cosmic Carnot engine [52, 8, 19], while infrared geometric modes provide the primary entropy transport required to sustain a stationary nonequilibrium state.

The second structural ingredient is geometric. We show that the appropriate tangent geometry for large-scale cosmic dynamics is not Riemannian but *Carnot–Carathéodory*, modeled locally by a Heisenberg or more general step-two Carnot group [33, 7, 46]. Such geometries contain an intrinsic infrared frequency  $\sigma$ , arising from the noncommutativity of their horizontal and vertical directions.

A central role in this framework is played not by a new fundamental constant, but by an emergent infrared rate that characterizes the steady-state coarse-graining of the exterior system. In Carnot–Carathéodory geometry this rate appears as a mesoscopic spectral scale  $\sigma$ , reflecting the timescale on which horizontal and vertical degrees of freedom mix under irreversible entropy flow. Crucially,  $\sigma$  is not imposed a priori: it is selected dynamically by the requirement that entropy export to the horizon be balanced by entropy-acceptance channels in the exterior. In the resulting steady state,  $\sigma$  adjusts to the cosmological expansion rate, yielding  $\sigma \sim H$  as a consistency condition rather than a postulate [45, 48]. Once this identification is made, a number of apparently independent cosmic phenomena become different expressions of the same mesoscopic scale: rotation curves, baryon equilibrium, and the equilibrium temperature of the photon bath all follow directly from  $\sigma$ .

Crucially, the parameter  $\sigma$  should not be interpreted as an exactly conserved microscopic quantity. Rather, it is a thermodynamic state variable characterizing the stationary mesoscopic exterior, analogous to temperature or chemical potential in ordinary nonequilibrium systems. Local gravitational excitations and horizon fluxes generically induce fluctuations in  $\sigma$ , but coarse-grained entropy

production drives relaxation toward a stable stationary value  $\sigma_*$  determined by global entropy throughput.

The framework that emerges is a *horizon-coupled steady-state cosmology* in which baryons, radiation, and infrared geometric modes continuously circulate entropy and conserved charge between the exterior and its horizons. Rather than invoking phenomenologically distinct components—dark matter, dark energy, primordial baryogenesis, and a relic radiation field—the model derives their observational signatures from a single mesoscopic mechanism. Galactic rotation curves arise from sub-Riemannian kinematics; the cosmic radiation field is a thermodynamic equilibrium sustained by geometric confinement and ordinary astrophysical heating; and the baryon density is maintained by the compensating source required by horizon thermodynamics. All of these features are controlled by the same mesoscopic rate selected by the horizon-coupled steady state.

The remainder of the introduction situates this framework in relation to MOND and  $\Lambda$ CDM and prepares the ground for the detailed continuity, geometry, and thermodynamic analysis that follows.

## 1.1 MOND as an Implicit Sub-Riemannian Theory

In its original Bekenstein–Milgrom formulation [4, 45, 25], MOND is defined by a nonlinear Lagrangian for the gravitational potential,

$$\mathcal{L}_{\text{MOND}} = -\frac{a_0^2}{8\pi G} F\left(\frac{|\nabla\Phi|^2}{a_0^2}\right) + \rho\Phi,$$

which yields a modified Poisson equation

$$\nabla \cdot \left[ \mu\left(\frac{|\nabla\Phi|}{a_0}\right) \nabla\Phi \right] = 4\pi G\rho.$$

Because the operator acting on  $\Phi$  is no longer the Euclidean Laplacian but a *directionally weighted* one, MOND dynamics are governed by an anisotropic diffusion operator resembling a horizontal sub-Laplacian on a Carnot manifold. The system propagates information preferentially along a distinguished set of directions (those where  $|\nabla\Phi|$  is small), in close analogy with the Heisenberg horizontal distribution.

This formal similarity is striking: the MOND kinetic operator is not far from the quadratic form obtained from a Heisenberg or general Carnot–Carathéodory tangent geometry, in which the Laplacian is replaced by a horizontal sum of squares. In both cases the resulting dynamics are effectively sub-Riemannian, and the corresponding spectral scale plays the role of an emergent acceleration or frequency.

What MOND lacks, however, is a *mechanism* for the scale  $a_0$ . It is inserted by hand and remains unexplained. In the present framework, by contrast, the mesoscopic spectral scale  $\sigma$  arises from the geometry itself and is dynamically locked to the Hubble rate through horizon thermodynamics. Thus

$$a_0 \sim \sigma \sim H_0,$$

giving a natural origin for the empirical MOND scale.

From this viewpoint MOND may be interpreted as a phenomenological glimpse of a deeper geometric structure—a nonlinear diffusion equation that partially encodes sub-Riemannian kinematics, but without identifying the underlying noncommutative tangent geometry or its thermodynamic origin.

Although the present framework captures a great deal of the infrared kinematics encoded in MOND—indeed, MOND can be viewed as a phenomenological glimpse of the correct variational structure—it remains only a theory of geometry and kinematics, not yet a full dynamical theory. We specify a noncommutative Carnot tangent geometry (Heisenberg type in the bulk, compact sub-Riemannian structure at horizons), derive the associated Hamiltonian flows, and explore their phenomenological consequences. What is missing is the analogue of the Einstein field equations: no law that tells the geometry how to evolve in response to matter, nor how the noncommutative tangent cone co-evolves with stress–energy. Several routes to such dynamics suggest themselves—effective four-dimensional stress–energy, synthetic curvature conditions in the sense of metric–measure geometry, or a phase-space reduction of a higher-dimensional vacuum—but none is yet sufficiently natural or transparent to serve as the fundamental field equation. Even the classical propagation of fields on a fixed sub-Lorentzian Carnot background is only partially understood. While Maxwell theory has been formulated on certain Carnot groups, the extension to a physically relevant sub-Lorentzian Hamiltonian is nontrivial. It may be that the correct approach is to identify the appropriate action principle: an analogue of the Einstein–Hilbert action adapted to the Carnot geometry, or a Lagrangian for fields compatible with the noncommutative phase space. MOND points in the right conceptual direction, but a complete dynamical theory lies beyond our current reach.

## 1.2 The $\Lambda$ CDM framework and its conceptual fragmentation

Modern cosmology rests on the empirical success of the  $\Lambda$ CDM model in fitting a wide range of observations: the Hubble–Lemaître law, the angular power spectrum of the cosmic microwave background (CMB), the large-scale distribution of galaxies, and the statistics of gravitational lensing, among others [1, 72, 51]. At the same time, the theoretical underpinnings of this framework remain conceptually fragmented. The standard model requires, as independent ingredients, a cold dark matter component to explain galactic and cluster dynamics, a dark energy component to drive late-time acceleration, an inflationary phase introduced to address horizon and flatness problems, and a hot primordial radiation era to account for the CMB. Each ingredient is phenomenologically successful in its own domain, but their mutual relations are largely kinematic rather than dynamical or thermodynamic.

From the standpoint of entropy flow and charge conservation, this fragmentation is significant. None of the components of  $\Lambda$ CDM communicate thermodynamically (in a unified, ongoing balance-law sense): the entropy generated

by structure formation, the entropy sequestered behind horizons, and the observed radiation density are not linked by a common continuity principle. The model provides no mechanism by which the cosmic baryon density, radiation density, and expansion rate should be related to one another in a stationary universe. Instead, each is set by separate initial conditions or phenomenological parameters.

The mesoscopic framework developed here replaces this modular structure with a set of coupled balance laws governing charge flow, entropy flow, and horizon thermodynamics. In this view, the observed cosmic densities and kinematics arise from ongoing equilibrium conditions rather than primordial initial states. The question is therefore not whether  $\Lambda$ CDM fits current observations—it does—but whether its component parts reflect a unified physical process or a set of independent empirical patches. The present work explores the possibility that a single mesoscopic scale  $\sigma$ , arising from the Carnot–Carathéodory tangent geometry, underlies both local kinematics and global thermodynamic balance. Throughout this work,  $\sigma$  should be understood not as a fundamental parameter but as an emergent bookkeeping rate characterizing the steady-state coarse-graining of an open, horizon-coupled system.

## 2 Heisenberg Kinematics and Radial Potentials

The galactic disc is modeled, to leading mesoscopic order, by the Heisenberg group

$$\mathcal{H} = \mathbb{R} \times \mathbb{C}, \quad (s, z)(s', z') = (s + s' + \Im(\bar{z}z'), z + z'),$$

whose tangent symplectic geometry naturally produces the mesoscopic frequency scale  $\sigma$  that governs large-radius rotation curves. This section develops the explicit Hamiltonian mechanics of this system.

### 2.1 Canonical one-form and horizontal momenta

The canonical one-form on  $T^*\mathcal{H}$  is

$$\psi = \sigma ds + \zeta dz + \bar{\zeta} d\bar{z},$$

with corresponding symplectic form  $\omega = d\psi$  and Poisson bracket defined by  $\omega^{-1}$ .

Define the horizontal momenta

$$P = \zeta - \frac{i}{2} \bar{z} \sigma, \quad \bar{P} = \bar{\zeta} + \frac{i}{2} z \sigma,$$

which satisfy the central relation

$$\{P, \bar{P}\} = i\sigma.$$

The Hamiltonian vector fields  $\hat{P}, \hat{\bar{P}}$  descend to the standard Heisenberg horizontal frame on  $\mathcal{H}$ .

## 2.2 Free Hamiltonian in polar coordinates

Take the free Hamiltonian to be

$$K = 2P\bar{P}.$$

In the abelian limit  $\sigma \rightarrow 0$ , this reduces to the usual free particle Hamiltonian  $K = \frac{1}{2}(p_x^2 + p_y^2)$ .

Introduce polar coordinates  $z = re^{i\theta}$  and conjugate momenta  $R, L$  via

$$\psi = R dr + L d\theta + \sigma ds.$$

A standard computation yields

$$P = -\frac{ie^{-i\theta}}{2} \left( \frac{L}{r} + iR + r\sigma \right),$$

and hence

$$K = 2P\bar{P} = \frac{1}{2} \left( R^2 + \frac{(L + r^2\sigma)^2}{r^2} \right). \quad (1)$$

With canonical Poisson brackets

$$\{r, R\} = 1, \quad \{\theta, L\} = 1, \quad \{s, \sigma\} = 1,$$

Hamilton's equations for the free motion are

$$\dot{r} = \{r, K\} = R, \quad (2)$$

$$\dot{\theta} = \{\theta, K\} = \frac{L + r^2\sigma}{r^2}, \quad (3)$$

$$\dot{s} = \{s, K\} = L + r^2\sigma, \quad (4)$$

$$\dot{R} = \{R, K\} = \frac{L^2}{r^3} - \sigma^2 r, \quad (5)$$

$$\dot{L} = \dot{\sigma} = 0. \quad (6)$$

Thus even in the absence of a potential, generic trajectories in the  $(r, \theta)$ -plane are curved, with a characteristic mesoscopic frequency  $\sigma$ .

## 2.3 Adding a radial potential

Add a central potential  $V(r)$  and consider the full Hamiltonian

$$H = K + V(r) = \frac{1}{2} \left( R^2 + \frac{(L + r^2\sigma)^2}{r^2} \right) + V(r).$$

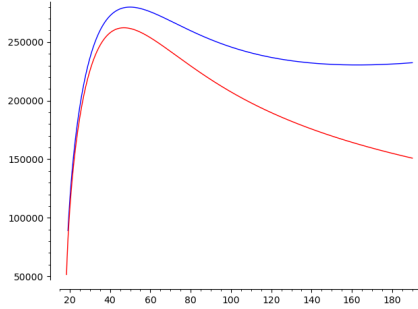


Figure 1: Rotation curve, with a naive exponential (Freeman) decay matter model, for M31 galaxy. Top curve: nonzero  $\sigma$ ; bottom curve:  $\sigma = 0$ . This uses the following parameters:  $G = 2.26954 \times 10^{-69} \text{ kpc}^3/\text{kg} \cdot \text{s}^2$ ,  $M = 2 \times 10^{42} \text{ kg}$  (mass of a typical galaxy like M31),  $\sigma = 10^{-17} \text{ s}^{-1} \approx 5H_0$ ,  $r_0 = 10 \text{ kpc}$  (scale parameter).

Hamilton's equations become

$$\dot{r} = R, \quad (7)$$

$$\dot{\theta} = \frac{L + r^2\sigma}{r^2}, \quad (8)$$

$$\dot{s} = L + r^2\sigma, \quad (9)$$

$$\dot{R} = \frac{L^2}{r^3} - \sigma^2 r - V'(r), \quad (10)$$

$$\dot{L} = \dot{\sigma} = 0. \quad (11)$$

For radial infall with  $\dot{\theta} = 0$  we have  $L = -r^2\sigma$ , and hence

$$\ddot{r} = -V'(r).$$

Thus  $V(r) = -m/r$  yields the inverse-square law.

## 2.4 Circular orbits and rotational velocity

For circular orbits of constant radius  $r = r_0$  we have  $R = \dot{R} = 0$ , so

$$\frac{L^2}{r^3} - \sigma^2 r - V'(r) = 0, \quad (12)$$

i.e.

$$L^2 = \sigma^2 r^4 + r^3 V'(r). \quad (13)$$

In the limit  $\sigma \rightarrow 0$ , this becomes the Newtonian condition  $L^2 = r^3 V'(r)$ .

The tangential velocity is

$$v(r) = r\dot{\theta} = \frac{L + r^2\sigma}{r}.$$

Using (13), we obtain

$$v(r) = \sigma r \pm \sqrt{\sigma^2 r^2 + v_N^2(r)}, \quad (14)$$

where  $v_N^2(r) = rV'(r)$  is the Newtonian circular velocity.

Equation (14) is the basic phenomenological prediction of the Heisenberg tangent geometry: the Newtonian velocity is modified by a geometric term  $\sigma r$ , with the two contributions combining nonlinearly.

## 2.5 Virial theorem

Let  $G = Rr$ . Then

$$\dot{G} = \{G, H\}.$$

A short calculation yields

$$\{G, H\} = R^2 + \frac{L^2}{r^2} - \sigma^2 r^2 - rV'(r). \quad (15)$$

For orbits confined to the galactic disc,  $G$  is bounded, and the usual virial theorem gives

$$\left\langle R^2 + \frac{L^2}{r^2} - \sigma^2 r^2 - rV'(r) \right\rangle = 0,$$

with  $\langle - \rangle$  the long-time average along the flow. For circular orbits ( $R = 0$ ), this reduces to (13).

For orbits that remain confined to the galactic disc,  $G$  is bounded and the usual virial theorem implies

$$\left\langle R^2 + \frac{L^2}{r^2} - \sigma^2 r^2 - rV'(r) \right\rangle = 0,$$

where  $\langle - \rangle$  denotes the long-time average along the flow. Under an ergodic hypothesis, this extends to the spatial average over the disc. In particular, for circular orbits ( $R = 0$ ) the virial identity is equivalent to the circular-balance condition (13).

In the present framework the virial relation acquires an additional term because the horizontal momenta on the Heisenberg group are not canonically conjugate to the radial coordinate in the Euclidean sense. The effective Hamiltonian for circular motion contains a contribution  $\frac{1}{2}\sigma^2 r^2$  arising from the noncommutative structure of the horizontal bundle, and this term survives the time average that produces the virial theorem. The result is a modified virial balance

$$\langle v^2 \rangle = \frac{GM(r)}{r} + \sigma^2 r^2,$$

so that the flat (or slowly rising) rotation curve follows naturally when the mesoscopic scale  $\sigma$  equals the Hubble rate  $H$ . In this sense the virial equilibrium of a galaxy is tied directly to the same mesoscopic scale that controls the horizon-exterior entropy balance.

### 3 Bulk Carnot Geometry and the Origin of $\sigma$

The Heisenberg model of Section 2 captures the *tangent* Carnot–Carathéodory (CC) geometry experienced by test particles moving in a two-dimensional galactic disc. In this section we indicate, at a schematic level, how such a tangent model arises from a higher-dimensional bulk geometry, and how the distinguished mesoscopic scale  $\sigma$  appears as the unique frequency associated with that bulk structure.

#### 3.1 A (3,3) nilpotent model

Consider a six-dimensional step-two nilpotent Lie algebra

$$\mathfrak{n} = \mathfrak{g}_- \oplus \mathfrak{g}_+,$$

where  $\mathfrak{g}_- \cong \mathbb{R}^3$  is “horizontal” and  $\mathfrak{g}_+ \cong \mathbb{R}^3$  is central. Physically,  $\mathfrak{g}_-$  represents ordinary spatial directions and  $\mathfrak{g}_+$  encodes noncommutative “phase” directions associated with angular structure. Let  $(x^i)$  be linear coordinates on  $\mathfrak{g}_-$  and  $(h_i)$  coordinates on  $\mathfrak{g}_+$ , with conjugate momenta  $(p_i)$  and  $(\omega_i)$ ,  $i = 1, 2, 3$ . We equip the phase space

$$(x^i, h_i, p_i, \omega_i)$$

with the standard symplectic form

$$\sum_i dp_i \wedge dx^i + \sum_i d\omega_i \wedge dh_i.$$

Define the *horizontal momenta*

$$P_i = p_i + (\omega \times x)_i, \quad i = 1, 2, 3, \tag{16}$$

where  $(\omega \times x)_i = \epsilon_{ijk} \omega_j x_k$  is the usual Euclidean cross product. A short computation gives the Poisson brackets

$$\{P_i, P_j\} = \epsilon_{ijk} \omega_k, \quad \{\omega_i, \cdot\} = 0, \tag{17}$$

so the  $\omega_k$  are central and the  $P_i$  generate a three-step nilpotent algebra with three-dimensional center. In particular, for fixed  $\omega$  this is a (3,3) Carnot group: the horizontal layer  $\mathfrak{g}_-$  is spanned by the  $P_i$ , while the central layer  $\mathfrak{g}_+$  is spanned by the  $\omega_k$ .

The free (kinetic) Hamiltonian is

$$K = \frac{1}{2} \delta^{ij} P_i P_j = \frac{1}{2} (P_x^2 + P_y^2 + P_z^2), \tag{18}$$

so that the corresponding Hamiltonian vector fields reproduce the horizontal frame of the (3,3) Carnot group. The key point is that for fixed  $\omega$  the only invariant quantity carried by the central layer is its Euclidean norm  $|\omega|$ . This norm sets a distinguished frequency scale in the free dynamics: the generic free

trajectories are curved with curvature proportional to  $|\omega|$ , in close analogy with cyclotron orbits in a magnetic field.

Radial potentials  $V(r)$ , with  $r^2 = x \cdot x$ , can be added without disturbing this structure by taking

$$H = K + V(r).$$

The horizontal geometry remains Carnot, and the noncommutativity of the momenta continues to enforce a characteristic mesoscopic scale  $|\omega|$  in the motion.

### 3.2 Planar motions and the Heisenberg limit

The Heisenberg model used for galactic discs appears as a planar subgeometry of the  $(3, 3)$  system. Suppose the free trajectory remains confined to a plane—for example,  $z = \text{constant}$ —and does not degenerate to motion along a straight line. The equations of motion then imply

$$p_z = 0, \quad \omega_x = \omega_y = 0,$$

so that only the central parameter  $\omega_z$  survives. In this regime the horizontal momenta reduce to

$$P_x = p_x + \omega_z y, \tag{19}$$

$$P_y = p_y - \omega_z x, \tag{20}$$

with bracket

$$\{P_x, P_y\} = \omega_z,$$

and the Hamiltonian

$$K = \frac{1}{2}(P_x^2 + P_y^2)$$

is exactly the Heisenberg kinetic energy studied in Section 2 after the identification  $\sigma \equiv \omega_z$ . Thus the two-dimensional Heisenberg geometry governing disc kinematics is the natural planar reduction of a three-dimensional  $(3, 3)$  Carnot geometry.

In particular, the mesoscopic frequency  $\sigma$  that appears in the radial Hamiltonian

$$K = \frac{1}{2}(R^2 + (L + \sigma r^2)^2/r^2)$$

is nothing more than the modulus of the central element  $\omega$  in the underlying  $(3, 3)$  Carnot group. At the purely geometric level,  $\sigma$  is the unique invariant scale associated with the noncommutative horizontal structure.

### 3.3 Embedding in a sub-Lorentzian bulk

The nilpotent model described above should be regarded as the *tangent* geometry of a more global, curved spacetime. One convenient way to organize such bulk models is via an involutive decomposition of a semisimple Lie algebra. Let

$\mathfrak{g}$  be a real semisimple Lie algebra equipped with an involution  $\theta : \mathfrak{g} \rightarrow \mathfrak{g}$ , and write

$$\mathfrak{g} = \mathfrak{g}_+ \oplus \mathfrak{g}_-$$

for the  $\pm 1$  eigenspaces. The subspace  $\mathfrak{g}_-$  carries an indefinite quadratic form  $Q$  (the restriction of the Killing form), and the bracket satisfies

$$[\mathfrak{g}_-, \mathfrak{g}_-] \subset \mathfrak{g}_+.$$

In this setting  $\mathfrak{g}_-$  plays the role of a horizontal subspace and  $\mathfrak{g}_+$  the “vertical” directions generated by their commutators. A *sub-Lorentzian* CC metric is obtained by declaring  $\mathfrak{g}_-$  to be the horizontal bundle and  $Q$  its metric.

Explicit examples include:

- $\mathfrak{g} = \mathfrak{sp}(4, \mathbb{R}) \cong \mathfrak{so}(2, 3)$ , whose symmetric space models a noncommutative de Sitter-like bulk;
- $\mathfrak{g} = \mathfrak{sp}(1, 1) \cong \mathfrak{so}(1, 4)$ , giving an anti-de Sitter-like bulk.

In each case, an appropriate choice of involution  $\theta$  yields a four-dimensional horizontal subspace  $\mathfrak{g}_-$  with Lorentzian signature  $(1, 3)$  and a compatible Hamiltonian

$$K = \frac{1}{2} Q^{ab} P_a P_b$$

constructed from the corresponding momenta  $P_a$ .

To recover the Carnot limit relevant for mesoscopic kinematics, one introduces a small parameter  $\varepsilon$  that rescales the Lie algebra as

$$\mathfrak{g}_- \mapsto \mathfrak{g}_-, \quad \mathfrak{g}_+ \mapsto \varepsilon^2 \mathfrak{g}_+,$$

and truncates the Lie bracket modulo  $O(\varepsilon^3)$ . In the limit  $\varepsilon \rightarrow 0$  the bulk geometry degenerates to a step-two Carnot group whose horizontal layer is  $\mathfrak{g}_-$  and whose center is  $\mathfrak{g}_+$ . At this level the only surviving invariant scale is the norm of the central element  $\omega \in \mathfrak{g}_+$ , which we identify with the mesoscopic frequency  $\sigma$ .

### 3.4 Geometric interpretation of the mesoscopic scale

From the bulk standpoint, the frequency  $\sigma$  appearing in Heisenberg kinematics and in the mesoscopic balance laws has a simple interpretation: it is the unique infrared scale associated with the curvature and noncommutativity of the CC tangent geometry. In the semisimple bulk model it is proportional to the inverse curvature radius of the corresponding de Sitter or anti-de Sitter space; in the nilpotent limit it appears as the norm  $|\omega|$  of the central element defining the Carnot structure.

Horizon thermodynamics then ties this geometric scale to the cosmic expansion rate through the entropy-balance and continuity relations: stationarity of the mesoscopic medium selects

$$\sigma \sim H,$$

so that the same scale governs

- the curvature of horizontal geodesics in the Heisenberg limit (flattened rotation curves),
- the mixing and effective confinement of photons in the CC geometry (thermal radiation),
- and the excitation of long-wavelength geometric modes that balance horizon entropy production.

In this way the bulk CC geometry provides a concrete origin for the mesoscopic spectral scale  $\sigma$  that underlies the kinematic and thermodynamic phenomena analyzed in the rest of the paper.

## 4 Mesoscopic Continuity Equations

The microscopic conservation laws of quantum field theory must be translated into a coarse-grained, horizon-coupled framework appropriate to expanding spacetimes with nontrivial tangent geometry. At mesoscopic scales—intermediate between local particle interactions and global cosmological averages—the relevant observables satisfy continuity equations modified by irreversible exchange with causally inaccessible sectors.

We work in comoving coordinates on a spatially expanding background with scale factor  $a(t)$  and Hubble parameter  $H = \dot{a}/a$ . Let  $n_X(t)$  denote the *physical* (proper) number density of any conserved or effectively conserved charge  $X$ . Integrating the associated current  $J_X^\mu$  over a comoving control volume whose boundary becomes null at the cosmological horizon, and allowing degrees of freedom to exit the exterior Hilbert space through causal decoupling, yields the general balance law [73, 21, 58]

$$\partial_t n_X + 3Hn_X = -\Phi_X + \Gamma_X. \quad (21)$$

Here  $\Phi_X$  is the physical loss rate (per unit volume) of  $X$ -carrying degrees of freedom from the observer-accessible sector, while  $\Gamma_X$  is the corresponding source term required by global charge conservation in the full spacetime description.

The two additional terms  $\Phi_X$  and  $\Gamma_X$  encode the essential mesoscopic physics:

- **Exterior loss flux  $\Phi_X$ :** the rate at which charge-carrying excitations are transported into causally inaccessible sectors—such as cosmological horizons or, on sufficiently long timescales, compact objects—and cease to contribute to the reduced exterior density operator.
- **Compensating source  $\Gamma_X$ :** the effective creation rate required to maintain mesoscopic charge balance in the exterior description when  $X$ -carrying degrees of freedom are irreversibly exported. This term reflects the open-system thermodynamics of the exterior and may be parameterized in terms of an *exterior entropy-exchange scale*  $T_{\text{ext}}$ , which governs the energetic cost of processing entropy through the open channel. It should

not be confused with the radiative/KMS temperature of the photon bath ( $T_\gamma \simeq 2.7\text{ K}$ ), which acts as a passive buffer and need not control  $\Gamma_X$ .

In this section we make these objects precise for the physically relevant charge  $X = B$  (baryon number). The same open-system formalism applies to any conserved quantum number whose irreversible export from the exterior can alter its effective density; this includes lepton number and other global or weakly gauged charges. Electric charge is excluded from this class, since its long-range gauge field imprints the total charge on the exterior region and prevents horizon-mediated depletion.

## 4.1 Observer-Dependence and Causal Partitioning

An important note is that the causal horizon invoked throughout this work should not be interpreted as an observer-independent physical boundary [66, 70]. Horizons in semiclassical gravity are inherently observer-relative: an observer freely crossing another's horizon does not encounter any local singularity, and each observer traces over degrees of freedom inaccessible to the other.

The role of the horizon in the present framework is therefore not ontological but operational. For any semiclassical observer, the causal structure induces a natural partition of the global Hilbert space into accessible and inaccessible sectors. Tracing over the latter renders the exterior an open quantum system, with irreversible entropy fluxes governed by modular dynamics [15, 18, 66, 9].

All thermodynamic statements in this work refer to this observer-relative exterior system. Physical predictions depend only on the universality of causal partitioning, not on the existence of a preferred or absolute horizon.

## 4.2 Coarse-grained currents and null boundaries

Let  $V(t)$  be a comoving volume whose boundary is everywhere timelike except at the cosmological horizon, where the causal structure degenerates. Formally,

$$\frac{d}{dt} \int_{V(t)} J_X^0 d^3x = - \int_{\partial V(t)} J_X^i dS_i + \int_{\partial V_{\text{hor}}} J_X^\mu k_\mu dA,$$

where  $k^\mu$  is the null generator of the horizon [69]. The first term gives the usual bulk flux; the second term represents loss of charge into the interior degrees of freedom. After dividing by the comoving volume and taking  $V \rightarrow \infty$ , one obtains the averaged flux  $\Phi_X$  that appears in (21).

Crucially,  $\Phi_X$  depends only on the *asymptotic* charge content of matter streams approaching the horizon and not on the microscopic details of local interactions. This reflects the fact that horizon absorption is a kinematic process governed by the causal structure of spacetime.

## 4.3 Entropy biases and compensating source terms

Tracing over causally inaccessible degrees of freedom induces an information-theoretic bias in the reduced exterior state. In an open quantum system, this

bias need not correspond to thermal equilibrium with a bath; rather, it reflects the fact that the reduced density operator maximizes entropy subject to the constraints imposed by the coarse-grained exterior observables [15, 63].

In the present context, the irreversible export of charge-carrying degrees of freedom across a causal horizon alters the entropy of the inaccessible sector in a charge-dependent manner. The exterior state therefore acquires an effective bias proportional to the entropy gradient

$$\frac{\partial S_{\text{inacc}}}{\partial Q_X},$$

evaluated on the traced-over sector. This quantity plays the role of a generalized thermodynamic force, biasing exterior fluctuations without introducing a physical horizon temperature or an equilibrium ensemble.

For baryon number, this entropy bias favors configurations in which the exterior charge deficit induced by horizon export is statistically compensated. In an irreversible nonequilibrium steady state, such a bias generically produces a compensating source term whose rate is set by the mesoscopic coarse-graining timescale rather than by a thermal bath [63, 23].

Accordingly, we parameterize the baryon creation rate as

$$\Gamma_B \sim \sigma \mathcal{F}_B,$$

where  $\sigma$  is the mesoscopic spectral scale introduced by the Carnot–Carathéodory tangent geometry, and  $\mathcal{F}_B$  is a dimensionless functional encoding the entropy bias induced by baryon transport into inaccessible sectors. This term appears as the source  $\Gamma_B$  in the mesoscopic continuity equation (21).

#### 4.4 Baryon continuity equation

Specializing to  $X = B$ , and writing the physical baryon density as  $n_B$ , we obtain

$$\partial_t n_B + 3Hn_B = -\Phi_B + \Gamma_B. \quad (22)$$

The interpretation is as follows:

- The expansion term  $3Hn_B$  represents the dilution of baryon density in physical volumes due to cosmological expansion.
- The flux  $\Phi_B$  accounts for the loss of baryon-carrying degrees of freedom from the observer-accessible sector, through transport into causally inaccessible regions such as cosmological horizons and, on sufficiently long timescales, compact objects.
- The source  $\Gamma_B$  represents a compensating baryon production term in the exterior description, induced by irreversible export of baryon number and required to maintain mesoscopic charge balance in a steady-state regime.

In a statistically stationary cosmological medium—understood as a coarse-grained steady state averaged over timescales long compared to the mesoscopic scale—one may set  $\partial_t n_B = 0$ , yielding the balance condition

$$3Hn_B = -\Phi_B + \Gamma_B.$$

This relation determines the steady-state baryon density once the cosmic expansion rate  $H$  and the exterior entropy-exchange and transport properties governing  $\Phi_B$  and  $\Gamma_B$  are fixed.

#### 4.5 Scaling, dimensional analysis, and the role of $\sigma$

The mesoscopic spectral scale  $\sigma$  arising from the Heisenberg (or more general Carnot–Carathéodory) tangent geometry enters the baryon continuity equation as the characteristic *rate* governing irreversible coarse-graining and long-wavelength mode mixing in the exterior system. It does not represent a temperature or equilibrium scale, but rather the inverse timescale over which exterior observables are reorganized by mesoscopic kinematics.

In the present framework, the compensating source term  $\Gamma_B$  is controlled by two ingredients: an entropy bias induced by the irreversible export of baryon number from the exterior sector, and the mesoscopic rate at which this bias is dynamically realized. Dimensional analysis therefore implies

$$\Gamma_B \sim \alpha_B \sigma,$$

where  $\alpha_B$  is a dimensionful coefficient. This coefficient encodes the efficiency with which entropy bias is converted into baryon-carrying exterior degrees of freedom, and depends on the structure of the available exterior channels rather than on any thermal properties of a radiation bath.

Observational analyses of galactic rotation curves [44, 25] indicate that the same mesoscopic scale satisfies  $\sigma \approx H_0$ . In a statistically stationary cosmological medium, the baryon continuity equation then implies that the physical baryon density is set parametrically by the cosmic expansion rate,

$$n_B \sim \frac{\Phi_B}{H_0} + O(1),$$

up to dimensionless factors determined by the details of baryon loss and entropy processing.

This closes the mesoscopic system: the same geometric scale  $\sigma$  that governs infrared kinematics and rotational dynamics also controls the long-term baryon balance of the universe in a nonequilibrium steady-state description.

### 5 The Cosmic Microwave Background as a Steady-State Radiative Equilibrium

The cosmic microwave background (CMB) is traditionally interpreted as relic radiation from a hot early epoch. In the framework developed here, the CMB

instead arises as the stationary radiative sector of an open quantum system, whose exterior degrees of freedom equilibrate to a fixed *radiative* (KMS) temperature with respect to the physical time flow of finite observers [14, 63]. This temperature,

$$T_{\text{CMB}} \simeq 2.7 \text{ K},$$

characterizes the photon–neutrino bath described by the reduced exterior density matrix and reflects the thermodynamic state of the resolved ultraviolet and mid-infrared field degrees of freedom.

This radiative temperature must be sharply distinguished from the *entropy-acceptance temperature* of the horizon. The cosmological horizon does not act as a radiative heat bath but as an effectively zero-temperature entropy sink, capable of absorbing entropy with negligible energy cost. The observed CMB temperature therefore does not represent a temperature of the horizon itself, nor a relic of a primordial epoch, but is a property of the exterior state–flow pair  $(\mathcal{A}_{\text{ext}}, \tau_t)$  governing late-time observers.

## 5.1 Why a stationary 2.7 K bath is thermodynamically natural

The exterior radiation field interacts rapidly with baryons, dust, plasma, and starlight [50, 56], and it mixes efficiently under the horizon-coupled Carnot–Carathéodory (CC) geometry. These processes ensure that the photon bath thermalizes on timescales  $\ll \sigma^{-1}$ , far shorter than the Hubble time. The bath thus functions as a *fast thermalizer*: any injected power is quickly redistributed, and any perturbation away from a thermal spectrum is smoothed by geometric mixing.<sup>1</sup>

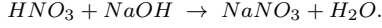
---

<sup>1</sup>The role played here by the photon bath is closely analogous to the use of *free-energy buffers* in chemistry and biophysics. In such systems (for example, the ATP/ADP/P<sub>i</sub> couple in cellular metabolism or standard redox buffers in electrochemistry), a regulated intermediate reservoir maintains an approximately stationary intensive parameter (chemical potential, redox potential, or effective temperature) while large free-energy fluxes pass through it. Entropy production is not minimized locally in the buffer but is exported to the ultimate environment, allowing irreversible processes to proceed without large excursions of the buffered variable.

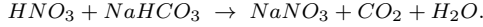
The photon bath in the present framework plays an analogous role: it redistributes free energy while remaining near a stationary KMS state, and it is not the final entropy sink of the system.

As a simple laboratory analogue, consider a buffered acid–base titration in which acid is slowly added to a bicarbonate solution. Over a wide range of added acid, the system irreversibly degrades free energy while the *buffered intensive variable* (the proton chemical potential, or pH) remains nearly constant; once the buffering capacity is exhausted, this regulation fails and the pH rapidly decreases.

By contrast, adding nitric acid directly to a sodium hydroxide solution produces a strongly exothermic neutralization in which temperature and local chemical–potential gradients change rapidly,



Introducing sodium bicarbonate moderates this interaction by providing an intermediate buffered channel in which free energy is absorbed and redistributed with smaller excursions of intensive variables,



Because the photon bath occupies only a tiny fraction of the total free-energy budget of the exterior, maintaining its temperature requires negligible energy [27, 50]. In particular, the free energy liberated by horizon entropy export is many orders of magnitude larger than the radiative energy needed to sustain a  $T_{\text{CMB}} \simeq 2.7$  K bath. As a result, the photon field is maintained at its equilibrium temperature even when ultrasoft gravitational modes “leak” entropy across the horizon. The required replenishment is thermodynamically cheap.

## 5.2 Why the photon bath does not cool under expansion

In standard FRW reasoning, radiation redshifts as  $a^{-4}$  and cools unless it is continually replenished [74, 21]. In the present framework, redshift represents not a loss of energy to “nothing” but the transfer of energy into the infrared geometric sector, where it contributes to the free-energy account that ultimately drives entropy export across the horizon. The photon bath does not drain away; it is continually reheated by absorbing an exceedingly small fraction of the free energy liberated by the irreversible sequestration of matter and structure into the horizon.

If the photon temperature were momentarily to fall below its stationary value, the bath would absorb additional free energy until equilibrium was restored. Because the required energy is minuscule compared to the available free-energy flux, this re-equilibration occurs with negligible effect on the global free-energy budget. Thus radiation maintains a stable KMS temperature set by the exterior state, rather than by initial conditions.

## 5.3 Conceptual summary

The observed CMB temperature is therefore interpreted not as a relic of a hot initial state but as the stationary thermal temperature of the photon–neutrino sector in a horizon-coupled nonequilibrium steady state. Within this framework, a photon bath at the observed temperature is dynamically stable and thermodynamically inexpensive to maintain. In particular, such a bath persists near 2.7 K because:

1. it is a fast thermalizer of injected free energy;
2. maintaining its temperature requires negligible power compared to the free-energy flux associated with horizon entropy export;
3. redshift losses feed the infrared geometric sector rather than depleting the exterior of energy; and
4. any deficit is corrected by tiny adjustments in the absorbed free-energy flux, rather than by bulk photon creation.

---

In both cases the total entropy production is comparable, but the buffered pathway spreads dissipation over a larger phase space and suppresses violent local responses.

These considerations do not, by themselves, fix the numerical value of the photon temperature; rather, they show that once the temperature is selected by infrared geometric and entropic constraints, it is robustly maintained against expansion and perturbations. This interpretation situates the CMB within the same mesoscopic thermodynamic framework that governs baryon balance and global entropy flow, and it prepares the ground for the horizon-coupled thermodynamics developed in the next section.

## 6 Horizon-Coupled Thermodynamics

The mesoscopic continuity equations derived in Section 4 describe the balance of conserved charges in an expanding spacetime with horizon exchange. We now incorporate the complementary requirement of *entropy balance*. In a horizon-coupled cosmology, entropy is not conserved as a comoving density, but flows irreversibly through the exterior system and into a causal sink. Stationarity must therefore be formulated as a balance of entropy *fluxes*, rather than as a closed-system conservation law.

The thermodynamic structure developed in this section is that of an open, nonequilibrium steady state. Entropy is continuously produced, transported, and exported, yet no macroscopic entropy reservoir accumulates entropy secularly. To make this explicit, we distinguish three extensive entropy sectors:

$$S_{\text{obs}}, \quad S_{\text{BH}}, \quad S_{\text{hor}},$$

denoting respectively the entropy of observer-accessible degrees of freedom, the Bekenstein–Hawking entropy of black holes within the cosmological causal wedge, and the entropy of the cosmological horizon.

The exterior entropy is defined as

$$S_{\text{ext}} \equiv S_{\text{obs}} + S_{\text{BH}}, \quad (23)$$

and in the late-time steady state all extensive exterior entropies are stationary:

$$\dot{S}_{\text{obs}} = 0, \quad \dot{S}_{\text{BH}} = 0, \quad \dot{S}_{\text{ext}} = 0. \quad (24)$$

Stationarity here refers to the *total* entropy in each sector, not to the absence of entropy flux. Each sector functions as a throughput reservoir whose inflow and outflow of entropy balance exactly in steady state.

Gravitational collapse, accretion, and structure formation continuously transfer entropy from observer-accessible degrees of freedom into black-hole microstates, while an equal entropy flux transfers black-hole microstates into the cosmological horizon. The black-hole sector therefore acts as an intermediate entropy amplifier: it neither accumulates nor depletes entropy in steady state, but mediates irreversible entropy flow between the exterior medium and the horizon.

The cosmological horizon is the unique entropy sink. Its entropy increases monotonically,

$$\dot{S}_{\text{hor}} > 0, \quad (25)$$

ensuring consistency with the second law for the combined system. The apparent constancy of  $S_{\text{ext}}$  does not signal reversibility or equilibrium. Rather, it reflects a balance of entropy fluxes in an open system.

Thermodynamically, the exterior operates as an *irreversible Carnot engine*. Free energy is processed within the exterior at an effective temperature  $T_{\text{ext}}$ , amplified into large amounts of entropy by gravitational collapse, and ultimately dumped into the cosmological horizon, which functions as an effectively zero-temperature reservoir. Because  $T_{\text{hor}} \ll T_{\text{ext}}$ , the entropy increase of the horizon associated with a given energy flux exceeds the entropy throughput of the exterior sectors, guaranteeing strictly positive net entropy production despite the stationarity of  $S_{\text{obs}}$  and  $S_{\text{BH}}$ .

With this bookkeeping fixed,<sup>2</sup> the remainder of this section formulates the mesoscopic continuity equations governing entropy throughput, identifies the infrared geometric channel responsible for entropy export and return, and shows how these fluxes enforce a self-consistent steady state with stationary exterior entropies.

**Entropy export versus horizon entropy.** A notational distinction is essential. Throughout this section,  $\dot{S}_{\text{cos}}$  (and its density  $\dot{s}_{\text{cos}}$ ) denotes an *entropy flux*—the rate at which exterior entropy  $S_{\text{ext}}$  is transported across the cosmological horizon and removed from the exterior Hilbert space as causal access is lost due to expansion. It is therefore an *outgoing flux of exterior entropy*, not the time derivative of the entropy of the horizon itself.

By contrast,  $\dot{S}_{\text{hor}}$  denotes the rate of change of the entropy associated with the cosmological horizon as a thermodynamic system. These two quantities are not equal. The second law for the combined exterior–horizon system requires

$$\dot{S}_{\text{hor}} \geq \dot{S}_{\text{cos}}, \quad (26)$$

with strict inequality whenever entropy is produced irreversibly in the transfer of exported degrees of freedom into horizon microstates. In the language of nonequilibrium thermodynamics,  $\dot{S}_{\text{cos}}$  is an entropy *current*, while  $\dot{S}_{\text{hor}}$  includes both this current and the additional entropy production associated with coupling to an effectively cold reservoir. Failure to distinguish these quantities would amount to confusing entropy transport with entropy production.

---

<sup>2</sup>A subtle but important point concerns the role of black-hole entropy in the exterior bookkeeping. Black holes amplify entropy through accretion, but the microscopic degrees of freedom responsible for the Bekenstein–Hawking entropy are causally tied to the same irreversible channel that exports entropy to the cosmological horizon. From a mesoscopic standpoint, it is therefore equally consistent to regard black-hole entropy as (i) part of the instantaneous exterior entropy, or (ii) entropy already irreversibly coupled to a future causal boundary.

These two descriptions differ only by a bookkeeping convention and have no physical consequence for the balance laws. What is invariant is the *entropy export rate* and the associated free-energy release. All subsequent equations depend only on this flux, not on the notional location of the entropy at intermediate times.

**Entropy export and stationarity.** In the bookkeeping adopted here, black-hole entropy is included in the exterior entropy  $S_{\text{ext}} = S_{\text{obs}} + S_{\text{BH}}$ . Although black-hole entropy is continually generated by collapse and accretion, it does not accumulate secularly. In a horizon-coupled steady state, the rate at which entropy is channeled into black-hole microstates is exactly balanced by the rate at which exterior entropy is exported across the cosmological horizon as causal access is lost due to expansion.

Black holes therefore act as entropy amplifiers and staging reservoirs within the exterior system. They neither create nor destroy entropy in the global sense; rather, they mediate an irreversible entropy flux from the exterior medium into the horizon. The cosmological horizon serves as the unique entropy sink, while the detailed partition of exterior entropy into observer-accessible and black-hole components plays no role in the balance laws.

As a consequence, entropy production within the exterior does not imply secular growth of the total exterior entropy. Stationarity is achieved dynamically through a balance of entropy fluxes. In steady state,

$$\dot{S}_{\text{ext}} \approx 0, \quad (27)$$

even though entropy is continually exported from the exterior and the entropy of the horizon increases monotonically in accordance with the second law.

**Entropy continuity equation.** Let  $s_{\text{ext}}(t)$  denote the coarse-grained physical entropy density of the exterior system. Applying Reynolds transport to a comoving world-tube bounded by the cosmological horizon yields the mesoscopic entropy balance equation [71]

$$\dot{s}_{\text{ext}} + 3H s_{\text{ext}} = -\dot{s}_{\text{cos}} + \dot{s}_{\text{IR}}, \quad (28)$$

where:

- $\dot{s}_{\text{cos}} > 0$  is the entropy *flux density* exported from the exterior across the cosmological horizon, i.e. the rate at which exterior entropy is removed from the exterior Hilbert space by loss of causal access due to expansion; and
- $\dot{s}_{\text{IR}} > 0$  is the rate at which expansion-driven infrared geometric modes inject entropy into the exterior system.

The term  $3H s_{\text{ext}}$  represents the kinematic dilution of physical entropy density due to cosmic expansion; it is the advective contribution associated with the time-dependent exterior volume and should not be interpreted as a separate entropy export channel. By contrast,  $\dot{s}_{\text{cos}}$  represents an irreversible entropy current across the horizon. Black-hole entropy production does not appear as an independent source term: because the total black-hole entropy  $S_{\text{BH}}$  is stationary in steady state, its production by accretion is exactly balanced by export across the horizon and is therefore contained implicitly in  $\dot{s}_{\text{cos}}$ .

**Stationary exterior entropy density.** In a horizon-coupled steady state the physical entropy density of the exterior is approximately stationary,

$$\dot{s}_{\text{ext}} \approx 0. \quad (29)$$

Under this condition, Eq. (28) reduces to the algebraic balance relation

$$3H s_{\text{ext}} = \dot{s}_{\text{IR}} - \dot{s}_{\text{cos}}, \quad (30)$$

which fixes the *volumetric entropy return rate* required for stationarity. The dilution of entropy density by cosmic expansion and the irreversible export of exterior entropy across the horizon must be exactly compensated, in steady state, by entropy supplied through expansion-induced infrared geometric degrees of freedom.

## 6.1 Entropy production and horizon export

At the semiclassical level, black-hole formation and growth are governed by the Bekenstein–Hawking area law [6, 71]. Matter accretion produces a large amount of entropy per unit accreted energy, amplifying entropy within the exterior system. In the present framework this amplification does not lead to secular growth of exterior entropy. Instead, the entropy generated by black-hole growth is transferred to the cosmological horizon on cosmological timescales, contributing to the irreversible increase of horizon entropy while leaving  $S_{\text{ext}}$  stationary.

The baryon flux  $\Phi_B$  introduced in Section 4 contributes directly to this entropy processing. Baryon sequestration into black holes enhances entropy amplification and thereby increases the export rate  $\dot{s}_{\text{cos}}$ . The resulting thermodynamic imbalance is compensated by the baryon creation term  $\Gamma_B$  in the baryon continuity equation (22), restoring a stationary exterior baryon density.

Photons and neutrinos also cross the cosmological horizon, but they do not control the entropy balance. Although a cold photon bath can carry large entropy per unit energy, routing the free-energy budget primarily into electromagnetic heating does not maximize entropy throughput into the ultimate cold reservoir. The dominant steady-state entropy circuit is instead gravitational and infrared: collapse and accretion amplify entropy, while expansion-driven infrared geometric modes provide the channel that exports this entropy irreversibly to the cosmological horizon. In this sense the photon–neutrino sector acts as a passive thermometer of the medium, whereas the infrared gravitational sector is the active carrier that closes the entropy budget in Eq. (28).

## 6.2 IR entropy from cosmic expansion

Cosmic expansion excites long-wavelength gravitational and geometric modes in the mesoscopic Carnot–Carathéodory geometry. These infrared modes carry entropy without being constrained by baryon or lepton charges and can be

produced in enormous numbers at small energy cost. Their net contribution to the entropy budget is encoded in  $\dot{s}_{\text{IR}}$  in (28).

Dimensional considerations and the kinematics of the Carnot tangent geometry imply that the excitation rate of IR modes scales with the distinguished mesoscopic frequency  $\sigma$ . When  $\sigma$  is locked to the Hubble rate  $H$ , the spectrum of IR modes behaves as a standing-wave system constrained by the global causal structure. The sign of  $\dot{s}_{\text{IR}}$  is such that expansion *adds* entropy to the exterior sector: on mesoscopic scales the production of long-wavelength geometric modes increases the exterior entropy density and counteracts the loss to horizons, allowing a stationary solution of (28).

From the standpoint of the combined system,  $\dot{S}_{\text{IR}}$  is the unique large channel through which expansion-driven geometry can return entropy to the mesoscopic medium. It is the entropy analogue of the creation term  $\Gamma_B$  in the baryon continuity equation: both are horizon-induced, infrared processes that restore stationarity in the presence of continuous accretion.

### 6.3 Grand-canonical constraints for the reduced exterior state

Tracing over horizon-inaccessible degrees of freedom yields a reduced exterior state that is naturally of grand-canonical type [62, 12]. In particular [10], the reduced density operator takes the schematic form

$$\rho_{\text{ext}} \propto \exp \left[ -K_{\text{mod}} - \sum_X \alpha_X Q_X \right], \quad (31)$$

where  $K_{\text{mod}}$  is the modular generator associated with the horizon-defined factorization and the  $\alpha_X$  encode the conjugate biases (chemical potentials) enforcing conditional entropy maximization at fixed exterior charges.

In the present framework, the temperature  $T_{\text{ext}}$  plays a single, unambiguous physical role. It governs the entropy-processing capacity of the exterior medium and sets the scale for the production of infrared modes and baryons that compensate expansion-driven dilution. The associated mesoscopic source terms are therefore controlled by  $T_{\text{ext}}$ , which functions as an entropy-return temperature rather than a horizon temperature.

The photon bath acts as a rapidly equilibrating, passive buffer that records this temperature spectrally. Its near-Planckian distribution reflects the stationary value of  $T_{\text{ext}}$  but does not itself drive entropy return or baryon repopulation, in close analogy with buffered intermediate reservoirs in chemical thermodynamics.

By contrast, the cosmological horizon functions as an effectively zero-temperature entropy sink. Because it absorbs entropy at negligible energetic cost, it does not participate in the entropy-return channel and does not set the scale of infrared production or chemical bias. Its role is purely absorptive, not regulatory.

In particular, the baryon bias may be written schematically as

$$\mu_B \equiv T_{\text{ext}} \alpha_B, \quad (32)$$

so that  $\mu_B > 0$  corresponds to a reduced exterior state that favors baryon repopulation when baryon-carrying degrees of freedom are exported across horizons. In steady state the baryon source term adjusts so that  $\Gamma_B = \Phi_B - 3Hn_B$ , fixing the stationary exterior density.

#### 6.4 Stationarity and coupled balance laws

The entropy continuity equation (28) and the baryon continuity equation (22) together determine the large-scale thermodynamic and kinematic state of an expanding universe whose mesoscopic structure is governed by the spectral scale  $\sigma$ .

Explicitly, the coupled mesoscopic balance laws are

$$\dot{s}_{\text{ext}} + 3Hs_{\text{ext}} = -\dot{s}_{\text{cos}} + \dot{s}_{\text{IR}}, \quad (33)$$

$$\dot{n}_B + 3Hn_B = -\Phi_B + \Gamma_B. \quad (34)$$

In a steady-state cosmological medium one has  $\dot{s}_{\text{ext}} = 0$  and  $\dot{n}_B = 0$ , and (33)–(34) reduce to the algebraic relations

$$\dot{s}_{\text{IR}} = 3Hs_{\text{ext}} + \dot{s}_{\text{cos}}, \quad 3Hn_B = -\Phi_B + \Gamma_B. \quad (35)$$

The first equation expresses the global second law for the combined horizon-exterior system; the second fixes the equilibrium baryon density once the horizon-induced fluxes  $\Phi_B$  and  $\Gamma_B$  are specified.

Because both  $\dot{s}_{\text{IR}}$  and  $\Gamma_B$  scale with the mesoscopic frequency  $\sigma$ , the expansion rate  $H$ , the cosmic baryon density, and the horizon thermodynamics are all governed by the same infrared scale.

The next subsection analyzes in more detail how horizon-induced entropy flow enforces mesoscopic baryon creation in such a steady state.

#### 6.5 Entropy Balance, Horizon Charges, and the Necessity of Baryon Creation

The mesoscopic exterior universe is not a closed thermodynamic system. Cosmological expansion continually removes degrees of freedom from the causal wedge of late-time observers, exporting both entropy and conserved charges into horizon-inaccessible sectors. Any steady-state description must therefore account not only for conserved currents but for the irreversible *loss of access* to those currents.

From the standpoint of the full quantum field theory, baryon number is exactly conserved. From the standpoint of the reduced exterior state, however, baryon density decreases as baryon-carrying worldlines are transported across the cosmological horizon. Black-hole accretion provides an additional localized realization of the same mechanism, sequestering baryon number into horizon-adjacent, exponentially redshifted modes. In neither case is baryon number destroyed; what changes is the factorization of the global Hilbert space into accessible and inaccessible sectors.

Coarse-graining over the inaccessible sector therefore produces an exterior density operator with a positive baryon chemical potential  $\mu_B > 0$ . Restoring steady state does not require the return of the original infalling baryons—a process exponentially suppressed by horizon redshift—but rather the appearance of new baryons in the exterior sector. Baryon creation is thus not an ad hoc assumption but the thermodynamically preferred response of an open system subject to continuous horizon-induced depletion.

The free energy required for baryon realization is supplied by entropy export into horizon microstates. Black-hole Hawking radiation is negligible for astrophysical masses; instead, entropy balance is achieved through the excitation of ultra-soft infrared modes associated with cosmological expansion. These modes can carry arbitrarily large entropy at negligible energy cost, liberating free energy sufficient to offset the rest-mass cost of baryon materialization by many orders of magnitude. At the mesoscopic level the baryon therefore appears first *in potentia*, as a grand-canonical bias in the reduced exterior state; a localized ultraviolet proton emerges only where local energy conditions permit.

**Why lepton number does not impose a thermodynamic constraint.** Although both baryon number  $B$  and lepton number  $L$  are exactly conserved in the full quantum field theory at the energies relevant here, they play very different roles in the thermodynamics of the mesoscopic exterior. The difference is not microscopic but energetic.

Baryons are heavy, long-lived, and gravitationally bound. Their removal from the exterior through cosmological expansion or black-hole accretion produces a genuine deficit in the reduced exterior density operator. Each lost baryon carries an entropy cost proportional to the inverse horizon temperature, and the exterior therefore develops a nonzero baryon chemical potential. Steady-state balance forces baryon creation.

Leptons, by contrast, are thermodynamically inexpensive. Once sufficient free energy is available to realize baryons, the additional energy required to produce the accompanying leptons needed for charge neutrality is negligible by comparison. Electron production therefore adjusts automatically to whatever baryon population emerges and never limits the equilibrium.

Any residual excess of lepton number is carried almost entirely by neutrinos. Because neutrinos interact only weakly, they decouple from the exterior free-energy recycling loop, redshift with the radiation field, and are gradually transported out of the causal wedge of late-time observers by cosmic expansion. This lepton background has no significant back-reaction on the mesoscopic state and does not influence the baryon chemical potential.

Thus lepton number must be conserved globally, but it does not constrain the steady state. Lepton creation is not an independent thermodynamic requirement; it is a trivial corollary of baryon realization and charge neutrality. The only conserved charge whose loss forces a macroscopic response in a horizon-coupled steady state is baryon number.

## 6.6 Baryon number continuity

Let  $\rho_B(t)$  denote the physical baryonic mass density contained in the exterior region accessible to late-time observers. Although the underlying quantum field theory exactly conserves the baryon current, the exterior is an *open system*: cosmological expansion continually transports baryon-carrying degrees of freedom across the cosmological horizon, removing them from the exterior Hilbert space. Baryon number therefore does not obey a closed comoving conservation law in the reduced description.

At mesoscopic scales the appropriate continuity equation on an expanding background takes the form

$$\dot{\rho}_B + 3H\rho_B = \dot{\rho}_B^{(\text{create})} - \dot{\rho}_B^{(\text{loss})}, \quad (36)$$

where  $\dot{\rho}_B^{(\text{create})}$  denotes the rate at which baryonic mass is injected into the exterior sector, and  $\dot{\rho}_B^{(\text{loss})}$  denotes the rate at which baryonic mass is exported from the exterior Hilbert space. The loss term represents a *flux across a causal boundary* rather than local destruction of baryon number.

The dominant contribution to  $\dot{\rho}_B^{(\text{loss})}$  arises from transport of baryon-carrying degrees of freedom across the cosmological horizon. Localized black-hole accretion provides an additional, spatially inhomogeneous contribution but does not control the homogeneous baryon balance of the universe. It is therefore convenient to write

$$\dot{\rho}_B^{(\text{loss})} = \dot{\rho}_{\text{cos}} + \dot{\rho}_{\text{acc}}, \quad (37)$$

where  $\dot{\rho}_{\text{cos}}$  denotes the horizon-export term and  $\dot{\rho}_{\text{acc}}$  the baryonic mass flux captured by black holes.

In a stationary exterior description,  $\dot{\rho}_B = 0$ , and Eq. (36) reduces to the steady-state balance condition

$$\dot{\rho}_B^{(\text{create})} = 3H\rho_B + \dot{\rho}_{\text{cos}} + \dot{\rho}_{\text{acc}}. \quad (38)$$

The term  $3H\rho_B$  reflects the kinematic dilution of physical density in an expanding volume, while  $\dot{\rho}_{\text{cos}}$  encodes irreversible export of baryon number from the causal wedge of late-time observers.

The purpose of comparing  $\dot{\rho}_B^{(\text{create})}$  with the black-hole accretion rate density  $\dot{\rho}_{\text{acc}}$  is not to suggest a causal link between baryon creation and black-hole growth, but to provide an empirical scale against which the required replenishment rate may be judged. The steady-state condition  $\dot{\rho}_B^{(\text{create})} \sim 3H\rho_B$  fixes the magnitude of baryon injection required by cosmological expansion and horizon export, independent of any localized collapse phenomena. By contrast,  $\dot{\rho}_{\text{acc}}$  is an observationally accessible tracer of baryonic mass processing in the late universe.

Observationally [32], the ratio of baryonic mass density to black-hole mass density lies in the range  $\rho_B/\rho_{\text{BH}} \sim 10^2\text{--}10^3$ , while the ratio of the cosmic star-formation rate density to the black-hole accretion rate density is also of order  $10^3$ . The fact that these independently inferred ratios are of similar magnitude

indicates that the baryon replenishment required to maintain a stationary exterior medium is not parametrically large compared to known late-time baryonic processing rates. Black-hole growth thus serves as a useful empirical yardstick, while remaining a subleading sink in the global baryon balance.

From this perspective, baryon “creation” in a steady-state universe is not a microscopic violation of baryon number but the open-system response of the exterior sector to continual charge export across the cosmological horizon. Black-hole accretion enters only as a correction to this global balance.

**Remark.** The same bookkeeping that enforces baryon balance also constrains the lepton budget in the neutrino sector. In steady state, the cosmological electron-type neutrino and antineutrino backgrounds (with local sources such as supernovae, neutron stars, and active galactic nuclei excised) must obey a mesoscopic continuity equation of the schematic form

$$\dot{n}_{\nu_e} + \dot{n}_{\bar{\nu}_e} + 3H(n_{\nu_e} + n_{\bar{\nu}_e}) = S_\nu(\sigma). \quad (39)$$

Here  $S_\nu(\sigma)$  encodes both neutrino production from weak processes near compact objects and the antineutrino flux associated with infrared baryon repopulation. As in the baryon case, this source term is not free: it is fixed by the same horizon-coupled balance laws that determine the baryon creation rate and the net rate at which lepton number is transported out of the cosmological causal wedge by expansion.

The large-scale  $\nu_e$ – $\bar{\nu}_e$  background therefore furnishes a conceptually sharp consistency condition: after subtracting local astrophysical contributions, the relic electron-type neutrino density should match the value implied by the balance equation for the observed expansion rate  $H$ .

In practice, however, this test is extremely challenging. Most proposed detection strategies for the cosmic neutrino background are sensitive only to some combination of  $n_{\nu_e}$  and  $n_{\bar{\nu}_e}$ , with limited ability to distinguish neutrinos from antineutrinos, while  $\nu_e \bar{\nu}_e$  annihilation into  $e^+ e^-$  can further obscure the relation between the individual number densities and the underlying source terms. The neutrino sector therefore provides the cleanest setting in the model where the frequency scale  $\sigma$  is tied *directly* to the Hubble rate via a continuity equation, with minimal mediation by buffered degrees of freedom, but exploiting this link observationally would require unprecedented control over both the relic neutrino background and its  $\nu_e$ – $\bar{\nu}_e$  composition.

## 6.7 Why Entropy Returns in the Infrared

The mesoscopic framework developed here posits that the dominant channel by which entropy is returned from horizons to the exterior sector is infrared and geometric rather than ultraviolet and particulate. That is, the entropy flow responsible for restoring stationarity appears primarily as long-wavelength curvature and graviton-like modes, not as a burst of high-energy quanta or an uncontrolled proliferation of cold photons. In this subsection we clarify why this must be the case once relativistic causality and the horizon-defined factorization of the exterior Hilbert space are taken seriously.

The relevant causal partition is set by the *cosmological horizon*. In an expanding FRW spacetime, baryon-carrying degrees of freedom are transported out of the causal wedge of late-time observers at a finite FRW time, even though no local microphysical process “destroys” the baryon along its worldline. From the standpoint of local quantum field theory, a proton that eventually crosses a black-hole horizon experiences nothing special at the crossing itself: in a freely falling frame the short-distance physics of QCD and the local Hilbert space factorization remain intact. Any description in which the proton is literally annihilated at the horizon is therefore unphysical. What changes is the causal accessibility of that proton to the exterior sector.

From the exterior viewpoint, the loss of causal access produces a mesoscopic depletion of baryon number. The expectation value of the exterior baryon current obeys

$$\nabla_\mu \langle J_B^\mu \rangle_{\text{ext}} = -\Phi_B + \Gamma_B,$$

where  $\Phi_B > 0$  encodes the export of baryon number from the exterior Hilbert space and  $\Gamma_B$  is the compensating source term required to maintain a stationary exterior density. At the level of the full Hilbert space no charge is lost, but for the reduced exterior state a “hole” opens in the baryon sector. As discussed in Section 6.5, this depletion drives a thermodynamically favored re-equilibration of the exterior medium.

The crucial consistency condition is not tied to any particular infalling worldline but to the horizon-defined factorization of the quantum state. Compensating baryons produced in the exterior sector must lie outside the cosmological causal wedge associated with the lost degrees of freedom. This requirement follows directly from the open-system interpretation of  $\Gamma_B$ : the compensating charge represents degrees of freedom that were previously inaccessible to the exterior and must remain so with respect to the horizon that defines that exterior.

It is nevertheless useful to phrase this requirement heuristically in terms of local observers. From the viewpoint of an infalling proton, local QFT remains valid and the horizon crossing is innocuous. Any compensating baryons that were causally accessible along the same worldline would therefore appear as a duplication of baryon number within a single connected causal domain. This picture should be understood as an intuition aid rather than the fundamental mechanism enforcing charge balance; the primary causal partition is set by the cosmological horizon itself.

Once this horizon-defined separation is recognized, the infrared character of the entropy return channel follows naturally. Ultraviolet excitations—hard photons, short-wavelength particles, or local scattering processes—populate the same light cones and remain confined to the same local field algebra. They do not alter the causal partition of spacetime and therefore cannot implement the large-scale reorganization of accessible versus inaccessible degrees of freedom required by horizon-coupled equilibration.

Infrared geometric modes, by contrast, are tied directly to horizon-scale physics. Long-wavelength gravitons and curvature perturbations modify the

redshift structure, the effective causal wedges, and the entanglement between interior and exterior sectors on mesoscopic scales. Such modes can carry large amounts of entropy at small energy cost and are unconstrained by baryon or lepton number. They therefore provide a natural channel through which the exterior state can re-equilibrate while respecting both local QFT and the global horizon-defined factorization of the Hilbert space.

From this perspective, graviton production plays a structural rather than a microscopic role in the baryon continuity equation. It is not invoked as a direct source of entropy but as the collective geometric response that enforces consistent causal separation between exterior and inaccessible degrees of freedom. Baryon creation is therefore *necessarily* an infrared phenomenon in this framework: it is encoded in long-wavelength geometric modes that are invisible to any single local inertial frame but manifest in the global causal structure set by the cosmological horizon.

This also clarifies why entropy is returned primarily in the infrared rather than the ultraviolet. UV channels do not modify causal structure and thus cannot mediate horizon-scale equilibration. IR geometric modes alone (i) carry large entropy at minimal energy cost, (ii) remain neutral under all conserved charges, and (iii) implement the horizon-defined separation required by relativistic causality. For these reasons the mesoscopic steady state routes entropy flow into long-wavelength geometry rather than into an unchecked proliferation of UV quanta.

## 6.8 Free Energy and Internal Dissipation

The exterior system is maintained at a fixed KMS temperature  $T_{\text{ext}}$ , while entropy is continuously exported to the horizon at negligible energetic cost. The exterior free energy,

$$F_{\text{ext}} = E_{\text{ext}} - T_{\text{ext}} S_{\text{ext}}, \quad (40)$$

therefore changes according to

$$\dot{F}_{\text{ext}} = -T_{\text{ext}} \dot{S}_{\text{export}}. \quad (41)$$

High free energy corresponds to abundant internal entropy-production channels (structure formation, collapse, black-hole growth). Low free energy signals that these internal channels are exhausted: chemical potentials are flat, gradients are weak, and further internal rearrangements no longer produce entropy.

## 6.9 Feedback and Relaxation Toward $\sigma_*$

The relaxation of  $\sigma$  follows from a feedback between free energy, structure persistence, and geometric dissipation:

**Large  $\sigma$ .** If  $\sigma$  is too large, geometric correlations decay rapidly and structure formation is suppressed. Entropy production drops, reducing the entropy flux to the horizon. With fewer irreversible processes active, correlations persist longer and the effective decay rate inferred from long-time dynamics decreases. Thus excessively large  $\sigma$  self-quenches.

**Small  $\sigma$ .** If  $\sigma$  is too small, geometric correlations persist and structure forms efficiently, but entropy export is throttled by the slow relaxation rate. Entropy accumulates in the exterior, lowering free energy and saturating internal dissipation channels. Once internal entropy production is exhausted, the second law requires entropy to be exported geometrically, and correlations lose their structural supports. This shortens correlation lifetimes and increases the effective decay rate, driving  $\sigma$  upward.

**Fixed Point.** The value  $\sigma_*$  is therefore selected by the condition

$$\frac{d}{d\sigma} \dot{S}_{\text{export}}(\sigma) \Big|_{\sigma=\sigma_*} = 0, \quad (42)$$

corresponding to maximal entropy throughput to the horizon. This fixed point is stable: deviations of  $\sigma$  in either direction reduce entropy export and induce geometric back-reaction that restores  $\sigma$  toward  $\sigma_*$ .

## 6.10 Infrared Universality

Because the feedback operates only on long-wavelength correlations and does not depend on microscopic physics, the selected value  $\sigma_*$  is an infrared quantity. At late times the only available timescale is the horizon crossing time, so

$$\sigma_* \sim H_0, \quad (43)$$

up to order-unity factors. The Carnot–Carathéodory tangent geometry discussed earlier is thus understood as the geometric fixed point associated with entropy–maximizing horizon coupling.

## 6.11 Summary

The relaxation of  $\sigma$  does not proceed through a dynamical equation for  $\sigma(t)$ , but through self-consistent selection. Excessively rapid geometric relaxation destroys the structures required for entropy production, while excessively slow relaxation exhausts internal dissipation and forces entropy export. The observed value  $\sigma_*$  maximizes entropy throughput to the horizon and represents the unique stable infrared relaxation rate compatible with a nonequilibrium steady state.

## 6.12 High- $\sigma$ Regime: Hot, Inefficient Structure Formation and Suppressed Black-Hole Sequestration

To build intuition for the  $\sigma$ -selection mechanism, it is useful to contrast two qualitative regimes. Recall that  $\sigma^{-1}$  is the characteristic timescale for the decay of large-scale geometric correlations and directional memory into horizon-coupled degrees of freedom. Large  $\sigma$  therefore corresponds to *rapid geometric relaxation*: anisotropies are erased quickly, long-wavelength correlations do not persist, and coarse-grained mixing acts aggressively.

**Hot formation.** In this high- $\sigma$  regime, gravitational structure has less time to self-organize into deep, long-lived potential wells before correlation information is mixed away. Collapse proceeds in a more impulsive, less coherent manner, so that baryons typically thermalize at higher effective temperatures during assembly (in the sense of larger velocity dispersion and stronger shock heating). Qualitatively, the system forms stars “hot”: gas is stirred and heated faster than it can cool and settle into thin disks, and the star-formation history is more bursty and feedback-dominated.

**Why this suppresses black-hole sequestration.** Efficient sequestration of mass-energy into black holes requires sustained, coherent inflow: cold gas must lose angular momentum, remain bound, and feed a compact nucleus over many dynamical times. Rapid geometric mixing frustrates this in two complementary ways:

1. *Shallow wells and disrupted inflow.* When correlations are erased quickly, gravitational potentials remain comparatively shallow and time-variable. Gas inflow is therefore easily reheated and re-ejected by feedback, preventing the long, cold accretion episodes that efficiently grow black holes.
2. *Premature equilibration of large-scale anisotropies.* The anisotropies and coherent torques that normally drive angular momentum transport (bars, mergers, triaxiality, filamentary feeding) are less persistent. Without long-lived nonaxisymmetric structure, angular momentum loss is inefficient and nuclear fueling is throttled.

The net effect is that high  $\sigma$  increases the *rate* at which geometric information is exported, but reduces the *efficiency* with which baryonic mass is processed into high-entropy gravitational states. Since black holes are the dominant entropy amplifiers per unit energy, this suppression directly reduces the long-time entropy throughput to the horizon. In other words, excessively large  $\sigma$  produces a universe that is locally “hot” (in the sense of violent, high-dispersion assembly) but globally inefficient at entropy amplification and sequestration.

**Interpretation.** This provides a concrete physical mechanism for why very large  $\sigma$  is not self-consistent in a nonequilibrium steady state: rapid mixing

speeds entropy export only transiently, while simultaneously starving the black-hole channel that supplies the bulk of gravitational entropy. The system is therefore driven away from the high- $\sigma$  regime toward the entropy-throughput optimum  $\sigma_*$ .

### 6.13 Why Free Energy Is Not Exhaustively Dissipated into Infrared Gravitational Modes

Although infrared gravitational modes represent the energetically cheapest carriers of entropy, the exterior system does not dissipate all available free energy directly into gravitons. The reason is that populating infrared geometric degrees of freedom is itself a form of irreversible mixing that erases large-scale correlations and directional memory. Excessive geometric relaxation suppresses the formation of coherent gravitational structures—deep potential wells, sustained anisotropies, and long-lived inflows—that are required for efficient entropy amplification through collapse and black-hole growth. While infrared gravitons provide an efficient sink for entropy, they do not by themselves amplify entropy; that role is played by nonlinear gravitational structures whose formation depends on the persistence of correlations over many dynamical times. Free energy therefore cannot be optimally discharged by immediate conversion into infrared modes alone. Instead, the system must retain sufficient free energy to support structure formation, allowing entropy to be processed and amplified before being exported geometrically. The resulting balance between correlation persistence and geometric relaxation selects a finite infrared decay rate and prevents the degenerate limit in which free energy is dissipated directly into gravitons without prior structural processing.

In a spacetime with a positive cosmological constant, the dominant large-scale response to excess free energy may be interpreted, at a coarse-grained level, as the continual injection of infrared geometric degrees of freedom through expansion. While this process need not be described microscopically as graviton emission, it is morally equivalent in thermodynamic terms: free energy is converted directly into long-wavelength geometric structure that dilutes correlations, redshifts resolved modes, and enlarges the available configuration space without prior processing through nonlinear structure formation. In this degenerate limit, free energy is discharged primarily by geometric expansion itself, rather than being routed through entropy-amplifying channels such as collapse and black-hole growth. The present framework instead describes a more general nonequilibrium regime in which expansion is only one outlet among several, and where free energy must be partially retained to sustain the structures that maximize long-time entropy throughput before entropy is exported to infrared geometric modes.

## 7 Entropy–Acceptance Temperature and the Horizon as a Cold Sink

In gravitational systems far from equilibrium, multiple notions of “temperature” coexist and must be carefully distinguished. The temperature relevant for entropy bookkeeping is not, in general, the radiative or spectral temperature associated with particle emission, but rather the thermodynamic derivative governing entropy acceptance. Throughout this work we therefore distinguish between *radiative (KMS) temperatures* and *entropy–acceptance temperatures*.

### 7.1 Entropy–Acceptance Temperature

For any open subsystem exchanging entropy with its environment, we define the entropy–acceptance temperature by the Clausius relation

$$T_{\text{acc}} \equiv \frac{\delta E_{\text{grav}}}{\delta S_{\text{grav}}}, \quad (44)$$

where  $\delta E_{\text{grav}}$  is the change in gravitational energy required to absorb an entropy increment  $\delta S_{\text{grav}}$ . This quantity orders subsystems by their ability to accept entropy [71]: entropy flows from larger  $dE/dS$  to smaller  $dE/dS$ . In this sense, a “colder” subsystem is one that can absorb entropy at lower energetic cost.

This definition is independent of radiative emission and applies equally to non-stationary and non-Killing horizons.

### 7.2 Black Holes as Cold Entropy Amplifiers

For a stationary black hole, the entropy–acceptance temperature coincides with the Hawking temperature [5, 71],

$$T_{\text{BH}} = \left( \frac{\partial E}{\partial S} \right)_{\text{BH}} = \frac{\hbar c^3}{8\pi k_B GM}. \quad (45)$$

Astrophysical black holes therefore have extremely small  $T_{\text{BH}}$ . This low temperature does not indicate inefficiency; rather, it reflects the fact that adding a small amount of energy opens an enormous gravitational phase space. Black holes are thus thermodynamically cold while simultaneously acting as highly efficient entropy amplifiers, converting modest input entropy (e.g. from QCD degrees of freedom) into vastly larger gravitational entropy [5, 71].

### 7.3 The Cosmological Horizon as an Effective Zero–Temperature Sink

The cosmological horizon in the present framework differs qualitatively from a stationary black hole horizon [31, 71]. It does not correspond to a fixed Killing generator and does not radiate in the Hawking sense. Instead, it functions as

an infrared sink for gravitational entropy produced elsewhere in the exterior region.

For entropy absorbed by the horizon, the associated energetic cost is negligible compared to that required for black hole entropy growth [31]. Operationally,

$$\delta E_{\text{horizon}} \approx 0 \quad \text{for} \quad \delta S_{\text{grav}} > 0, \quad (46)$$

so that

$$T_{\text{horizon}}^{(\text{acc})} = \frac{\delta E_{\text{horizon}}}{\delta S_{\text{grav}}} \approx 0 \quad (47)$$

to the precision relevant for exterior gravitational bookkeeping. In this entropy-acceptance sense, the cosmological horizon is colder than any black hole and acts as the terminal entropy sink of the universe.

## 7.4 Entropy Cascade

With these definitions, the thermodynamic ordering of subsystems is unambiguous:

$$\left( \frac{dE}{dS} \right)_{\text{matter}} > \left( \frac{dE}{dS} \right)_{\text{BH}} > \left( \frac{dE}{dS} \right)_{\text{horizon}} \approx 0. \quad (48)$$

Entropy flows from ordinary matter into black holes, where it is greatly amplified into gravitational degrees of freedom, and is ultimately sequestered by the cosmological horizon at negligible energetic cost. This hierarchy underlies the nonequilibrium steady state described in this work.

# 8 Minimal Thermodynamic Structure: Cold Entropy Export and Free-Energy Balance

The thermodynamic content of the model is deliberately minimal and can be stated independently of any microscopic details. The exterior region is treated as an open system coupled to a cold entropy reservoir, identified with the cosmological horizon. The essential features are as follows.

## 8.1 Cold Entropy Export

Entropy is continuously removed from the exterior description as degrees of freedom become horizon-coupled and are traced out [47, 11, 64]. This entropy export occurs at effectively zero energetic cost:

$$\delta E_{\text{ext}} \approx 0, \quad \delta S_{\text{ext}} < 0. \quad (49)$$

The reservoir absorbs entropy without returning energy [41, 8], and its state is not altered by this exchange. No heat flow is associated with this process; only information and distinguishability are lost from the exterior algebra.

## 8.2 Fixed Radiative Temperature of the Exterior

The resolved radiative sector of the exterior system remains locked to a finite KMS temperature [34, 14],

$$T_{\text{rad}} \simeq 2.7 \text{ K}, \quad (50)$$

with respect to the physical time of finite observers [27]. This temperature characterizes the equilibrium state of the photon–neutrino bath [43] and other rapidly mixing radiative degrees of freedom, and does not govern the effective temperature of infrared geometric modes or horizon–coupled degrees of freedom. The horizon functions as an information–erasing boundary condition rather than as a thermal medium.

## 8.3 Free–Energy Increase

At fixed exterior temperature, the loss of entropy implies an increase in free energy [16, 53, 23],

$$F_{\text{ext}} = E_{\text{ext}} - T_{\text{ext}} S_{\text{ext}}, \quad (51)$$

so that

$$\delta F_{\text{ext}} = -T_{\text{ext}} \delta S_{\text{ext}} > 0. \quad (52)$$

Removing entropy at zero energetic cost therefore drives the exterior system out of equilibrium by raising its free energy. This increase does not correspond to heating or energy injection; rather, it represents an excess capacity for irreversible reorganization.

## 8.4 Chemical–Potential Imbalance

The raised free energy manifests as shifts in the chemical potentials associated with resolved degrees of freedom [20]. For any approximately conserved quantity  $N_i$ ,

$$\mu_i = \left( \frac{\partial F_{\text{ext}}}{\partial N_i} \right)_T, \quad (53)$$

entropy loss drives the system away from equilibrium values  $\mu_i = 0$ . In particular, chemical potentials associated with baryon number and with the number of resolved gravitational degrees of freedom (“tiles”) become nonzero when entropy is exported to the horizon.

## 8.5 Restoration of Equilibrium

At fixed temperature, equilibrium is restored by reducing free energy. The most efficient mechanism is the appearance of new low–energy, high–entropy degrees of freedom, which lowers  $F_{\text{ext}}$  without requiring external energy input. In the present framework this takes the form of:

- repopulation of resolved gravitational degrees of freedom (tile creation), and

- rebalancing of baryon number within the resolved exterior sector.

This process is not thermal pair production and does not require  $kT \sim m$ . Rather, it is the open-system response of a finite-temperature exterior whose entropy is continuously exported to a cold reservoir.

## 8.6 Summary

The thermodynamic cycle may therefore be summarized succinctly:

$$\begin{aligned} \text{cold entropy export} &\Rightarrow \text{free-energy increase} \Rightarrow & (54) \\ &\text{chemical-potential imbalance} \Rightarrow \text{repopulation of degrees of freedom.} \end{aligned}$$

All energetic content remains within the exterior system; only entropy is removed. The horizon functions as a zero-temperature entropy sink, while the exterior maintains a finite equilibrium temperature through continual reorganization.

## 9 Minimum Exterior Temperature and Entropy-Sink Selection

A recurring concern is whether the horizon-driven entropy export invoked in this framework can supply sufficient free energy to support (i) baryon repopulation of the exterior and (ii) the steady-state expansion implied by tile creation, without assuming a high exterior temperature. Here we show that the *minimum* effective temperature required is extraordinarily low,  $T_{\min} \sim 10^{-11}\text{--}10^{-10}$  K, and explain why photon heating to  $T_\gamma \simeq 2.7$  K remains thermodynamically natural despite this.

### 9.1 Free-energy balance and minimum temperature

For an open system exchanging entropy with a reservoir, the available free-energy production rate associated with entropy export is

$$\dot{F}_{\text{avail}} \simeq T_{\text{ext}} \dot{S}_{\text{out}}. \quad (55)$$

In a horizon-coupled steady state, black holes are removed from the exterior at a rate set by the Hubble expansion [5, 37, 22], so the entropy export per unit volume is

$$\dot{s}_{\text{out}} \simeq 3H s_{\text{BH}}, \quad (56)$$

where  $s_{\text{BH}}$  is the comoving black-hole entropy density.

To maintain a constant baryon mass density  $\rho_b$  against dilution, a conservative upper bound on the required volumetric power is

$$\dot{u}_b \simeq 3H \rho_b c^2. \quad (57)$$

Additional expansion-support channels (e.g. IR geometric modes) can be included via an effective energy density  $\rho_{\text{exp}}$ , giving

$$\dot{u}_{\text{req}} \simeq 3H(\rho_b + \rho_{\text{exp}})c^2. \quad (58)$$

Matching free-energy supply to demand,

$$T_{\text{ext}} \dot{s}_{\text{out}} = \dot{u}_{\text{req}}, \quad (59)$$

and noting that the common factor  $3H$  cancels, we obtain the minimum required exterior temperature

$$T_{\text{min}} \simeq \frac{(\rho_b + \rho_{\text{exp}})c^2}{s_{\text{BH}}}. \quad (60)$$

The black-hole entropy density may be written as

$$s_{\text{BH}} \simeq \rho_{\text{BH}} \frac{S_{\text{BH}}}{M}, \quad \frac{S_{\text{BH}}}{M} = \frac{4\pi k_B G}{\hbar c} M, \quad (61)$$

where  $\rho_{\text{BH}}$  is the black-hole mass density and  $M$  a characteristic black-hole mass. Substituting,

$$T_{\text{min}} \simeq \frac{\hbar c^3}{4\pi k_B G} \frac{\rho_b + \rho_{\text{exp}}}{\rho_{\text{BH}} M}. \quad (62)$$

Using representative present-day values [59] ( $\rho_b \simeq 0.05\rho_c$ ,  $\rho_{\text{BH}} \sim 4 \times 10^5 M_{\odot} \text{Mpc}^{-3}$ ,  $M \sim 10^8 M_{\odot}$ ), one finds

$$T_{\text{min}} \sim 10^{-11} \text{--} 10^{-10} \text{K}, \quad (63)$$

even if  $\rho_{\text{exp}}$  is taken comparable to the observed dark-energy density. Thus the entropy export associated with black-hole horizon crossing provides an ample free-energy budget at an extremely low effective exterior temperature.

## 9.2 Why photons are *not* the dominant entropy sink

The existence of a low  $T_{\text{min}}$  does not imply that the optimal use of available free energy is to “dump it into photons.” In a horizon-coupled nonequilibrium steady state, the relevant selection rule is not to maximize the instantaneous entropy increase of the *local* bath, but to maximize the *net entropy throughput* into the ultimate cold reservoir (the horizon), i.e. to maximize the entropy exported per unit free energy expended.

A convenient back-of-the-envelope measure of “entropy yield per joule” for a channel is the effective ratio

$$\frac{dS}{dE} \sim \frac{1}{T_{\text{eff}}}, \quad (64)$$

where  $T_{\text{eff}}$  is the temperature of the degrees of freedom that actually absorb the entropy in that channel.

**Photon bath.** For a thermal photon population [16] at temperature  $T_\gamma$ ,

$$\left. \frac{dS}{dE} \right|_\gamma = \frac{1}{T_\gamma}. \quad (65)$$

At  $T_\gamma \simeq 2.7$  K, this ratio is large compared to many *local, nonrelativistic* dissipation channels, which explains why the photon bath can act as a convenient *buffer* for modest excess free energy. However, its low entropy elasticity implies that even small entropy injection rapidly raises  $T_\gamma$ , rendering photon heating an inefficient channel for sustained entropy throughput compared to horizon-mediated or ultrasoft geometric sinks.

**Black holes and horizon-coupled storage.** However, the dominant entropy sink in the present architecture is the creation and export of *cold entropy* in black-hole/horizon degrees of freedom. For a Schwarzschild black hole [5, 37],

$$S_{\text{BH}} = \frac{4\pi k_B G}{\hbar c} M^2, \quad T_H = \frac{\hbar c^3}{8\pi k_B G} \frac{1}{M}, \quad (66)$$

so

$$\frac{dS_{\text{BH}}}{dE} = \frac{dS_{\text{BH}}}{d(Mc^2)} = \frac{1}{T_H}. \quad (67)$$

Because  $T_H$  is extraordinarily small for astrophysical black holes, the entropy yield per joule in the black-hole channel is correspondingly enormous [22]. For example, for  $M \sim 10^8 M_\odot$  one has  $T_H \sim 10^{-16}$  K, so

$$\frac{(dS/dE)_{\text{BH}}}{(dS/dE)_\gamma} = \frac{T_\gamma}{T_H} \sim 10^{15}-10^{16}. \quad (68)$$

Thus, per unit energy invested, increasing black-hole (and ultimately horizon) entropy is vastly more effective than heating a 2.7 K photon bath.

**Thermodynamic ordering of channels.** This establishes the intended hierarchy: available free energy is preferentially routed into processes that *build cold entropy that can be exported*, namely baryon repopulation and subsequent accretion/sequestration into black holes, followed by horizon depletion. Photon heating is not the optimal entropy sink; rather, the photon bath functions as an intermediary that (i) rapidly equilibrates and (ii) buffers small mismatches between injection and export. The steady-state value  $T_\gamma \simeq 2.7$  K should therefore be interpreted not as the temperature of the exterior reservoir, but as a dynamically selected “thermometer” temperature fixed by balance between entropy injection, angular mixing/thermalization, and infrared leakage into geometric and horizon-coupled modes.

## 10 Stationary Solutions and Cosmological Implications

The coupled continuity and entropy balance equations developed in Sections 4 and 6 determine the large-scale thermodynamic and kinematic state of an expanding universe whose mesoscopic structure is governed by a distinguished spectral scale  $\sigma$ . In this section we analyze the stationary solutions of this system and derive their physical implications for rotation curves, radiation fields, baryon equilibrium, and the linkage between cosmic expansion and horizon thermodynamics.

This section should be read as an analysis of scaling relations and structural consistency rather than as a closed-form solution of the full dynamical system. Numerical coefficients and detailed microphysics are deliberately suppressed in favor of identifying the unique infrared scale governing stationary cosmological behavior.

### 10.1 The stationary system

Combining the baryon continuity equation

$$\partial_t n_B + 3Hn_B = -\Phi_B + \Gamma_B,$$

with the steady-state entropy balance (coarse-grained over a comoving patch),

$$3H S_{\text{ext}} = -\dot{S}_{\text{cos}} + \dot{S}_{\text{IR}},$$

we obtain the stationary-state system

$$3Hn_B = -\Phi_B + \Gamma_B, \quad (69)$$

$$\dot{S}_{\text{IR}} = 3H S_{\text{ext}} + \dot{S}_{\text{cos}}. \quad (70)$$

The first equation fixes the baryon number density once  $H$ ,  $\Phi_B$ , and  $\Gamma_B$  are specified. The second determines the expansion rate  $H$  itself through a competition between accretion-driven horizon entropy production and IR entropy removal by expansion.

Because both  $\Phi_B$  and  $\Gamma_B$  depend on horizon-coupled acceptance scales and effective chemical potentials, and because these quantities scale as  $\sigma$ , the entire system is governed by the single mesoscopic scale  $\sigma$ .

### 10.2 Determination of the expansion rate

The entropy fluxes admit the schematic scalings [53, 23]

$$\dot{S}_{\text{hor}} \sim +\frac{F_{\text{proc}}}{T_{\text{acc}}}, \quad \dot{S}_{\text{IR}} \sim -\kappa H,$$

where  $F_{\text{proc}}$  is the net free-energy flux processed through collapse, accretion, and horizon-sequestering channels (with the radiative bath acting as a fast thermalizer but not the dominant reservoir), and  $T_{\text{acc}}$  is the effective entropy–acceptance temperature of the horizon-coupled sink [41, 31].

Setting  $\dot{S}_{\text{hor}} + \dot{S}_{\text{IR}} = 0$  yields

$$H \sim \frac{F_{\text{proc}}}{\kappa T_{\text{acc}}}.$$

In the present framework the acceptance scale is set by the mesoscopic frequency  $\sigma$  (equivalently  $k_B T_{\text{acc}} \sim \hbar \sigma$  in units where this identification is meaningful), giving the scaling relation

$$H \sim \sigma,$$

consistent with the mesoscopic frequency inferred independently from galactic kinematics [44].

### 10.3 Baryon equilibrium

Given  $H \sim \sigma$ , the baryon continuity equation in steady state becomes

$$3\sigma n_B = -\Phi_B + \Gamma_B.$$

The horizon-induced creation rate satisfies  $\Gamma_B \propto \sigma$ , while the flux  $\Phi_B$  is constrained by the black hole population and the long-term behavior of the radiation field. Thus the equilibrium baryon density satisfies

$$n_B \sim \frac{\Phi_B}{\sigma} + O(1),$$

consistent with the observed near-constancy of cosmic baryon density without appeal to early-universe baryogenesis [50].

### 10.4 Stationary radiation density

The radiation energy density in the exterior is fixed by thermodynamic balance, not by direct thermal contact with the horizon. Entropy export across the horizon continually injects free energy into the exterior subsystem, which must be absorbed by available degrees of freedom. Because the photon bath thermalizes rapidly and has a large phase space [27, 14], it acts as an efficient sink for a small fraction of this free energy, maintaining a stationary blackbody distribution.

Dimensional analysis then implies that the stationary radiation density scales [16] with the characteristic infrared rate  $\sigma$ ,

$$u_\gamma \sim \sigma^4,$$

up to numerical factors set by the efficiency of free-energy transfer. With the empirical identification [54]  $\sigma \approx H_0$ , this yields a radiation density of the observed order of magnitude.

Stability of the stationary state does not rely on redshift loss alone. If the radiation density rises above equilibrium, excess energy is diverted into ultrasoft geometric modes [13] and entropy-export channels. If it falls below equilibrium, free energy released by ongoing horizon-coupled processes and nuclear activity in the exterior reheats the photon bath.

Re-equilibration of the photon bath around its stationary temperature carries a negligible energetic cost; the only substantive requirement is that the exterior supply a steady, low-level radiative output sufficient to balance the slow leakage of radiation into ultrasoft geometric modes.

The observed CMB temperature therefore reflects a dynamic balance between free-energy injection, rapid thermalization, and slow leakage into infrared geometric degrees of freedom.

## 10.5 Rotation curves and macroscopic geometry

Section 2 established that the large-radius rotation curve satisfies

$$v(r) = \sigma r \pm \sqrt{\sigma^2 r^2 + v_N^2(r)}.$$

For  $r$  sufficiently large, the Newtonian contribution becomes subdominant and the velocity approaches the linear asymptote

$$v(r) \sim 2\sigma r.$$

Because  $\sigma = H_0$ , this implies a universal outer velocity profile directly tied to cosmic expansion. The success of this relation in describing flattened and rising rotation curves [55, 44] across a wide range of galactic systems supports the underlying mesoscopic geometric picture.

(Deviations from this asymptote are expected in systems with strong environmental coupling or incomplete IR equilibration.)

## 10.6 Global consistency and observational tests

The horizon-coupled mesoscopic framework yields a cosmology in which [50, 17]:

- the Hubble rate arises dynamically from thermodynamic balance,
- the cosmic radiation density is set by thermodynamic balance in a horizon-coupled open system,
- the baryon density is maintained by horizon-induced creation,
- galactic rotation curves reflect the same spectral scale  $\sigma$ ,
- and all of these quantities remain stationary without a hot big bang [50].

These predictions can be tested through:

1. detailed comparison of rotation curve slopes with the inferred Hubble parameter in low-redshift systems,
2. measurements of the CMB energy density independent of big bang assumptions,
3. examination of baryon deficits and black hole mass densities as probes of  $\Phi_B$ ,
4. and potential detection of horizon-driven neutrino or photon excitations corresponding to  $\Gamma_B$ .

The unified appearance of  $\sigma$  across these phenomena suggests that the mesoscopic structure of spacetime—approximated here by a Heisenberg or general Carnot tangent model—provides the missing link between local galactic dynamics and global cosmological equilibrium.

## 11 Photon Confinement, Carnot Mixing, and Blackbody Equilibrium

A central feature of the mesoscopic framework developed in this work is that, in a Carnot–Carathéodory geometry [46], the propagation and mixing of photon degrees of freedom give rise to an *effectively cavity-like* statistical behavior on cosmological scales. In this setting, the cosmic radiation field is naturally described as a stationary photon bath characterized by a KMS distribution at late times.

The role of cosmological expansion in this framework is not to establish equilibrium through local interactions, but to provide the large-scale kinematic conditions under which horizon coupling and mesoscopic mixing lead to a stable blackbody spectrum. This section formalizes the physical basis for this effective confinement, outlines the mixing properties implied by the sub–Laplacian, and shows how the observed cosmic blackbody spectrum [29] can be understood within an open–system, steady–state description of the cosmological exterior.

### 11.1 Effective confinement in Carnot–Carathéodory geometry

A distinctive feature of Carnot–Carathéodory (CC) geometries such as the Heisenberg group is that null geodesics are governed by the horizontal distribution rather than by the full tangent bundle. In the Heisenberg case, the Hamiltonian flow is generated by the horizontal momenta  $(P, \bar{P})$  with the central coordinate  $s$  playing the role of a gauge parameter. The resulting geodesics are not straight rays but curved horizontal trajectories analogous to cyclotron orbits [30]: they have a characteristic curvature set by the mesoscopic scale  $\sigma$  and possess a finite geometric “return time” even in the absence of any scattering.

Thus photons do not stream radially to infinity along Euclidean null lines. Instead, their horizontal projections undergo recurrent motion, revisiting neighborhoods of their initial position after a time of order  $\sigma^{-1}$ . Motion in the central (“vertical”) direction corresponds to the noncommutative phase of the Heisenberg group and carries no physical displacement once one projects onto the underlying abelian quotient. The physically relevant dynamics is therefore entirely horizontal, and it is this horizontal cyclotron-like structure that produces effective confinement.

Because the CC geodesic flow forces recurrence, the mesoscopic medium behaves as a *photon cavity* [57] even in the absence of appreciable baryonic opacity. Scattering, absorption, and re-emission merely enhance the mixing that the geometry already enforces. The photon distribution function  $f(t, x, \omega)$  therefore evolves primarily under the horizontal Heisenberg generators,

$$\partial_t f + X_1 f + X_2 f = C[f],$$

with  $C[f]$  encoding subdominant interactions with the baryonic medium. The geometric confinement supplied by the CC structure ensures that radiation remains trapped and repeatedly reprocessed on timescales long compared to  $H^{-1}$ , permitting the establishment of an approximately Planckian stationary state, with relaxation governed by the geometric mixing scale  $\sigma$ .

## 11.2 Sub-Laplacian mixing and ergodicity

The geometric mixing mechanism arises from the sub-Laplacian [30, 67]

$$\Delta_{\text{sub}} = X_1^2 + X_2^2,$$

whose heat kernel is well known to satisfy strong regularity, rapid decay away from characteristic directions, and a spectral gap above the ground state [30, 67]. These properties imply that solutions to the kinetic equation are driven toward equilibrium on timescales much shorter than cosmological expansion.

Although angular mixing is not fully isotropic, the sub-Laplacian provides sufficient ergodicity for the photon bath to become well-mixed. Together with continuous emission and absorption in the radiating medium, the radiation field therefore approaches a distribution function of the form [57]

$$f(\omega) = \frac{1}{\exp(\omega/T_{\text{rad}}) - 1},$$

independent of spatial position and angular direction up to mesoscopic corrections, where  $T_{\text{rad}}$  is the effective temperature of the steady-state radiating medium.

## 11.3 A plausible origin of the CMB angular power spectrum from horizon mixing

The key empirical challenge for any steady-state reinterpretation of the CMB is not the existence of a Planck spectrum (which follows naturally from cavity



Figure 2: Two typical geodesics on a sub-Riemannian  $SU(2)$ , stereographically projected onto  $\mathbb{R}^3$ . The mixing occurs on Clifford tori, over smaller angular regions relative to the Hopf fibration than Euclidean mixing. See Appendix A.1. Efficiency of the angular mixing, as well as the smaller angular scales over which it occurs, is thus to be expected given the ergodicity of the geodesic flow on Clifford tori.

mixing and redshift balance), but the detailed *angular* statistics encoded in the power spectrum  $C_\ell$ . Here we outline a conservative mechanism by which a horizon-coupled Carnot–Carathéodory (CC) geometry can generate a nearly isotropic, approximately scale-invariant low- $\ell$  spectrum with a high- $\ell$  damping tail, and can admit peak-like structure without invoking a primordial acoustic epoch. We emphasize that this subsection is not intended as a derivation of the observed acoustic peak structure, but as a demonstration that horizon-coupled Carnot geometry naturally supports a stationary angular power spectrum with the correct qualitative features.

**Angular mixing as diffusion on the horizon.** On large scales the CC geometry induces rapid angular “stirring” of null directions: photon trajectories do not propagate as straight Euclidean rays but undergo recurrent horizontal motion and continual deflection by horizon-scale geometric fluctuations. Coarse-grained on times  $\Delta t \gg \sigma^{-1}$ , the net effect on the observed sky map can be modeled as *angular diffusion* generated by an effective mixing operator  $\mathcal{L}_\Omega$  acting on functions of direction  $\Omega \in S^2$ . Denoting the fractional temperature anisotropy by  $\Theta(\Omega, t) = \delta T(\Omega, t)/T$ , we write the simplest effective equation

$$\partial_t \Theta(\Omega, t) = -\nu \mathcal{L}_\Omega \Theta(\Omega, t) - \gamma \Theta(\Omega, t) + \xi(\Omega, t), \quad (71)$$

where  $\nu \sim \sigma$  sets the mixing rate,  $\gamma$  represents slow damping (e.g. finite optical depth, redshift smoothing, or leakage into other degrees of freedom), and  $\xi$  is a stationary forcing term representing continual inhomogeneous emissivity and horizon-adjacent geometric fluctuations. This is the angular analogue of an Ornstein–Uhlenbeck process [75]: diffusion drives isotropy, forcing sustains fluctuations, and a stationary  $C_\ell$  results.

**Why this produces a  $C_\ell$  at all.** If  $\mathcal{L}_\Omega$  is approximately rotationally symmetric after coarse-graining, its eigenfunctions are (to good approximation) the spherical harmonics  $Y_{\ell m}$  with eigenvalues  $\lambda_\ell \simeq \ell(\ell + 1)$ . Then each harmonic coefficient  $\Theta_{\ell m}(t)$  obeys

$$\dot{\Theta}_{\ell m} = -(\nu \lambda_\ell + \gamma) \Theta_{\ell m} + \xi_{\ell m}(t).$$

For stationary forcing with variance  $\langle |\xi_{\ell m}|^2 \rangle = P_\ell$ , the steady-state variance is

$$C_\ell \equiv \frac{1}{2\ell+1} \sum_m \langle |\Theta_{\ell m}|^2 \rangle \propto \frac{P_\ell}{\nu \ell(\ell+1) + \gamma}. \quad (72)$$

Equation (72) immediately yields two robust qualitative features: (i) diffusion generically produces a high- $\ell$  damping tail because the decay rate grows like  $\ell(\ell+1)$ , and (ii) the low- $\ell$  slope is controlled by the large-scale spectrum of the forcing  $P_\ell$  rather than by initial conditions.

**Where “peaks” can come from in a steady state.** In this picture the analog of the usual “transfer function” is the frequency- and scale-dependence of the forcing and damping, not a one-time acoustic episode. Peak-like structure in  $C_\ell$  can arise if either:

1. the forcing has a finite coherence angle (equivalently, a preferred correlation length on the horizon), producing a band-limited  $P_\ell$ ; or
2.  $\mathcal{L}_\Omega$  is not exactly the Laplacian but a CC-induced *sub*-Laplacian whose spectrum is close to  $\ell(\ell+1)$  but with a mild splitting or dispersion at intermediate  $\ell$  (as is typical of anisotropic diffusion operators).

Both mechanisms are natural in a horizon-coupled setting: the exterior sets a temperature and a characteristic mixing time  $\sigma^{-1}$ , while the CC geometry supplies a preferred mesoscopic scale that can act as a coherence length. Importantly, no fine tuning is required to obtain the gross features: angular diffusion automatically yields isotropy and a damping tail, while stationary forcing fixes the overall amplitude.

**What is and is not claimed.** We do not claim here to reproduce the full precision Planck spectrum from first principles. The claim is more modest: once the horizon-coupled CC geometry is treated as generating an effective angular diffusion operator on the sky, a stationary  $C_\ell$  with the correct qualitative structure follows naturally. A complete quantitative match reduces to determining the effective operator  $\mathcal{L}_\Omega$  and the forcing spectrum  $P_\ell$  from the underlying IR geometric sector, which is a tractable but separate technical problem.

#### 11.4 Photon Heating, Geometric Thermalization, and the Absence of Radiative Runaway

In the horizon-coupled steady state developed in this work, the cosmic photon bath is neither a relic of an early hot phase nor a passive background subject only to adiabatic redshift. Rather, it is a dynamically maintained subsystem, continuously heated by the absorption of free energy generated by irreversible entropy export into horizons, and continuously cooled through its coupling to the expanding geometric infrared sector.

**Continuous photon heating.** When matter collapses and accretes across a horizon, a large amount of *cold entropy* is removed from the exterior region. This raises the free energy of the remaining exterior degrees of freedom, which must be dissipated through available channels. Ordinary radiative processes in baryonic matter (stellar emission, bremsstrahlung, line radiation, and reprocessing by dust and gas) provide one such channel, continuously injecting energy into the photon field [57]. Photon heating is therefore ongoing and unavoidable in a stationary horizon-coupled universe: it is the radiative expression of free energy absorption in the exterior sector.

**Why photons do not dominate entropy throughput.** Despite being energetically inexpensive, photons are *poor entropy sinks* in the present framework. The dominant entropy-recapture channel is instead carried by long-wavelength geometric and curvature modes [13] associated with the infrared sector of the Carnot–Carathéodory (CC) tangent geometry. These modes can absorb large entropy per unit energy and are unconstrained by baryonic or electromagnetic quantum numbers. From a thermodynamic standpoint, exporting entropy into IR geometric degrees of freedom is therefore far more efficient than dumping it into a bath of increasingly cold photons. As a result, the photon field remains a secondary, slaved subsystem: it is heated by free energy absorption but does not control the global entropy balance.

## 11.5 Structural relation between entropy–acceptance and KMS temperatures

The effectively zero entropy–acceptance temperature associated with the cosmological horizon should not be confused with the  $T \simeq 2.7\text{ K}$  KMS temperature characterizing the exterior radiation field. These two temperatures are linked by the open-system structure of the theory, but not by their magnitudes.

Both quantities arise as thermodynamic derivatives of the same entropy balance, taken with respect to different variables. The exterior KMS temperature  $T_{\text{ext}}$  characterizes the stationary state of exterior observables with respect to the physical time flow of finite observers and governs entropy processing and particle production in the exterior medium. By contrast, the entropy–acceptance temperature associated with the horizon reflects the energetic cost of absorbing entropy into inaccessible degrees of freedom and is effectively zero. It does not characterize a thermal bath and does not regulate exterior dynamics.

The fact that these two temperatures differ parametrically is not a tension but a structural feature of an open, irreversible cosmological system. The photon bath records the value of  $T_{\text{ext}}$  spectrally as a passive buffer, while the horizon functions solely as an entropy sink. No phenomenological relation between their magnitudes is implied or required.

**Compatibility with steady-state energy balance.** Although the photon temperature is geometrically admitted, the existence of a stationary state re-

quires consistency with the coarse-grained energy balance equation

$$\dot{\rho}_\gamma + 4H\rho_\gamma = \dot{\rho}_\gamma^{(\text{net})}, \quad (73)$$

where  $\dot{\rho}_\gamma^{(\text{net})}$  denotes the net radiative heating rate from baryonic processes. In equilibrium, this reduces to

$$4H\rho_\gamma = \dot{\rho}_\gamma^{(\text{net})}, \quad (74)$$

which should be read not as a temperature-setting relation but as a *compatibility condition*: only those steady states in which baryonic emissivity is sufficient to maintain the geometrically imposed photon energy density are dynamically allowed.<sup>3</sup>

**Absence of cold-photon runaway.** At first sight, the photon field might appear free to absorb arbitrarily large entropy by producing vast numbers of ultra-soft photons. In the present framework, however, such a runaway is thermodynamically disfavored. Because IR geometric modes dominate entropy transport at far lower free-energy cost [53, 23], the system preferentially routes entropy into the geometric sector rather than into extreme photon occupation numbers. The photon bath therefore relaxes toward a KMS form admitted by the CC mixing dynamics, with an effective temperature  $T_{\text{ext}}$  determined by the steady-state routing of free energy among available channels; its total energy density is then slaved to the expansion rate, while excess entropy is exported through geometric degrees of freedom. A microscopic comparison of the relative entropic efficiencies of cold-photon production and IR geometric excitation lies beyond the scope of this mesoscopic treatment, but the hierarchy of channels suffices to exclude radiative overproduction in the steady state.

In this sense, the cosmic radiation field behaves as a blackbody in an effectively confining CC medium [29], whose near-KMS form is stabilized by rapid mesoscopic mixing and whose energy density is maintained by continuous free-energy absorption in the exterior.

---

<sup>3</sup>As a purely heuristic consistency check, one may combine the observed Hubble rate with standard FRW-based estimates of the present-day bolometric luminosity density of galaxies [2, 36] in the steady-state relation  $4H\rho_\gamma = \dot{\rho}_\gamma^{(\text{net})}$ . Doing so yields an equilibrium photon temperature in the kelvin range, typically of order  $T_\gamma \sim 1$  K, rather than picokelvin or gigakelvin scales. This estimate should not be interpreted as a prediction of the photon temperature, which in the present framework is fixed by the geometric KMS periodicity of the stationary mesoscopic state, as enforced by the CC modular flow and its compatibility with the horizon-imposed causal structure. Its sole purpose is to demonstrate that known astrophysical heating rates are not grossly inconsistent with maintaining a photon bath at a few kelvin. Because both the luminosity density and the comoving volume element entering this estimate are inferred under an abelian FRW prior, while the present model replaces this by a non-abelian Carnot–Carathéodory geometry on Hubble scales, order-unity deviations are neither unexpected nor significant.

## 12 Entropy Throughput and the Origin of Apparent Expansion

The late-time cosmological exterior in the present framework is not a closed thermodynamic system but an open nonequilibrium steady state (NESS) [15, 63]. Matter, radiation, and geometric excitations continually enter and exit the resolved exterior description through irreversible coupling to black-hole interiors and horizon-adjacent infrared (IR) degrees of freedom. The purpose of this section is to show how this steady-state entropy throughput gives rise to phenomena normally attributed to cosmological expansion, while the local Carnot–Carathéodory (CC) tangent geometry remains stationary as a mesoscopic constitutive law.

### 12.1 The exterior as an open thermodynamic system

The cosmological exterior is defined operationally as the subsystem whose degrees of freedom remain resolvable by finite observers. Black-hole interiors and horizon-coupled or ultrasoft IR modes are excluded: they are irreversibly traced over in the reduced description [15]. As a result, the exterior continuously exchanges entropy and degrees of freedom with its environment and cannot be treated as a closed system.

The essential elements of this open-system architecture are [15, 63]:

1. the cosmological horizon, which acts as an effectively infinite entropy sink through irreversible tracing of inaccessible degrees of freedom;
2. black holes, which efficiently destroy correlations and organized structure during collapse and accretion;
3. a working medium consisting of baryons, photons, and long-wavelength geometric excitations governed locally by the CC tangent law; and
4. compensating repopulation of the working medium through horizon-coupled processes.

No finite hot reservoir is required. Entropy production is driven by the irreversible destruction of structure, while entropy removal is enforced by the horizon’s unbounded capacity [13, 76].

### 12.2 Free energy stored in resolved degrees of freedom

The thermodynamically relevant quantity in this framework is not conserved matter–energy but free energy stored in distinguishable, resolvable degrees of freedom. Let  $\rho$  denote the coarse-grained exterior state and let  $\rho_*$  be the stationary reference state selected by the horizon-coupled IR sector, assumed to be KMS with respect to the emergent mesoscopic time flow. The available free energy is

$$F_{\text{dof}}(\rho) \equiv F(\rho) - F(\rho_*) = T_{\text{ext}} S(\rho \parallel \rho_*), \quad (75)$$

where  $S(\rho\|\rho_*)$  is the relative entropy [68, 24]. This quantity measures free energy stored in correlations, gradients, and organized structure rather [68] than in rest mass. Here  $T_{\text{ext}}$  is the entropy–acceptance temperature associated with the resolved exterior degrees of freedom. It is not the Hawking temperature of any horizon, nor the temperature of the photon bath, but an effective intensive parameter governing the conversion of entropy removal into available free energy in the reduced description.

Although black holes are radiatively cold in the Hawking sense, they are thermodynamically effective entropy generators because collapse and accretion irreversibly convert structured exterior degrees of freedom into black–hole interior entropy. Since black–hole interiors are excluded from the exterior algebra, this entropy is traced out of the reduced description and constitutes an irreversible entropy flux out of the exterior system.

### 12.3 Steady-state entropy balance

The coarse-grained entropy of the exterior obeys [63, 23]

$$\dot{S}_{\text{ext}} = \sigma - J_S, \quad (76)$$

where  $\sigma \geq 0$  is the entropy production rate and  $J_S$  is the entropy flux into the traced-out sector. In the late-time steady state,

$$\langle \dot{S}_{\text{ext}} \rangle = 0 \quad \Rightarrow \quad \langle \sigma \rangle = \langle J_S \rangle. \quad (77)$$

Entropy does not accumulate in the exterior [42]. Instead, free energy is continually generated through structure formation, destroyed by collapse and accretion, and exported from the exterior description through irreversible tracing of black–hole interior and horizon–coupled degrees of freedom at the same average rate.

### 12.4 Stationary CC geometry and timescale separation

The CC tangent geometry and its associated mixing operator  $\mathcal{L}_{\text{CC}}$  govern local propagation, causal structure, and spectral mixing. This geometry is not a dynamical state variable. It is the rapidly re-attained fixed point of local equilibration with the horizon-coupled IR sector [78].

On timescales [78]  $\tau_{\text{mix}} \ll H^{-1}$ , local observables relax back to this stationary CC structure. At the same time, the global exterior state evolves slowly because resolvable degrees of freedom are continually removed from the description. The coexistence of fast local equilibration and slow global drift is the defining signature of the nonequilibrium steady state realized here.

### 12.5 Resolved degrees of freedom, “tiles,” and apparent expansion

In the present framework, the fundamental bookkeeping object is not matter or energy but the number of resolved degrees–of–freedom units (“tiles”) comprising

ing the exterior description. Each tile carries a finite information and entropy capacity. Tiles are irreversibly removed from the exterior when their degrees of freedom become entangled with horizon-coupled modes or black-hole interior states and are therefore traced over in the reduced description [15, 76].

In a nonequilibrium steady state, the loss of tiles must be exactly balanced by the creation of new tiles in the exterior sector. This effective conservation of tile number is not a dynamical law but a consistency requirement of the steady-state coarse-graining. It forces the resolved domain to grow so that finite densities of matter, radiation, and entropy can be maintained.

This growth produces increasing mean separations, cosmological redshift, and dilution relations without invoking any microscopic pressure, force, or local metric stretching. Apparent expansion is therefore the macroscopic manifestation of tile creation required to maintain a stationary exterior description under continuous entropy sequestration.

Equivalently, “expansion” in this framework is not postulated as a local geometric deformation but emerges as a bookkeeping drift induced by time-dependent coarse-graining [78, 42]. At each epoch  $t$ , finite observers access only an exterior algebra of observables,

$$\mathcal{A}_{\text{ext}}(t) = \text{Tr}_{\text{hor+IR}}(\mathcal{A}_{\text{full}}),$$

obtained by tracing over horizon-interior and ultrasoft infrared degrees of freedom. As the horizon continually partitions the quantum state, the effective observable algebra and its resolved phase-space volume drift in time. Stationarity of physical densities in the reduced theory therefore requires a compensating rescaling of the effective spatial measure, which appears observationally as an expansion law with rate  $H$ .

The tile picture is a mnemonic for this behavior: the number of resolved degrees-of-freedom units defining the exterior description remains fixed by the coarse-graining scheme, while their effective physical support grows as modes are traced out and replenished.

## 12.6 Free–Energy Throughput and Entropy Export: Quantitative Closure

In this subsection we collect several independent order-of-magnitude estimates for the free–energy fluxes required to maintain a stationary late–time exterior, and compare them with the free energy made available by entropy export into the traced–out sector (black–hole interiors and horizon–coupled IR modes).. The purpose is not to derive detailed microphysics, but to establish that the steady–state bookkeeping closes at the observed scales.

Throughout, all quantities are evaluated per unit *physical* volume, and we take  $H \simeq H_0$ .

**Photon bath stationarity.** A stationary photon bath at temperature  $T_\gamma$  in an expanding background requires continuous replenishment to offset redshift

and dilution. The radiation energy density obeys

$$\dot{\rho}_\gamma + 4H\rho_\gamma = \dot{\rho}_{\text{inj}}.$$

Imposing  $\dot{\rho}_\gamma = 0$  gives the required injection rate

$$\dot{\rho}_{\text{inj}}^{(\gamma)} = 4H\rho_\gamma. \quad (78)$$

For a blackbody bath at  $T_\gamma \simeq 2.7 \text{ K}$ ,  $\rho_\gamma = a_{\text{rad}} T_\gamma^4 \simeq 4 \times 10^{-14} \text{ J m}^{-3}$ , so

$$\dot{\rho}_{\text{inj}}^{(\gamma)} \sim 4 \times 10^{-31} \text{ W m}^{-3}.$$

This is an extremely small free-energy requirement.

**Stationarity of baryon density.** Maintaining a constant baryon mass density  $\rho_b$  against expansion requires

$$\dot{\rho}_b + 3H\rho_b = Q_b, \quad \Rightarrow \quad \dot{\rho}_{\text{inj}}^{(b)} = 3H\rho_b.$$

With  $\rho_b \simeq 4 \times 10^{-11} \text{ J m}^{-3}$ ,

$$\dot{\rho}_{\text{inj}}^{(b)} \sim 2 \times 10^{-28} \text{ W m}^{-3}. \quad (79)$$

This term dominates over the photon requirement by several orders of magnitude, but remains small on absolute scales.

**Free-energy scale associated with expansion.** If the expansion is interpreted as the continuous creation of long-wavelength gravitational degrees of freedom, the relevant free-energy scale admits a convenient comparison with the dark-energy density  $\rho_\Lambda$ .<sup>4</sup> For a constant  $\rho_\Lambda$ , the energy contained in a physical volume grows as  $E_\Lambda = \rho_\Lambda V$ , yielding a power density

$$P_{\text{exp}} = \frac{\dot{E}_\Lambda}{V} = 3H\rho_\Lambda \sim 3 \times 10^{-27} \text{ W m}^{-3}. \quad (80)$$

Here  $\rho_\Lambda$  is used purely as an effective parameter encoding the observational profile of expansion, not as a fundamental vacuum energy density. This scale exceeds the combined photon and baryon stationarity requirements by roughly two orders of magnitude, leaving substantial free-energy throughput available.

**Entropy export from black-hole accretion (black holes traced out).** In the present bookkeeping, black holes are not part of the exterior algebra: their interior degrees of freedom are irreversibly traced out. Entropy generated by black-hole growth therefore constitutes an entropy flux out of the exterior system.

---

<sup>4</sup>Our ansatz here is that required throughput scale can be compared after the fact with the effective dark-energy density inferred in  $\Lambda$ CDM fits

For a Schwarzschild black hole of mass  $M$ , the first law gives

$$dE = T_{\text{BH}}(M) dS_{\text{BH}}, \quad T_{\text{BH}}(M) = \frac{\hbar c^3}{8\pi G k_B M}.$$

If exterior energy  $\dot{E}_{\text{in}} = \dot{M}_{\text{in}} c^2$  crosses the horizon, the associated entropy production rate is

$$\dot{S}_{\text{BH}} = \frac{\dot{E}_{\text{in}}}{T_{\text{BH}}(M)}.$$

Since black holes are excluded from the exterior algebra, this entropy is traced out of the reduced description. Per unit physical volume, the entropy export rate is therefore

$$\dot{s}_{\text{out}}^{(\text{BH})} = \int dM n_{\text{BH}}(M) \frac{\dot{M}_{\text{in}}(M) c^2}{T_{\text{BH}}(M)} \equiv \frac{\dot{u}_{\text{in}}^{(\text{tot})}}{T_{\text{BH}}^{\text{eff}}}, \quad (81)$$

where  $\dot{u}_{\text{in}}^{(\text{tot})}$  is the total energy flux into black-hole mass per unit volume and  $T_{\text{BH}}^{\text{eff}}$  is the accretion-weighted effective Hawking temperature.

**Free energy produced by cold entropy export.** If this entropy is traced out into a much colder reservoir (the cosmological horizon), then the maximum free-energy production rate in the exterior is

$$P_{\text{free}}^{(\text{BH})} \approx (T_{\text{ext}} - T_{\text{sink}}) \dot{s}_{\text{out}}^{(\text{BH})} \approx T_{\text{ext}} \frac{\dot{u}_{\text{in}}^{(\text{tot})}}{T_{\text{BH}}^{\text{eff}}}, \quad (82)$$

where  $T_{\text{ext}}$  is the entropy-acceptance temperature of the exterior degrees of freedom and  $T_{\text{sink}} \ll T_{\text{ext}}$  has been assumed.

Using the observed late-time cosmic black-hole accretion rate density,  $\dot{u}_{\text{in}}^{(\text{tot})} \sim 10^{-33} - 10^{-34} \text{ W m}^{-3}$ , and accretion dominated by supermassive black holes with  $T_{\text{BH}}^{\text{eff}} \sim 10^{-17} - 10^{-15} \text{ K}$ , one finds

$$P_{\text{free}}^{(\text{BH})} \sim \left( \frac{T_{\text{ext}}}{10^{-9} \text{ K}} \right) \times 10^{-27} \text{ W m}^{-3}.$$

**Closure.** Taken together, these estimates show that:

- the free energy required to maintain a stationary photon bath and baryon density is extremely small;
- the expansion naturally provides a free-energy throughput at the  $3H\rho_{\Lambda}$  scale;
- irreversible entropy export through black-hole growth (with black-hole interiors excluded from the exterior algebra) provides an entropy sink capable of supporting the required free-energy throughput at the observed expansion scale.

This quantitative coincidence supports the interpretation of the late-time Universe as a horizon-coupled nonequilibrium steady state.

## 12.7 Sanity check on the entropy–export engine: required $T_{\text{ext}}$

We now perform a quantitative sanity check on the entropy–export mechanism, under the explicit assumption that black holes are *not* part of the exterior algebra. Black–hole interiors are traced out, and the growth of black–hole entropy therefore constitutes an irreversible entropy flux *out* of the exterior system. The purpose of this subsection is to determine the range of exterior entropy–acceptance temperatures  $T_{\text{ext}}$  required for this entropy export to support the free–energy throughput associated with baryon creation and effective “tile creation,” as inferred phenomenologically from the observed expansion scale.

**Entropy export from black–hole accretion.** For a Schwarzschild black hole of mass  $M$ , the first law gives

$$dE = T_{\text{BH}}(M) dS_{\text{BH}}, \quad T_{\text{BH}}(M) = \frac{\hbar c^3}{8\pi G k_B M}. \quad (83)$$

If exterior energy  $\dot{E}_{\text{in}} = \dot{M}_{\text{in}} c^2$  crosses the horizon, the associated entropy production rate is

$$\dot{S}_{\text{BH}} = \frac{\dot{E}_{\text{in}}}{T_{\text{BH}}(M)}. \quad (84)$$

Since black holes are excluded from the exterior algebra, this entropy is counted as an entropy flux into the traced–out sector. Per unit physical volume, the total entropy export rate is therefore

$$\dot{s}_{\text{out}}^{(\text{BH})} = \int dM n_{\text{BH}}(M) \frac{\dot{M}_{\text{in}}(M) c^2}{T_{\text{BH}}(M)} \equiv \frac{\dot{u}_{\text{in}}^{(\text{tot})}}{T_{\text{BH}}^{\text{eff}}}, \quad (85)$$

where  $\dot{u}_{\text{in}}^{(\text{tot})}$  is the total energy flux into black–hole mass per unit volume, and  $T_{\text{BH}}^{\text{eff}}$  denotes the accretion–weighted harmonic mean Hawking temperature.

**Free energy liberated by entropy removal.** Entropy export into an effectively zero–temperature sink produces available free energy in the exterior bookkeeping at the rate

$$\dot{f}_{\text{avail}}^{(\text{BH})} = (T_{\text{ext}} - T_{\text{sink}}) \dot{s}_{\text{out}}^{(\text{BH})} \approx T_{\text{ext}} \dot{s}_{\text{out}}^{(\text{BH})} = T_{\text{ext}} \frac{\dot{u}_{\text{in}}^{(\text{tot})}}{T_{\text{BH}}^{\text{eff}}}, \quad (86)$$

where  $T_{\text{ext}}$  is the entropy–acceptance temperature of the resolved exterior degrees of freedom and  $T_{\text{sink}} \simeq 0$  has been assumed.

This free–energy production is a statement about the coarse–grained availability of work in the reduced description; it does not represent a radiative luminosity injected into the exterior.

**Observed accretion scale.** At late times, the cosmic mean black-hole accretion rate density is observationally inferred to be

$$\dot{\rho}_{\text{BH}}(z \simeq 0) \sim (3\text{--}6) \times 10^{-6} M_{\odot} \text{ yr}^{-1} \text{ Mpc}^{-3}, \quad (87)$$

corresponding to an energy deposition rate into black-hole mass of

$$\dot{u}_{\text{in}}^{(\text{tot})} \sim (5\text{--}10) \times 10^{-34} \text{ W m}^{-3}. \quad (88)$$

Black-hole growth at late times is dominated by supermassive black holes with typical masses in the range  $M \sim 10^7\text{--}10^9 M_{\odot}$ , for which the Hawking temperature lies in the interval

$$T_{\text{BH}}^{\text{eff}} \sim 10^{-17}\text{--}10^{-15} \text{ K}. \quad (89)$$

**Required free-energy throughput.** The phenomenological free-energy scale associated with “tile creation” may be estimated from the effective dark-energy density inferred in  $\Lambda$ CDM fits,

$$P_{\text{tile}} \equiv 3H_0\rho_{\Lambda}c^2 \sim (3\text{--}4) \times 10^{-27} \text{ W m}^{-3}. \quad (90)$$

Maintaining a stationary baryon density against dilution contributes a subleading requirement,

$$P_{\text{baryon}} \sim 3H_0\rho_b c^2 \sim \text{few} \times 10^{-28} \text{ W m}^{-3}, \quad (91)$$

so that the total required free-energy throughput is

$$P_{\text{req}} \approx P_{\text{tile}} + P_{\text{baryon}} \sim \text{few} \times 10^{-27} \text{ W m}^{-3}. \quad (92)$$

**Implied exterior temperature.** Equating the required throughput to the free-energy production rate Eq. (86) yields

$$T_{\text{ext}} \approx P_{\text{req}} \frac{T_{\text{BH}}^{\text{eff}}}{\dot{u}_{\text{in}}^{(\text{tot})}}. \quad (93)$$

Using the observational ranges above gives

$$T_{\text{ext}} \sim 10^{-10}\text{--}10^{-8} \text{ K}, \quad (94)$$

with a characteristic value of order

$$T_{\text{ext}} \sim \text{few} \times 10^{-9} \text{ K} \quad (95)$$

for accretion dominated by  $\sim 10^8 M_{\odot}$  black holes.

**Interpretation.** This nanoKelvin-scale temperature is not a thermal bath temperature of the photon field, but an effective entropy-acceptance temperature governing the free-energy bookkeeping of resolved degrees of freedom. Within the present framework, entropy removal through black-hole growth at observed rates is sufficient to support both baryon creation and the effective growth of the resolved exterior domain without introducing any additional energy reservoir.

## 13 Emergent Carnot–Carathéodory Geometry and the Horizon Fixed Point

The mesoscopic framework developed in this work assumes a non-Riemannian tangent structure of Carnot–Carathéodory (CC) type, characterized by a horizontal distribution, a degenerate vertical sector, and an associated sub-Laplacian generating large-scale mixing. In this section we argue that the CC tangent geometry is not merely a kinematical ansatz but an *emergent fixed point* selected by the thermodynamic requirements of a horizon-coupled nonequilibrium steady state.

The argument is not one of mathematical uniqueness. Rather, we show that a CC-type sub-Riemannian geometry provides a particularly efficient constitutive response of the exterior spacetime to three coupled constraints: (i) the presence of an observer-dependent horizon enforcing a 2.7 K KMS boundary condition, (ii) continuous inflow of thermodynamically cold entropy from collapsing matter and black holes, and (iii) the requirement that repopulated baryons have sufficient time to cool, mix, and condense into extremely high-entropy configurations before ultimately exiting the resolved exterior description.

### 13.1 The horizon as a thermodynamic boundary condition

For any timelike observer, the causal horizon defines an operational boundary across which degrees of freedom become permanently inaccessible. Tracing over those degrees of freedom induces a KMS state on the residual exterior algebra of observables [34]. Empirically, the cosmic radiation field is observed to be an almost perfect 2.7 K blackbody; in the open-system viewpoint adopted here, this is interpreted not as the fossil of an initial thermal episode but as a *horizon-imposed KMS boundary condition*.

In standard expanding FRW cosmology, the comoving horizon grows and its associated Gibbons–Hawking temperature decreases with time [31]. As a result, the horizon becomes progressively colder and more distant, weakening its thermodynamic coupling to entropy generated in the interior. By contrast, in the mesoscopic picture developed here, the effective horizon remains pinned near a fixed KMS temperature. The horizon does not cool away from the gravitational sector but remains thermodynamically “close” to it, maintaining efficient contact with entropy exported from collapsed structures.

The horizon itself is not a physical membrane and carries no independent local degrees of freedom. Its role is entirely encoded in the constraints it places on the exterior geometry: any viable mesoscopic tangent structure must (i) preserve the KMS state under large-scale transport, (ii) prevent rapid ballistic leakage of photons directly to the horizon, and (iii) accommodate a continuous entropy flux associated with matter collapse without destabilizing the cavity.

## 13.2 Cold entropy, collapse timescales, and geometric response

Black holes occupy a distinguished place in the entropy budget of the exterior sector. Their Hawking temperatures are extremely small [5, 37],  $T_{\text{BH}} \ll 1\text{K}$ , while their absolute entropies are enormous. The formation of a black hole therefore represents a substantial injection of *cold entropy* into the thermodynamic accounting of the exterior.

Crucially, black holes are not formed instantaneously. They are the end states of long baryonic cooling and condensation histories involving galaxy formation, star formation, and successive phases of collapse and accretion. A consistent mesoscopic geometry must therefore satisfy a dual requirement: it must efficiently export the entropy of mature collapsed objects to the horizon at late times, while simultaneously allowing repopulated baryons sufficient time to cool, mix, and assemble into high-entropy configurations at intermediate times.

These requirements strongly constrain the admissible tangent structures. A geometry that transports radiation and matter too efficiently toward the horizon would starve the system of collapsed entropy sources; one that confines matter indefinitely would violate the steady-state entropy balance.

## 13.3 Why purely Riemannian tangent geometries are disfavored

A purely Riemannian (or Euclidean) tangent geometry does not naturally satisfy these constraints. In such geometries, null geodesics free-stream, photons disperse ballistically, and there is no intrinsic mechanism for large-scale confinement or spectral mixing. Maintaining a stable  $2.7\text{K}$  KMS cavity would require fine-tuned boundary conditions, as radiation would continually leak toward the horizon without re-equilibration.

Moreover, attempting to absorb continuous cold-entropy inflow directly into Riemannian curvature degrees of freedom would tend to produce large-scale geometric distortions or instabilities, rather than the observed near-homogeneity of the late-time universe. From a thermodynamic standpoint, Riemannian tangent structures are too rigid to act as efficient steady-state mediators between cold-entropy production, cavity equilibration, and horizon export.

## 13.4 CC geometry as a thermodynamic fixed point

A Carnot–Carathéodory geometry [33] provides a natural resolution of these constraints. Horizontally constrained null propagation forces photons into recurrent trajectories on mesoscopic scales, while the associated sub-Laplacian induces strong mixing [38]. As a result, local perturbations in photon and baryon densities are rapidly homogenized, and the exterior remains in approximate KMS equilibrium with the horizon.

At the same time, the degenerate vertical sector supports ultrasoft geometric modes that act as entropy absorbers for the cold-entropy flux generated by

collapse. These modes do not represent propagating forces or local curvature dynamics; rather, they provide a channel through which entropy can be irreversibly sequestered without disrupting the local CC constitutive law.

Importantly, the CC geometry itself does *not* drive expansion. The large-scale expansion of the resolved exterior arises from tile bookkeeping and coarse-graining drift, as described in Sec. 12. The role of the CC geometry is instead to ensure that this expansion proceeds in a thermodynamically efficient and observationally consistent manner: photons are confined and mixed on intermediate timescales, baryons cool and condense before exiting the resolved description, and entropy is exported steadily to the horizon.

### 13.5 Fixed-point interpretation

The apparent circularity of this construction—the geometry is shaped by horizon thermodynamics, while horizon thermodynamics is defined relative to the geometry—is best understood as a fixed-point relation. The CC tangent structure and the horizon KMS state emerge together as a self-consistent solution of the open-system entropy balance.

Schematically, the steady state satisfies

$$\frac{dS_{\text{ext}}}{dt} = \Phi_{\text{prod}} - \Phi_{\text{hor}} = 0, \quad (96)$$

where  $\Phi_{\text{prod}}$  denotes entropy production from structure formation and collapse, and  $\Phi_{\text{hor}}$  denotes entropy export through horizon-coupled and geometric channels. At the fixed point, the exterior photon bath is approximately KMS with temperature 2.7 K, baryons have sufficient time to condense into high-entropy objects, and the CC tangent geometry remains stationary as a constitutive law.

In this sense, the Carnot–Carathéodory structure is not imposed but selected. It represents a thermodynamically efficient phase of spacetime geometry for a horizon-coupled exterior universe operating in a nonequilibrium steady state, with expansion governed by coarse-graining and tile creation rather than by local metric dynamics.

### 13.6 Relaxation of the Geometric Relaxation Rate $\sigma$

The parameter  $\sigma$  introduced in the preceding sections is not a dynamical field nor an externally tunable constant. Rather, it is an *emergent infrared relaxation rate* characterizing the long-time decay of geometric correlations into the horizon. In this section we explain how  $\sigma$  is dynamically selected and why the system relaxes [53] toward a unique entropy-maximizing value  $\sigma_*$ .

#### 13.6.1 Definition of $\sigma$

Operationally,  $\sigma$  is defined as the slowest nonzero decay rate of large-scale geometric correlations under coarse-graining,

$$\langle \mathcal{O}(t)\mathcal{O}(0) \rangle \sim e^{-\sigma t} \quad (t \rightarrow \infty), \quad (97)$$

where  $\mathcal{O}$  denotes long-wavelength geometric observables. Equivalently,  $\sigma^{-1}$  is the characteristic timescale on which directional information, anisotropies, and large-scale memory are irreversibly lost to horizon-coupled degrees of freedom.

Importantly,  $\sigma$  is inferred from the behavior of the geometry; it does not govern that behavior via an equation of motion.

### 13.6.2 Entropy Export and the Throughput Functional

Entropy transport to the horizon proceeds through geometric correlation decay. At fixed horizon scale and exterior temperature, the entropy export rate may be written schematically as

$$\dot{S}_{\text{export}}(\sigma) = \sigma \mathcal{I}_{\text{geom}}(\sigma), \quad (98)$$

where  $\mathcal{I}_{\text{geom}}(\sigma)$  measures the amount of long-lived geometric structure available to be erased. The two factors have opposite dependence on  $\sigma$ :

- Increasing  $\sigma$  accelerates relaxation and increases the transport rate per unit structure.
- Increasing  $\sigma$  also suppresses structure formation by erasing correlations before they can seed collapse, thereby reducing  $\mathcal{I}_{\text{geom}}$ .

As a result,  $\dot{S}_{\text{export}}(\sigma)$  generically possesses a single maximum at an intermediate value  $\sigma_*$ .

## 14 A Geometric Viewpoint on Luminosity Decay

The purpose of this section is to articulate a purely geometric mechanism by which observed luminosity may decay more rapidly with distance than in standard Friedmann–Robertson–Walker optics, without invoking absorption, scattering, or any explicit loss of energy. The key idea is that, in a mesoscopic Carnot–Carathéodory (CC) geometry, an observer’s angular degrees of freedom need not parameterize the full geometric extent of a propagating wavefront.

### 14.1 Wavefronts and angular accessibility

In ordinary Riemannian geometry, the null wavefront emitted by a point source at a fixed emission time is a smooth sphere whose area growth is faithfully tracked by angular coordinates at the observer. Angular resolution therefore provides a natural parametrization of the wavefront, and luminosity decay follows directly from the familiar area law.

In a CC geometry, the situation is more subtle. The wavefront remains an isodistance surface, but it may possess intrinsic geometric structure that is not resolved by the observer’s angular coordinates. In this case, the observer’s celestial sphere parameterizes only a *projection* of the true wavefront. Radiative

power is conserved on the full wavefront, but the fraction of that power accessible per observed solid angle may decrease with propagation distance.

Crucially, this effect need not arise from rapid angular mixing or local diffusion. Instead, it may be governed by an additional geometric “phase” direction whose evolution is characterized by an exceptionally low frequency. As a result, the loss of angular accessibility accumulates only over very long propagation times, becoming appreciable only on cosmological scales.

## 14.2 The Heisenberg group as a geometric toy model

The simplest setting in which this mechanism can be visualized explicitly is the  $2 + 1$ -dimensional Heisenberg group equipped with its standard Carnot–Carathéodory structure.

In this geometry, admissible curves are constrained to lie in a distinguished two-dimensional horizontal distribution. A defining feature of the space is that horizontal motion necessarily generates an additional geometric degree of freedom: when a horizontal trajectory sweeps out signed area in the horizontal plane, it accumulates displacement in a third (“vertical”) direction. This vertical coordinate records a phase history of the motion rather than a directly observable spatial separation.

Consider a point source at the origin emitting signals uniformly in all horizontal directions. At a fixed propagation time  $t$ , the set of points reached by horizontal geodesic arcs forms a Carnot–Carathéodory wavefront. Unlike a Euclidean circle, this wavefront contains structure associated with different amounts of vertical phase accumulation. Distinct geodesic arcs may arrive at nearly the same horizontal location and with nearly the same horizontal tangent direction, while differing substantially in their accumulated vertical phase.

Now place an observer at some horizontal distance from the source. The observer’s celestial “sky” consists of horizontal arrival directions. Near the source, horizontal angle remains a faithful label of the wavefront: different emission directions correspond to different arrival directions, and the observer’s angular coordinate distinguishes most of the wavefront’s structure.

As the propagation distance increases, the geometry enforces a different trade-off. Reaching larger horizontal distances requires geodesic arcs to accumulate substantial signed area, and hence substantial vertical phase. Small variations among long geodesics increasingly manifest as differences in phase history rather than differences in horizontal direction. Since the observer’s angular degrees of freedom do not resolve this phase, many geometrically distinct portions of the wavefront collapse onto the same observed direction.

From the observer’s perspective, the angular sky remains a circle of fixed length, but it parameterizes the wavefront with increasing multiplicity. The observer has access to a shrinking fraction of the wavefront’s intrinsic geometric measure, even though the wavefront itself continues to grow.

### 14.3 Distance and effective luminosity

This Heisenberg example captures the essential geometric mechanism. Radiative power is conserved on the full CC wavefront, but the observer’s angular coordinates fail to resolve an increasing portion of the wavefront’s structure as propagation time grows. Equivalently, the effective transverse area over which conserved power is distributed grows faster than the area accessible to image-forming angular degrees of freedom.

Phenomenologically, this can be expressed by writing the observed flux from a standard candle as

$$F_{\text{obs}}(z) = \frac{L}{4\pi A_{\text{eff}}(z)}, \quad (99)$$

where  $A_{\text{eff}}(z)$  denotes the effective geometric area of the CC wavefront relative to the observer’s accessible angular parametrization. In standard FRW optics,  $A_{\text{eff}}(z)$  reduces to the usual luminosity–distance area. In the CC framework, the geometric claim is simply that

$$A_{\text{eff}}(z) \text{ grows faster with distance than the apparent angular area resolved by the observer.} \quad (100)$$

The Heisenberg group illustrates how this can occur without any local loss mechanism: increasing propagation time shifts geometric information from angular separation into an unresolved phase direction. Because the characteristic frequency associated with this phase evolution is infrared, the effect is negligible at small distances and becomes relevant only over cosmological scales.

### 14.4 Interpretation

The resulting luminosity decay is therefore geometric in origin. It reflects a mismatch between the intrinsic growth of the wavefront in a CC geometry and the observer’s angular access to that wavefront, rather than any failure of energy conservation. Distance correlates with dimming because increasing propagation time increases the portion of the wavefront lying in geometric directions not resolved by the observer’s angular coordinates.

The Heisenberg example serves as a concrete toy model demonstrating how such an infrared bundle effect can arise purely from geometry, and how it naturally leads to a distance-dependent reduction of observed flux without invoking absorption, scattering, or local angular diffusion.

### 14.5 Local Phase Inheritance and Coarse–Grained Continuity

The “phase” variable appearing in the Carnot–Carathéodory description is not an internal label or conserved quantum number, but a geometric quantity encoding the accumulated transverse holonomy of horizontal transport. As such, it admits no globally preferred trivialization. Any attempt to assign a single,

exterior-wide phase reference would amount to introducing an unphysical background structure and would violate coarse-grained continuity by suppressing the very phase drift implied by the geometry.<sup>5</sup>

For this reason, newly created matter excitations cannot be globally phase-locked. Instead, matter must inherit the phase defined by its *local* CC environment at the spacetime region in which it is created. This inheritance is automatic: physical creation processes occur over finite regions and necessarily sample the ambient modular flow and horizontal frame. No additional postulate is required.

Phase continuity is preserved not by constancy but by smooth variation. The CC phase field varies gradually across the exterior, and locally created matter simply joins this existing structure without introducing discontinuities. There is therefore no preferred phase and no global synchronization condition, in direct analogy with the absence of global simultaneity in general relativity.

Once created, matter exhibits strong phase stiffness due to timelike motion, internal dynamics, and continual interaction, which rapidly re-anchors its phase to the local environment. Nevertheless, this stiffness is not absolute. Over sufficiently long proper times, even matter accumulates transverse holonomy incoherently, leading to slow phase drift on cosmological scales. This drift is parametrically weaker than that experienced by radiation, which propagates along null trajectories and therefore integrates the CC connection coherently over large distances.

The distinction between matter and radiation is thus not one of phase versus no-phase, but of *coherent versus incoherent accumulation*. Matter remains locally coherent and dynamically stable while gradually becoming relationally distant from a given observer's algebra. Radiation, by contrast, provides a sensitive probe of large-scale phase structure and reveals this drift observationally through flux diminution rather than local decoherence.

This local inheritance principle ensures that phase drift, horizon formation, and effective charge loss emerge continuously and without introducing hidden sectors or preferred reference structures, preserving the open-system and observer-relative character of the exterior description.

## 14.6 Single-packet CC phase drift and effective luminosity decay

The discussion above was framed in terms of wavefront accessibility and coarse-grained angular resolution. For a feasibility test, however, it is useful to isolate a simpler geometric picture based on the propagation of a *single localized photon wave packet*. Ensemble and bundle effects can be reintroduced later by superposition; at the present stage they are not essential.

---

<sup>5</sup>Note: Throughout this section, by phase we mean CC geometric phase (vertical displacement / holonomy), not wave phase. In the Heisenberg case, this is  $e^{is\sigma}$ .

**CC phase as a geometric observable.** In Carnot–Carathéodory geometries of Heisenberg type, horizontal transport generically accumulates displacement in the central direction. For a horizontal curve with coordinates  $(x(t), y(t))$ , the associated central coordinate  $\phi(t)$  is proportional (up to normalization) to the signed area swept by the horizontal projection,

$$\phi(t) \propto \int_0^t (x \dot{y} - y \dot{x}) dt. \quad (101)$$

Thus the CC phase is not an independent degree of freedom but a geometric holonomy recording the cumulative noncommutativity of horizontal transport.

**Long-time scaling and normalization.** In the Heisenberg model one can compute the central holonomy explicitly for the canonical constant-curvature horizontal motion, obtaining

$$\phi(t) = \frac{1}{\sigma} (t - \sin(\sigma t)) = \frac{t}{\sigma} + O(\sigma^{-1}). \quad (102)$$

Thus  $\phi$  grows linearly in  $t$  with slope  $1/\sigma$ , with only bounded oscillatory corrections. We therefore treat  $\phi$  as an area-type central coordinate; only the ratio  $\phi/\phi_0$  entering the response function is dimensionless.

**Phase-dependent luminosity response.** We assume that the observer’s image-forming algebra does not resolve the central (CC) coordinate directly. Instead, the contribution of an arriving photon to the perceived flux is effectively weighted by a *phase-luminosity response curve*

$$\ell(\phi) \in [0, 1], \quad \ell(0) = 1, \quad (103)$$

which encodes how arrivals with CC phase  $\phi$  are registered by the observer. The CC phase  $\phi$  is an area-type geometric quantity (central holonomy), and need not be dimensionless; only the ratio  $\phi/\phi_0$  entering the response function is dimensionless. As a conservative and analytically tractable choice, we adopt a Cauchy (Lorentzian) response,

$$\ell(\phi) = \frac{1}{1 + (\phi/\phi_0)^2}, \quad (104)$$

where  $\phi_0$  sets the effective phase-resolution scale of the observer. Arrivals with  $|\phi| \gg \phi_0$  are not sharply excluded, but are strongly suppressed.

**Effective luminosity decay.** For a single localized wave packet propagating for a time  $t$ , the observed flux is reduced according to

$$g(t) = \ell(\phi(t)). \quad (105)$$

Using the asymptotic Heisenberg scaling derived above,

$$\phi(t) = \frac{1}{\sigma} (t - \sin(\sigma t)) \simeq \frac{t}{\sigma},$$

the attenuation factor becomes

$$g(t) \simeq \frac{1}{1 + \left(\frac{t}{\sigma \phi_0}\right)^2}. \quad (106)$$

It is therefore convenient to introduce the characteristic onset timescale

$$\tau_0 \equiv \sigma \phi_0, \quad (107)$$

so that  $g(t) = (1 + (t/\tau_0)^2)^{-1}$ . The corresponding shift in distance modulus is

$$\Delta\mu(t) = 2.5 \log_{10} \left[ 1 + \left( \frac{t}{\tau_0} \right)^2 \right]. \quad (108)$$

Two qualitative features are immediate. First, the effect is negligible at small lookback times: for  $t \ll \tau_0$  one has  $\Delta\mu(t) \approx (2.5/\ln 10) (t/\tau_0)^2$ , so local distance calibrations are unaffected. Second, for propagation times of order the Hubble time,  $t \sim H_0^{-1}$ , and for an infrared scale dynamically selected such that  $\sigma \sim H_0$ , the attenuation becomes order unity when  $\tau_0$  itself is of Hubble order. In this regime, the observed luminosity suppression is a natural consequence of CC phase accumulation rather than an indication of photon loss or modified expansion kinematics.

**Relation to exponential parametrizations.** Over a finite redshift interval, the logarithmic slope of Eq. (106) defines an effective decay rate,

$$-\frac{d}{dt} \ln g(t) = \frac{2t}{\tau_0^2 + t^2}. \quad (109)$$

For  $t$  restricted to a narrow range around  $t \sim \tau_0$ , this quantity varies slowly and may be approximated by a constant. In such limited domains, phenomenological fits of the form  $\exp(-\varepsilon t)$  can serve as local surrogates for the underlying phase-selection law, but should not be interpreted as evidence for a fundamental exponential attenuation mechanism.

This single-packet picture isolates a purely geometric mechanism for anomalous luminosity suppression that becomes relevant only on cosmological scales, and does so without invoking photon destruction, scattering, or additional propagating degrees of freedom.

**Sanity check: observational scale of the phase-resolution parameter.** Using the asymptotic Heisenberg scaling from Eq. (102),

$$\phi(t) = \frac{1}{\sigma} (t - \sin(\sigma t)) = \frac{t}{\sigma} + O(\sigma^{-1}),$$

we approximate  $\phi(t) \simeq t/\sigma$  for the purpose of a crude observational anchor. The single-packet attenuation then becomes

$$g(t) = \ell(\phi(t)) \simeq \frac{1}{1 + \left(\frac{t}{\sigma \phi_0}\right)^2}. \quad (110)$$

It is convenient to define the onset time scale

$$\tau_0 \equiv \sigma \phi_0, \quad (111)$$

so that  $g(t) = (1 + (t/\tau_0)^2)^{-1}$  and

$$\Delta\mu(t) = 2.5 \log_{10} \left[ 1 + \left( \frac{t}{\tau_0} \right)^2 \right]. \quad (112)$$

Solving for  $\tau_0$  gives

$$\tau_0 = \frac{t}{\sqrt{10^{\Delta\mu/2.5} - 1}}. \quad (113)$$

As a visual reference, Type Ia supernova data show an apparent dimming of order  $\Delta\mu \simeq 0.2\text{--}0.3$  mag at redshifts  $z \simeq 0.4\text{--}0.6$ , corresponding to lookback times  $t \simeq 4\text{--}6$  Gyr for standard cosmological parameters. Taking  $\Delta\mu = 0.25$  mag at  $t = 5$  Gyr yields  $\tau_0 \simeq 10$  Gyr, i.e.  $\tau_0 \simeq 0.7 H_0^{-1}$  for  $H_0^{-1} \simeq 14$  Gyr.

Interpreting this in terms of the phase-resolution parameter gives

$$\phi_0 \simeq \frac{\tau_0}{\sigma}. \quad (114)$$

If the infrared scale is dynamically selected such that  $\sigma \sim H_0$ , this implies

$$\phi_0 \sim (0.5\text{--}0.9) H_0^{-2}, \quad (115)$$

i.e. the required phase-resolution scale is of the natural order set by the Hubble scale (in the units appropriate to the central CC coordinate), with no fine tuning.

#### 14.7 Vertical Mixing, Fat-Tailed Phase Occupation, and the Stability of the Photon Bath

The luminosity-decay mechanism introduced above must be interpreted with care when applied to diffuse radiation fields. A reduction in *recoverable* flux from a localized source does not, by itself, imply a catastrophic loss of photons from the exterior cavity. The distinction hinges on the distribution of radiation over the Carnot–Carathéodory vertical (central) degree of freedom.

Let  $p(\phi, t)$  denote the normalized occupation distribution of photons over the affine central coordinate  $\phi$ ,

$$\int_{-\infty}^{\infty} p(\phi, t) d\phi = 1, \quad (116)$$

and let  $\ell(\phi) \in [0, 1]$  denote the phenomenological phase–acceptance function encoding how radiation arriving at vertical displacement  $\phi$  contributes to image–forming observables. The effective observational efficiency is then

$$\eta(t) \equiv \int_{-\infty}^{\infty} p(\phi, t) \ell(\phi) d\phi. \quad (117)$$

For radiation emitted by a localized source,  $p(\phi, t)$  is initially narrow. Geometric CC phase drift and bundle spreading cause this distribution to broaden with propagation time, leading to a redshift–dependent suppression of  $\eta(t)$ . This is the origin of the effective luminosity decay discussed in Sec. 14.6.

The cosmic microwave background, however, occupies the opposite regime. Over cosmological timescales, the photon bath has undergone not only angular isotropization but also extensive *vertical mixing*. As a result, the CMB occupation distribution  $p_{\text{CMB}}(\phi)$  is expected to be extremely broad, with a fat tail extending over a large region of the affine central direction. When the characteristic width of  $p_{\text{CMB}}$  greatly exceeds the intrinsic scale  $\phi_0$  appearing in  $\ell(\phi)$ , the effective acceptance  $\eta_{\text{CMB}}$  becomes insensitive to further vertical spreading and remains close to unity.

In this regime, the CMB exhibits negligible effective photon loss despite the same geometric mechanisms that strongly suppress the recoverable flux from localized emitters. Any small residual leakage from the resolved observational channel can be easily offset by ordinary baryonic emission and rapid equilibration with the photon bath, even at low densities.

This picture also clarifies the role of photons as a large and robust free–energy buffer. Because free energy can be exported not only angularly but also into the vertical degrees of freedom, the photon bath possesses a large effective state space in which injected free energy can be redistributed while maintaining a near–stationary radiative (KMS) spectrum when projected onto the exterior observable algebra. The buffering capacity of the radiation field is therefore enhanced by vertical delocalization rather than undermined by it.

Importantly, this mechanism does not require the exclusion of layered or multimodal vertical populations. Such structures may arise for freshly produced or weakly mixed radiation. The CMB simply represents the late–time, strongly mixed attractor of the vertical dynamics, in which the occupation distribution is sufficiently broad that luminosity–decay effects do not translate into significant photon loss from the cavity.

## 14.8 Radiation and detection in the $(3, 3)$ Carnot geometry

The Heisenberg example serves as a pedagogical toy model, but the mesoscopic geometry relevant for the present framework is more naturally modeled by a step–2 Carnot group with horizontal and central dimensions  $(3, 3)$ . In this case the central fiber is three–dimensional,

$$Z \cong \Lambda^2 V \cong \mathbb{R}^3,$$

and the Carnot–Carathéodory “phase” accumulated by horizontal transport is no longer a scalar but a vector–valued geometric holonomy.

At first sight this appears to introduce a qualitative complication: the central holonomy may be decomposed into a magnitude and a direction,

$$\omega = \|\omega\|\hat{\omega}, \quad \hat{\omega} \in S^2,$$

suggesting an additional sphere of “phase directions” beyond the observer’s ordinary celestial sphere. If taken literally, one might worry that radiation emitted with all possible  $\hat{\omega}$  would free–stream and uniformly populate this vertical sphere at reception, erasing any distance–dependent selection effect.

This concern is resolved once the correct observable is identified. In the (3, 3) geometry, the vertical direction  $\hat{\omega}$  is not a physical emission angle and does not label distinct rays in spacetime. It is an internal axial label encoding the oriented bivector (area normal) generated by horizontal transport. Free streaming routes photons according to their horizontal directions alone; the vertical direction  $\hat{\omega}$  does not affect which spacetime points a ray can reach.

Crucially, the observer’s image–forming algebra is assumed to be rotationally invariant in the vertical sector. Detection does *not* depend on selecting a preferred cap or solid angle on the vertical sphere  $S^2$ . Instead, it depends only on the *magnitude* of the central displacement,

$$\|\omega\|,$$

that is, on how far the arriving ray has drifted away from the locally resolved sector of the vertical fiber. The resolved region is therefore a neighborhood of the origin in  $Z \cong \mathbb{R}^3$ , not a directional subset of  $S^2$ .

With this identification, the apparent emission–reception asymmetry disappears. Emission may populate  $\hat{\omega}$  isotropically without consequence. During propagation, Carnot–Carathéodory transport generates a systematic growth of  $\|\omega\|$  with distance, while preserving isotropy in  $\hat{\omega}$ . At reception, arrivals are weighted according to their radial distance from the origin in the vertical fiber. Luminosity diminution therefore arises from *radial escape in a noncompact central direction*, not from any directional selection on  $S^2$ .

In this sense, the (3, 3) case clarifies rather than complicates the geometric mechanism. The role played by the scalar phase in the Heisenberg model is taken over by the central magnitude  $\|\omega\|$ , while the additional directional structure of the center remains observationally silent. The luminosity decay mechanism thus survives intact: increasing propagation time shifts geometric information into an unresolved central sector whose extent grows without bound, reducing the fraction of the wavefront accessible to the observer’s angular parametrization without introducing anisotropy or violating energy conservation.

## 15 Late-Time Cosmology, Chemical Steady State, and the Origin of Quasars

In a horizon-coupled equilibrium universe, the observable sector is not a fossil left by a unique high-temperature episode but an open, slowly evolving system in which baryons, entropy, and chemical species are continually exchanged with causal horizons. Once the mesoscopic continuity equations are taken seriously, several assumptions inherited from  $\Lambda$ CDM invert: quasars become *late-time* thermodynamic states rather than early-time anomalies; nucleosynthesis becomes an *ongoing* process governed by stellar evolution and baryon replenishment; and the cosmic helium fraction arises as a *regulated equilibrium quantity*, not a primordial boundary condition. This section introduces these structural consequences and motivates the quantitative helium budget developed in Sec. 16.

### 15.1 Quasars as Terminal Galactic Attractors

Under standard cosmology, quasars require finely tuned early-time conditions: rapid black-hole growth, intense starbursts, and fast chemical enrichment at high redshift. These requirements are widely acknowledged to be contrived.

In a horizon-coupled equilibrium universe, the evolutionary arrow reverses. A galaxy that persists for Gyr–Tyr naturally undergoes secular baryon depletion through stellar collapse, metal cooling, neutronization, and horizon-mediated sequestration. Over sufficiently long times, the diffuse baryon reservoir contracts toward the center, while the stellar population processes a significant fraction of its gas into helium and heavier elements. The terminal state is a compact, thermodynamically regulated accretion structure feeding an overgrown SMBH.

The observed properties [61, 35, 26] of quasars— $10^8$ – $10^{10} M_\odot$  black holes, compact emitting regions, super-solar metallicities, and rapid variability—then follow naturally as signatures of *old galaxies in their final luminous phase*. Quasars appear not as youthful anomalies but as the late-time attractors of secular galactic evolution.

### 15.2 Nucleosynthesis Beyond the Primordial Paradigm

Standard cosmology treats light-element abundances as relics of a brief early nucleosynthesis epoch [65, 49]. The horizon-coupled framework replaces this with a slow, ongoing chemical cycle:

1. **Baryon return:** horizon exchange injects light species—primarily hydrogen, with minimal helium—into the diffuse reservoir.
2. **Stellar processing:** long-lived stellar populations continuously convert hydrogen into helium and produce metals according to IMF-weighted yields.

Because the exterior sector is not closed, its chemical composition reflects the *balance* among these processes rather than an imprinted thermal boundary

condition. Light-element abundances become emergent properties of long-term baryon cycling rather than diagnostic fossils of the early universe.

### 15.3 Preferential Metal Sequestration

A classical objection to stellar-driven helium production is that it would over-produce metals in a closed-box universe. The present framework avoids this by introducing a natural one-way sink for metals.

Metal-rich gas cools rapidly, condenses, and sinks into deep gravitational potentials, where it is preferentially accreted by SMBHs or trapped in dense nuclear regions. Observationally, the gas feeding active nuclei is already highly enriched, and metal-rich cores are ubiquitous in clusters and bulges. Over cosmic timescales, this hydrodynamic sorting removes metals from the exterior sector while leaving helium and hydrogen—much poorer coolants—distributed in the diffuse medium or expelled by AGN outflows.

Thus the exterior metallicity remains low even while helium is continually produced, eliminating the closed-box objection and enabling a chemically consistent steady state.

### 15.4 Chemical Equilibrium and the Helium Fixed Point

The three ingredients above—ongoing baryon return, continuous stellar processing, and preferential metal sequestration—drive the exterior sector toward a chemical steady state. The crucial point is that the *value* of the helium fraction is determined by stellar microphysics.

Stellar populations return only a fraction [77]

$$y_{\text{He}} \simeq 0.20 - 0.33$$

of the baryonic mass they process as newly synthesized helium. This yield is set by nuclear physics and the IMF, with negligible dependence on environment or cosmic epoch.

In a horizon-coupled universe, nearly all helium in the exterior sector must be produced through hydrogen burning, while helium losses into compact objects and horizon-sequestered modes occur slowly and roughly proportionally to the baryon cycle. A mesoscopic continuity equation then forces the helium mass fraction toward

$$Y_{\text{eq}} \approx \frac{y_{\text{He}}}{1 + \epsilon},$$

where  $\epsilon \ll 1$  encodes the slight excess sequestration of helium relative to hydrogen.

For empirically supported  $y_{\text{He}}$  in the range 0.20–0.33 and typical drain efficiencies  $\epsilon \sim 0.1\text{--}0.2$ , one finds

$$Y_{\text{eq}} \simeq 0.22 - 0.26,$$

in striking agreement with the observed [40, 3] cosmic helium fraction  $Y \simeq 0.24$ .

Thus the helium abundance is not a remnant of an early thermal episode but the *fixed point* of slow baryon cycling:

*The Universe has  $\sim 25\%$  helium because stars return  $\sim 25\%$  helium, and the horizon-regulated baryon cycle forces the exterior sector to inherit that ratio.*

## 15.5 Summary

These ingredients combine into a unified equilibrium picture:

- **Quasars** are the late-time thermodynamic attractors of galactic evolution.
- **Nucleosynthesis** is continuous rather than primordial, governed by stellar evolution and baryon return.
- **Metals** are efficiently removed into SMBHs, preventing over-enrichment.
- **Helium** is a fixed-point quantity determined by stellar nuclear yields and slow baryon cycling, not by a unique early-time epoch.

This motivates the detailed helium-budget analysis presented next in Sec. 16, where the equilibrium value  $Y \simeq 0.24$  emerges quantitatively from the mesoscopic continuity equation.

# 16 The Cosmic Helium Budget

A central phenomenological success of the horizon-coupled framework is that it naturally explains the near-universal cosmic helium fraction  $Y \simeq 0.24$  [40, 3] without invoking a primordial nucleosynthesis epoch. Helium is not a fossil boundary condition but a dynamically maintained quantity governed by stellar microphysics, baryon return, and slow gravitational sequestration.

This section develops the helium continuity equation, demonstrates the existence of a fixed point, and shows why that fixed point lies near the observed value.

## 16.1 Helium as a Mesoscopic Observable

Let  $\rho_{\text{He}}$  be the physical helium density in the exterior sector. In an expanding universe with horizon exchange and slow baryon loss,  $\rho_{\text{He}}$  obeys

$$\dot{\rho}_{\text{He}} + 3H \rho_{\text{He}} = S_{\text{He}} - L_{\text{He}}, \quad (118)$$

where:

- $S_{\text{He}}$  is the rate at which stellar populations convert hydrogen into helium and return it to the diffuse medium,
- $L_{\text{He}}$  is the net rate of helium removal into compact objects, deep potentials, and horizon-sequestered modes.

Horizon return contributes primarily hydrogen, so nearly all new helium must be produced through stellar burning. The helium fraction therefore tracks the ratio of stellar processing to global baryon cycling.

## 16.2 Equilibrium Condition

A mesoscopic equilibrium requires

$$\dot{\rho}_{\text{He}} \approx 0.$$

Applying this to (118) gives

$$S_{\text{He}} - L_{\text{He}} \simeq 3H \rho_{\text{He}}. \quad (119)$$

Writing  $\rho_{\text{He}} = Y \rho_b$  yields

$$\frac{S_{\text{He}} - L_{\text{He}}}{\rho_b} \simeq 3H Y \sim 10^{-18} \text{ s}^{-1}, \quad (120)$$

so only a few percent of the baryon mass must be processed into helium per 10 Gyr to maintain the observed helium density. This requirement is modest: typical stellar populations exceed it comfortably.

## 16.3 Microphysical Origin of the Helium Fixed Point

The equilibrium value itself is set by nuclear microphysics. The IMF-averaged helium yield

$$y_{\text{He}} \simeq 0.20 - 0.33$$

determines what fraction of processed hydrogen reappears as helium in stellar ejecta. Because helium losses scale weakly with the baryon drain, the continuity equation forces

$$Y_* \approx \frac{y_{\text{He}}}{1 + \epsilon}, \quad (121)$$

with  $\epsilon \ll 1$  quantifying the slight excess sequestration of helium relative to hydrogen.

For the empirical range of  $y_{\text{He}}$  and typical drain efficiencies,

$$Y_* \simeq 0.22 - 0.26,$$

precisely matching the observed cosmic helium fraction.

## 16.4 Role of Metal Sequestration

Although AGN outflows redistribute gas on galactic scales, quasars act as extremely efficient *net* metal sinks. Metal-rich gas cools rapidly and collapses into the nuclear region, where it cycles repeatedly through the accretion disk and broad-line region. The material that actually reaches these zones is enriched by

factors of 5–10 relative to the galactic ISM [35], so even a modest SMBH accretion rate permanently removes metals at a rate far disproportionate to its mass growth. By contrast, the gas expelled in winds and jets is dominated by hot, low-metallicity hydrogen and helium that is far more likely to escape to large radii. The result is a persistent asymmetry: metals experience a net inward flow and long-term sequestration, while helium and hydrogen remain diffusely distributed and readily mixed into the exterior reservoir.

This asymmetry—net metal sequestration and net helium retention—eliminates the closed-box overproduction problem and stabilizes the chemical equilibrium of the exterior sector.

## 16.5 Thermodynamic consumption of metals as an exterior principle

A common objection to late-time helium production is that stellar processing generates metals alongside helium, and that the integrated metal yield would over-enrich the diffuse cosmic reservoir. In a horizon–closed chemical evolution model this objection is decisive: metals behave as an approximately conserved tracer and accumulate in the background in proportion to the total processed mass.

In the present horizon–coupled nonequilibrium steady state, the relevant constraint is different. The exterior is not an isolated reactor but an open system with a persistent entropy sink. Steady state is maintained by a balance of *entropy throughput* rather than by conservation of chemical tracers. In such a setting, the long–time distribution of species is controlled not primarily by their production ratios, but by the existence of preferential *thermodynamic routes* by which exterior free energy is converted into entropy delivered to the sink.

**Consumption principle.** Metals constitute the most efficient intermediate route from diffuse exterior free energy to irreversible entropy export, because they (i) provide the most effective catalysis for radiative dissipation and cooling, (ii) enable the most rapid condensation into deep gravitational potentials, and hence (iii) promote the formation of compact, high–binding configurations that maximize entropy production under continued accretion and collapse. Consequently, in a horizon–coupled NESS the *dominant* fate of newly produced metals is not to homogenize as a passive background abundance, but to be *rapidly consumed* into condensation and accretion channels that feed the entropy sink.

This claim does not require that no metals escape in winds or jets. Rather, it asserts that thermodynamic balance places the escaping fraction much closer to “consumable” configurations than hydrogen and helium: even when metals are transported outward, they remain strongly biased toward phases and environments that re-enter condensation, precipitation, and reaccretion pathways on cosmological timescales. The exterior therefore supports a persistent asymmetry: hydrogen and helium can remain in long–lived diffuse reservoirs, while metals preferentially populate the short–lived, high–dissipation sector.

**Exterior consequence.** The metal continuity equation for the diffuse exterior must therefore include an effective *consumption* term  $C_Z$  representing transfer into condensed and accreting phases,

$$\dot{\rho}_Z + 3H\rho_Z = S_Z - L_Z - C_Z, \quad (122)$$

with  $C_Z$  parametrically larger (per unit abundance) than the corresponding consumption term for hydrogen and helium. In this regime, the steady-state background metallicity is controlled mainly by the competition between production  $S_Z$  and thermodynamic consumption  $C_Z$ , rather than by IMF-averaged yield ratios alone. The usual closed-box inference from “helium production” to “metal overproduction” is therefore inapplicable.

## 16.6 Interpretation

The helium fraction  $Y \simeq 0.24$  emerges as a regulated equilibrium of the exterior sector:

- horizon return supplies hydrogen,
- stellar populations convert a fixed fraction  $y_{\text{He}}$  into helium,
- metals are preferentially removed,
- helium drains slowly into compact objects and horizon-proximal modes,
- cosmic expansion sets the replenishment rate.

The long-term result is a stable fixed point  $Y_*$  determined by stellar yields and the slow baryon cycle. The cosmic helium fraction is therefore an *equilibrium property* of the late-time Universe rather than a relic of an early, high-temperature phase.

## 17 Concluding Remarks: Open-System Conservation, Entropy Production, and the Mesoscopic Universe

The central claim of this work is that the late-time Universe must be described as an *open* quantum-thermodynamic system. At the microscopic level, the conservation laws of quantum field theory are encoded in exact *local operator identities*,

$$\nabla_\mu J_X^\mu(x) = 0,$$

which hold pointwise on the full Hilbert space and express the local invariance of the underlying field algebra. In spacetimes admitting global Cauchy surfaces, these identities integrate to global conservation laws for charges defined on complete hypersurfaces.

In a horizon-dominated cosmology, however, the exterior region accessible to late-time observers is not a closed system and does not admit a global Cauchy surface. Cosmological and black-hole horizons partition the Hilbert space into accessible and inaccessible sectors, and the exterior is described by a *reduced* density matrix obtained by tracing over horizon degrees of freedom. From the standpoint of this reduced state, the microscopic identity  $\nabla_\mu J_X^\mu = 0$  no longer appears as a strict local continuity equation for coarse-grained densities. Instead, it manifests as an open-system balance law,

$$\partial_t n_X + 3H n_X = -\Phi_X + \Gamma_X,$$

where the flux  $\Phi_X$  represents the loss of charge into horizon-adjacent modes and the source term  $\Gamma_X$  represents the compensating inflow generated by the horizon-induced chemical potential. The apparent “local creation” terms that arise at mesoscopic scales are therefore not violations of microscopic locality or conservation, but the effective imprint of globally conserved currents on an open subsystem.

In the specific case of baryon number, this structure has decisive thermodynamic consequences. The exterior sector continuously loses baryon charge through cosmological expansion and black-hole accretion. A stationary late-time state can therefore exist only if the reduced density matrix repopulates baryon number at the same rate. The required baryon source  $\Gamma_B$  is not an additional dynamical assumption, but the joint consequence of (i) exact local QFT conservation laws, (ii) Hilbert-space factorization across horizons, and (iii) the requirement of stationarity for the exterior medium. The “baryon creation” discussed throughout this work is thus simply the exterior reappearance of globally conserved charge that has been sequestered in inaccessible degrees of freedom.

Entropy obeys an analogous but more dominant balance principle, with an important thermodynamic distinction. The exterior continuously exports entropy into black-hole and cosmological horizons, yet the combined horizon-exterior system must satisfy the second law. Crucially, this entropy export is accompanied by a *net liberation of free energy* in the exterior sector: sequestering degrees of freedom behind horizons increases the distinguishability of the remaining accessible states and therefore raises the exterior free-energy density relative to its instantaneous entropy content. Stationarity thus requires not only that entropy be returned to the exterior, but that this excess free energy be *dissipated through admissible channels*.

The dominant compensating channel is the excitation of long-wavelength geometric modes—infrared gravitons, curvature fluctuations, and Carnot–Carathéodory deformations—which can absorb entropy at extremely low effective temperatures. These modes provide a high-entropy, low-free-energy sink and therefore maximize entropy throughput per unit free energy expended. The resulting balance condition,

$$\dot{s}_{\text{hor}} + \dot{s}_{\text{IR}} = 0,$$

ensures that the exterior entropy density remains stationary, while the requirement that the liberated free energy be dissipated fixes the expansion rate  $H$

and dynamically ties it to the mesoscopic frequency scale  $\sigma$  characterizing the Carnot–Carathéodory tangent geometry.

Viewed thermodynamically, the late-time Universe is therefore not a heat engine in the traditional sense but a steady-state *free-energy dissipation system*. Entropy transport is dominated by infrared geometric modes, but free energy cannot be dissipated arbitrarily: causal structure, charge conservation, and dynamical stability severely restrict the available channels. Within the Standard Model, the only robust channel capable of absorbing a non-negligible fraction of the liberated free energy while remaining compatible with horizon separation is the baryon–accretion cycle. Low-entropy baryons are regenerated in the exterior, participate in structure formation, and ultimately fall into black holes, where they trigger a vast increase of horizon entropy. Although this channel carries only a small fraction of the total entropy flux, it plays a structurally essential role by providing the “work-like” dissipation required to stabilize the nonequilibrium steady state.

In this sense, baryons are not the dominant entropy carriers but the dominant *free-energy sinks* compatible with late-time cosmology. Their existence and continual regeneration are dictated not by microscopic baryogenesis, but by the macroscopic requirement that the exterior free-energy surplus generated by horizon entropy export be continuously neutralized.

The most delicate aspect of this framework is not the conservation of baryon number as a charge, but the appearance of *baryonic rest mass* in the exterior sector. This point is often misunderstood. The creation of baryons in the mesoscopic balance laws does not occur freely or abundantly, nor does it draw upon an unlimited energy reservoir. Rather, it is tightly constrained by the available *free energy* liberated by horizon-coupled entropy export.

When degrees of freedom are sequestered behind cosmological or black-hole horizons, the exterior does not merely lose entropy; it acquires a small but persistent surplus of free energy. This surplus arises because tracing over horizon degrees of freedom reduces the entropy of the accessible state faster than it reduces its energy, thereby increasing the exterior free energy  $F = E - TS$  relative to its instantaneous entropy content. In steady state, this free-energy excess must be dissipated through channels compatible with causality, conservation laws, and long-term dynamical stability.

The key point is that the free-energy flux available from horizon entropy export is enormous on cosmological timescales, while the rest-mass cost of baryon creation required to maintain stationarity is comparatively tiny. Only an extremely small fraction of the available free energy is needed to realize the observed baryon regeneration rate. The mesoscopic source term  $\Gamma_B$  is therefore not energetically problematic: it is parametrically suppressed by the ratio of the baryon rest-mass scale to the horizon-controlled free-energy throughput.

In this sense, baryon creation is not the dominant entropy-return mechanism, nor is it the primary sink of free energy. Infrared geometric modes absorb the overwhelming majority of the entropy at negligible energetic cost. Baryons play a different role: they provide a *discrete, chemically stable, and long-lived channel* through which a small but necessary portion of the liberated free energy

can be irreversibly converted into rest mass and ultimately delivered to black holes. Their creation is therefore not driven by entropy maximization, but by the requirement that the exterior free-energy surplus be neutralized in a way compatible with horizon separation.

From this perspective, the baryon–accretion cycle is not extravagant but economical. It consumes only a minute fraction of the available free energy, yet it enables the system to close its charge balance and to convert free energy into horizon entropy with maximal efficiency. The rarity of baryon creation is thus a feature, not a flaw: it reflects the fact that rest-mass realization is the most expensive available channel and is invoked only to the extent strictly required by steady-state balance.

This open-system framework also explains the ubiquity of the mesoscopic scale  $\sigma$  in late-time cosmology. The same frequency governs the excitation of infrared entropy-carrying modes, the grand-canonical bias fixing the baryon repopulation rate, the sub-Riemannian curvature of particle trajectories, and the mixing properties of the photon bath. As a result, the Hubble expansion rate, the asymptotic behavior of galactic rotation curves, and the equilibrium temperature of the cosmic radiation field are all controlled by a single geometric scale. The coincidence  $\sigma \approx H_0$  is therefore not accidental, but a direct consequence of horizon-coupled mesoscopic dynamics.

Much remains unresolved. A complete dynamical theory of Carnot–Carathéodory gravity, an action principle unifying infrared geometry with semiclassical horizon thermodynamics, and a microscopic derivation of the infrared entropy elasticity all remain open problems. Nevertheless, the analysis presented here demonstrates that once the open-system character enforced by horizons, the exact locality of QFT conservation laws, and the mesoscopic geometry of spacetime are taken seriously, a wide range of cosmological regularities follow from a single underlying scale. The unified appearance of  $\sigma$  across baryon balance, entropy flow, photon equilibrium, and galactic kinematics suggests a coherent and tightly constrained alternative to the fragmented phenomenology of the standard cosmological model. Whether this mesoscopic framework can be extended into a complete theory, and whether its predictions remain compatible with increasingly precise observational data, are questions that future work must decisively address.

## References

- [1] N. et al. (Planck Collaboration) Aghanim. Planck 2018 results. vi. cosmological parameters. *Astronomy and Astrophysics*, 641:A6, 2020.
- [2] S. K. Andrews, S. P. Driver, A. S. G. Robotham, M. Alpaslan, I. K. Baldry, et al. Galaxy and mass assembly: the evolution of the cosmic spectral energy distribution from  $z = 1$  to  $z = 0$ . *Monthly Notices of the Royal Astronomical Society*, 470(2):1342–1360, 2017.

- [3] Erik Aver, Keith A. Olive, and Evan D. Skillman. The effects of he i  $\lambda 10830$  on helium abundance determinations. *Journal of Cosmology and Astroparticle Physics*, 2015(07):011, 2015.
- [4] Jacob Bekenstein and Mordehai Milgrom. Does the missing mass problem signal the breakdown of newtonian gravity? *Astrophysical Journal*, 286:7–14, 1984.
- [5] Jacob D. Bekenstein. Black holes and entropy. *Physical Review D*, 7:2333–2346, 1973.
- [6] Jacob D. Bekenstein. Generalized second law of thermodynamics in black-hole physics. *Physical Review D*, 9(12):3292–3300, 1974.
- [7] André Bellaïche. The tangent space in sub-riemannian geometry. In *Sub-Riemannian Geometry*. Birkhäuser, 1996.
- [8] Eugenio Bianchi and Robert C. Myers. On the architecture of spacetime geometry. *Classical and Quantum Gravity*, 31(21):214002, 2014.
- [9] J. J. Bisognano and E. H. Wichmann. On the duality condition for a hermitian scalar field. *Journal of Mathematical Physics*, 16:985–1007, 1975.
- [10] Joseph J. Bisognano and Eyyvind H. Wichmann. On the duality condition for a hermitian scalar field. *Journal of Mathematical Physics*, 17(3):303–321, 1976.
- [11] Luca Bombelli, Rabinder K. Koul, Joohan Lee, and Rafael D. Sorkin. Quantum source of entropy for black holes. *Physical Review D*, 34(2):373–383, 1986.
- [12] H.-J. Borchers. On the use of modular groups in quantum field theory. *Annales de l'Institut Henri Poincaré (A) Physique théorique*, 63(4):331–382, 1995.
- [13] Raphael Bousso. The holographic principle, 2002.
- [14] Ola Bratteli and Derek W. Robinson. *Operator Algebras and Quantum Statistical Mechanics 2*. Springer, 1987.
- [15] Heinz-Peter Breuer and Francesco Petruccione. *The Theory of Open Quantum Systems*. Oxford University Press, 2002.
- [16] Herbert B. Callen. *Thermodynamics and an Introduction to Thermostatics*. Wiley, 2 edition, 1985.
- [17] Sean M. Carroll. *Spacetime and Geometry*. Addison-Wesley, 2004.
- [18] E. B. Davies. Markovian master equations. *Communications in Mathematical Physics*, 39:91–110, 1974.

- [19] S. R. de Groot and P. Mazur. *Non-Equilibrium Thermodynamics*. Dover, 1984.
- [20] S. R. De Groot and P. Mazur. *Non-Equilibrium Thermodynamics*. Dover, 1984.
- [21] Scott Dodelson. *Modern Cosmology*. Academic Press, 2003.
- [22] Chas A. Egan and Charles H. Lineweaver. A larger estimate of the entropy of the universe. *The Astrophysical Journal*, 710(2):1825–1834, 2010.
- [23] Massimiliano Esposito and Christian Van den Broeck. Entropy production in open systems. *Physical Review Letters*, 104(9):090601, 2010.
- [24] Massimiliano Esposito and Christian Van den Broeck. Second law and landauer principle far from equilibrium. *Europhysics Letters*, 95:40004, 2011.
- [25] Benoit Famaey and Stacy McGaugh. Modified newtonian dynamics (mond): Observational phenomenology and relativistic extensions. *Living Reviews in Relativity*, 15(10), 2012.
- [26] Xiaohui Fan, Chris L. Carilli, and Brian Keating. Observational constraints on cosmic reionization, 2006.
- [27] D. J. Fixsen. The temperature of the cosmic microwave background. *The Astrophysical Journal*, 707:916–920, 2009.
- [28] D. J. et al. Fixsen. The cosmic microwave background spectrum from the full cobe firas data set. *Astrophysical Journal*, 473:576, 1996.
- [29] Dale J. et al. Fixsen. The cosmic microwave background spectrum from the full cobe firas data set. *The Astrophysical Journal*, 473:576–587, 1996.
- [30] Bernard Gaveau. Principe de moindre action, propagation de la chaleur et estimées sous elliptiques sur certains groupes nilpotents. *Acta Mathematica*, 139:95–153, 1977.
- [31] Gary W. Gibbons and Stephen W. Hawking. Cosmological event horizons, thermodynamics, and particle creation. *Physical Review D*, 15(10):2738–2751, 1977.
- [32] Alister W. Graham. The local supermassive black hole mass density. *Monthly Notices of the Royal Astronomical Society: Letters*, 380(1):L15–L19, 2007.
- [33] Mikhail Gromov. Carnot–carathéodory spaces seen from within. In *Sub-Riemannian Geometry*. Birkhäuser, 1996.
- [34] Rudolf Haag, Nico M. Hugenoltz, and Marinus Winnink. On the equilibrium states in quantum statistical mechanics. *Communications in Mathematical Physics*, 5:215–236, 1967.

- [35] Fred Hamann and Gary Ferland. Elemental abundances in quasistellar objects: Star formation and galactic nuclear evolution at high redshifts. *Annual Review of Astronomy and Astrophysics*, 37:487–531, 1999.
- [36] M. G. Hauser and E. Dwek. The cosmic infrared background: Measurements and implications. *Annual Review of Astronomy and Astrophysics*, 39:249–307, 2001.
- [37] Stephen W. Hawking. Particle creation by black holes. *Communications in Mathematical Physics*, 43:199–220, 1975.
- [38] Lars Hörmander. Hypoelliptic second order differential equations. *Acta Mathematica*, 119:147–171, 1967.
- [39] Werner Israel. Thermo-field dynamics of black holes. *Physics Letters A*, 57(2):107–110, 1976.
- [40] Yuri I. Izotov and Trinh X. Thuan. Systematic effects and a new determination of the primordial helium abundance. *Astrophysical Journal*, 710:L67–L71, 2010.
- [41] Ted Jacobson. Thermodynamics of spacetime: The einstein equation of state. *Physical Review Letters*, 75(7):1260–1263, 1995.
- [42] Joel L. Lebowitz and Herbert Spohn. A gallavotti–cohen-type symmetry in the large deviation functional for stochastic dynamics. *Journal of Statistical Physics*, 95:333–365, 1999.
- [43] Julien Lesgourgues and Sergio Pastor. *Neutrino Cosmology*. Cambridge University Press, 2013.
- [44] Stacy S. McGaugh, Federico Lelli, and James M. Schombert. The radial acceleration relation in rotationally supported galaxies. *Physical Review Letters*, 117(20):201101, 2016.
- [45] M. Milgrom. A modification of the newtonian dynamics as a possible alternative to the hidden mass hypothesis. *Astrophysical Journal*, 270:365–370, 1983.
- [46] Richard Montgomery. *A Tour of Sub-Riemannian Geometries, Their Geodesics and Applications*. American Mathematical Society, 2002.
- [47] Michael A. Nielsen and Isaac L. Chuang. *Quantum Computation and Quantum Information*. Cambridge University Press, 10th anniversary edition, 2010.
- [48] T. Padmanabhan. Thermodynamical aspects of gravity: New insights. *Reports on Progress in Physics*, 73(4):046901, 2010.
- [49] Bernard E. J. Pagel. *Nucleosynthesis and Chemical Evolution of Galaxies*. Cambridge University Press, 1997.

- [50] P. J. E. Peebles. *Principles of Physical Cosmology*. Princeton University Press, 1993.
- [51] P. J. E. Peebles and B. Ratra. The cosmological constant and dark energy. *Reviews of Modern Physics*, 75:559–606, 2003.
- [52] R. Penrose. Singularities and time-asymmetry. *General Relativity: An Einstein Centenary Survey*, 1979.
- [53] Ilya Prigogine. *Introduction to Thermodynamics of Irreversible Processes*. Interscience, 1967.
- [54] Adam G. et al. Riess. A comprehensive measurement of the local value of the hubble constant, 2022.
- [55] Vera C. Rubin and W. Kent Ford. Rotational properties of 21 sc galaxies with a large range of luminosities and radii. *The Astrophysical Journal*, 238:471–487, 1980.
- [56] George B. Rybicki and Alan P. Lightman. *Radiative Processes in Astrophysics*. Wiley, 1979.
- [57] George B. Rybicki and Alan P. Lightman. *Radiative Processes in Astrophysics*. Wiley, 1979.
- [58] Barbara Ryden. *Introduction to Cosmology*. Cambridge University Press, 2 edition, 2016.
- [59] Francesco Shankar, David H. Weinberg, and Jordi Miralda-Escudé. Self-consistent models of the agn and black hole populations. *The Astrophysical Journal*, 690(1):20–41, 2009.
- [60] Y. Sofue and V. Rubin. Rotation curves of spiral galaxies, 2001.
- [61] Andrzej Sołtan. Masses of quasars. *Monthly Notices of the Royal Astronomical Society*, 200:115–122, 1982.
- [62] James Sorce. An intuitive construction of modular flow. 2023.
- [63] Herbert Spohn. Entropy production for quantum dynamical semigroups. *Journal of Mathematical Physics*, 19:1227–1230, 1978.
- [64] Mark Srednicki. Entropy and area. *Physical Review Letters*, 71(5):666–669, 1993.
- [65] Beatrice M. Tinsley. Evolution of the stars and gas in galaxies. *Fundamentals of Cosmic Physics*, 5:287–388, 1980.
- [66] William G. Unruh. Notes on black-hole evaporation. *Physical Review D*, 14:870–892, 1976.

- [67] N. Th. Varopoulos, L. Saloff-Coste, and T. Coulhon. Analysis and geometry on groups. *Cambridge Tracts in Mathematics*, 1992.
- [68] Vlatko Vedral. The role of relative entropy in quantum information theory. *Reviews of Modern Physics*, 74:197–234, 2002.
- [69] Robert M. Wald. *General Relativity*. University of Chicago Press, 1984.
- [70] Robert M. Wald. *Quantum Field Theory in Curved Spacetime and Black Hole Thermodynamics*. University of Chicago Press, 1994.
- [71] Robert M. Wald. The thermodynamics of black holes. *Living Reviews in Relativity*, 4(6), 2001.
- [72] S. Weinberg. *Cosmology*. Oxford University Press, 2008.
- [73] Steven Weinberg. *Cosmology*. Oxford University Press, 2008.
- [74] Steven Weinberg. *Cosmology*. Oxford University Press, 2008.
- [75] M. Wilkinson. Spherical ornstein-uhlenbeck processes. 2011.
- [76] Edward Witten. Aps medal for exceptional achievement in research: Invited article on entanglement entropy. *Reviews of Modern Physics*, 90:045003, 2018.
- [77] S. E. Woosley and T. A. Weaver. The evolution and explosion of massive stars. ii. explosive hydrodynamics and nucleosynthesis. *Astrophysical Journal Supplement Series*, 101:181–235, 1995.
- [78] Robert Zwanzig. *Nonequilibrium Statistical Mechanics*. Oxford University Press, 2001.

## A Curved model geometries

**Context and purpose.** The main text models the mesoscopic exterior by a Carnot–Carathéodory (CC) tangent law, whose simplest flat local model is the Heisenberg group (or more generally a step–two Carnot group) equipped with a canonical contact structure and a Hamiltonian geodesic flow. The aim of the present appendix is not to add new cosmological assumptions, but to record the corresponding *curved* homogeneous model geometries that play the same structural role:  $SU(2)$  and  $SL(2, \mathbb{R})$  are the constant–curvature deformations (positive and negative) of the Heisenberg model, while  $Sp(2)$  and  $Sp(1, 1)$  are the natural quaternionic analogues relevant to four–dimensional Euclidean and Lorentzian signatures. In each case the construction preserves the same ingredients used in the bulk: a contact (horizontal) distribution, an invariant quadratic (or norm) Hamiltonian, and the resulting second–order dynamics governed by the same step–two bracket structure. These models provide a concrete reference

class showing that the CC/Heisenberg tangent law admits geometrically natural global realizations and constant-curvature variants, so that the mesoscopic frequency scale  $\sigma$  should be viewed as an emergent kinematical rate associated with the underlying horizontal/vertical mixing rather than an ad hoc parameter.

### A.1 $SU(2)$

We shall work in  $\mathbb{C}^2$ . Let  $\epsilon(W \wedge Z)$  be the determinant of the  $2 \times 2$  matrix with columns  $Z, W \in \mathbb{C}^2$ . Let  $\epsilon(Z) := \epsilon(- \wedge Z)$ , so that  $W \cdot \epsilon(Z) = \epsilon(W \wedge Z)$ . In terms of the standard basis, we have  $\epsilon(Z) = [z_2, -z_1]$ , i.e.,

$$\epsilon = \begin{bmatrix} 0 & 1 \\ -1 & 0 \end{bmatrix}.$$

We also have

$$\epsilon(\epsilon(Z)) = -Z$$

and

$$\epsilon(Z) \cdot \epsilon(W) = Z \cdot W.$$

Let  $Z, P \in \mathbb{C}^2$ . Let  $\theta = P \cdot dZ + \bar{P} \cdot d\bar{Z}$ , and let  $d\theta$  define a Poisson bracket. Define  $M = \epsilon(P \wedge \bar{Z})$ ,  $\bar{M} = \epsilon(\bar{P} \wedge Z)$ , and  $H = M\bar{M}$ .

Note that  $Z \cdot \bar{Z}$  and  $P \cdot \bar{P}$  Poisson commute with  $H$ . Also, the symplectic gradient of  $H$  is tangent to the contact distribution  $\theta = i(Z \cdot d\bar{Z} - \bar{Z} \cdot dZ)$  on the 3-dimensional hypersurface  $Z \cdot \bar{Z} = 1$ .

Let  $N = \{M, M\} \in i\mathbb{R}$ . Then  $\dot{N} = \{N, H\} = 0$ . We have the Hamilton equations

$$\begin{aligned} \dot{Z} &= \{Z, H\} = \epsilon(\bar{Z})\bar{M} \\ \dot{\bar{Z}} &= \{\bar{Z}, H\} = \epsilon(Z)M. \end{aligned}$$

Taking another derivative on the first of these gives

$$\begin{aligned} \ddot{Z} &= \epsilon(\dot{\bar{Z}})\bar{M} + \epsilon(\bar{Z})\dot{\bar{M}} \\ &= \epsilon(\epsilon(Z))M\bar{M} - \epsilon(\bar{Z})\bar{M}N \\ &= -ZM\bar{M} - \dot{Z}N \end{aligned}$$

so that

$$\ddot{Z} + \dot{Z}N + ZM\bar{M} = 0.$$

The characteristic polynomial is  $\lambda^2 + \lambda N + M\bar{M}$ , with roots  $\lambda_1, \lambda_2$  given by

$$\lambda = -\frac{N}{2} \pm \frac{1}{2}\sqrt{N^2 - 4M\bar{M}} \in i\mathbb{R}.$$

We have  $N = -(\lambda_1 + \lambda_2)$  and  $H = \lambda_1\lambda_2$ .

Solutions have the form

$$Z = e^{\lambda_1 t}Z_1 + e^{\lambda_2 t}Z_2.$$

Note that, from  $Z \cdot \bar{Z} = 1$ , we have  $Z_1 \cdot \bar{Z}_2 = 0$ ,  $Z_1 \cdot \bar{Z}_1 + Z_2 \cdot \bar{Z}_2 = 1$ .

To find the relation between  $Z_1, Z_2, \lambda_1, \lambda_2$ , we first deduce a formula for  $M, \bar{M}$  in terms of  $\lambda_1, \lambda_2, Z_1, Z_2$ . We have on one hand

$$\epsilon(Z \wedge \dot{Z}) = \epsilon(Z \wedge \epsilon(\bar{Z}))\bar{M} = -Z \cdot \bar{Z}\bar{M} = -\bar{M}$$

On the other hand,

$$\begin{aligned}\epsilon(Z \wedge \dot{Z}) &= \epsilon((e^{\lambda_1 t} Z_1 + e^{\lambda_2 t} Z_2) \wedge (\lambda_1 e^{\lambda_1 t} Z_1 + \lambda_2 e^{\lambda_2 t} Z_2)) \\ &= (\lambda_2 - \lambda_1) e^{(\lambda_1 + \lambda_2)t} \epsilon(Z_1 \wedge Z_2).\end{aligned}$$

Thus

$$\begin{aligned}\bar{M} &= (\lambda_1 - \lambda_2) \epsilon(Z_1 \wedge Z_2) e^{-Nt} \\ M &= (\lambda_2 - \lambda_1) \epsilon(\bar{Z}_1 \wedge \bar{Z}_2) e^{Nt}.\end{aligned}\tag{123}$$

Next, we have

$$\begin{aligned}\dot{Z} &= \lambda_1 e^{\lambda_1 t} Z_1 + \lambda_2 e^{\lambda_2 t} Z_2 \\ \epsilon(\bar{Z})\bar{M} &= (e^{-\lambda_1 t} \epsilon(\bar{Z}_1) + e^{-\lambda_2 t} \epsilon(\bar{Z}_2))(\lambda_1 - \lambda_2) \epsilon(Z_1 \wedge Z_2) e^{-Nt}.\end{aligned}$$

Equating coefficients, we have

$$\begin{aligned}\lambda_1 Z_1 &= (\lambda_1 - \lambda_2) \epsilon(Z_1 \wedge Z_2) \epsilon(\bar{Z}_2) \\ \lambda_2 Z_2 &= (\lambda_1 - \lambda_2) \epsilon(Z_1 \wedge Z_2) \epsilon(\bar{Z}_1).\end{aligned}$$

Note that this can be rewritten in the equivalent form

$$\begin{aligned}\lambda_1 Z_1 &= \bar{M} e^{Nt} \epsilon(\bar{Z}_2) \\ \lambda_2 Z_2 &= \bar{M} e^{Nt} \epsilon(\bar{Z}_1).\end{aligned}\tag{124}$$

Taking the respective inner products with  $\epsilon(Z_2)$  and  $\epsilon(Z_1)$  gives

$$\begin{aligned}\lambda_1 \epsilon(Z_1 \wedge Z_2) &= (\lambda_1 - \lambda_2) \epsilon(Z_1 \wedge Z_2) Z_2 \cdot \bar{Z}_2 \\ \lambda_2 \epsilon(Z_2 \wedge Z_1) &= (\lambda_1 - \lambda_2) \epsilon(Z_1 \wedge Z_2) Z_1 \cdot \bar{Z}_1.\end{aligned}$$

So we find

$$\begin{aligned}Z_1 \cdot \bar{Z}_1 &= \frac{\lambda_2}{\lambda_2 - \lambda_1} \\ Z_2 \cdot \bar{Z}_2 &= \frac{\lambda_1}{\lambda_1 - \lambda_2}.\end{aligned}$$

(Note that we have the required relation  $Z_1 \cdot \bar{Z}_1 + Z_2 \cdot \bar{Z}_2 = 1$ .)

We now determine the evolution of the  $P$  variable. We have

$$\begin{aligned}\dot{P} &= \{P, H\} = \epsilon(\bar{P})M \\ \dot{\bar{P}} &= \{\bar{P}, H\} = \epsilon(P)\bar{M}.\end{aligned}$$

$$\begin{aligned}
\ddot{P} &= \epsilon(\dot{P})M + \epsilon(\bar{P})\dot{M} \\
&= \epsilon(\epsilon(P))M\bar{M} + \epsilon(\bar{P})MN \\
&= -PM\bar{M} + \dot{P}N.
\end{aligned}$$

So we have

$$\ddot{P} - \dot{P}N + PM\bar{M} = 0.$$

The roots are  $-\lambda_1 = \bar{\lambda}_1, -\lambda_2 = \bar{\lambda}_2$ .

Write  $P = e^{-\lambda_1 t}P_1 + e^{-\lambda_2 t}P_2$ . Then

$$\begin{aligned}
M &= \epsilon(P \wedge \bar{Z}) \\
&= e^{-(\lambda_1 + \lambda_2)t} \epsilon(P_1 \wedge \bar{Z}_2 + P_2 \wedge \bar{Z}_1) + e^{-2\lambda_1 t} \epsilon(P_1 \wedge \bar{Z}_1) + e^{-\lambda_2 t} \epsilon(P_2 \wedge \bar{Z}_2).
\end{aligned} \tag{125}$$

These last two terms must vanish identically, and so  $P_1 = A_1 \bar{Z}_1, P_2 = A_2 \bar{Z}_2$  for some constants  $A_1, A_2$  to be determined.

We have

$$\begin{aligned}
\dot{P} &= \epsilon(\bar{P})M \\
&= e^{\lambda_1 t} \bar{A}_1 \epsilon(Z_1)M + e^{\lambda_2 t} \bar{A}_2 \epsilon(Z_2)M \\
\dot{P} &= -e^{-\lambda_1 t} A_1 \lambda_1 \bar{Z}_1 - e^{-\lambda_2 t} A_2 \lambda_2 \bar{Z}_2.
\end{aligned}$$

Equating coefficients, we find

$$\begin{aligned}
Me^{-Nt} \bar{A}_1 \epsilon(Z_1) &= -A_2 \lambda_2 \bar{Z}_2 \\
Me^{-Nt} \bar{A}_2 \epsilon(Z_2) &= -A_1 \lambda_1 \bar{Z}_1.
\end{aligned}$$

But the terms on the left-hand side can be rewritten using (124) to give

$$\begin{aligned}
-\bar{A}_1 \lambda_2 \bar{Z}_2 &= -A_2 \lambda_2 \bar{Z}_2 \\
-\bar{A}_2 \lambda_1 \bar{Z}_1 &= -A_1 \lambda_1 \bar{Z}_1,
\end{aligned}$$

i.e.,  $\bar{A}_1 = A_2, \bar{A}_2 = A_1$ .

Turning again to (125), we have

$$\begin{aligned}
Me^{-Nt} &= \epsilon(P_1 \wedge \bar{Z}_1 + P_2 \wedge \bar{Z}_2) \\
&= (A_2 - A_1) \epsilon(\bar{Z}_1 \wedge \bar{Z}_2)
\end{aligned}$$

but by (123),  $Me^{-Nt} = (\lambda_2 - \lambda_1) \epsilon(\bar{Z}_1 \wedge \bar{Z}_2)$ , so we have  $A_2 - A_1 = \lambda_2 - \lambda_1$ .

The general solution is thus

$$\begin{aligned}
P &= A_1 e^{-\lambda_1 t} \bar{Z}_1 + A_2 e^{-\lambda_2 t} \bar{Z}_2 \\
A_1 &= \frac{\lambda_1 - \lambda_2}{2} + c \\
A_2 &= \frac{\lambda_2 - \lambda_1}{2} + c
\end{aligned}$$

where  $c$  is real.

### A.1.1 Clifford tori

Given a pair of non-zero vectors  $Z_1, Z_2 \in \mathbb{C}^2$  such that  $Z_1 \cdot \bar{Z}_1 + Z_2 \cdot \bar{Z}_2 = 1$  and  $Z_1 \cdot \bar{Z}_2 = 0$ , the subset of  $\mathbb{S}^3$ :

$$\{e^{i\theta}Z_1 + e^{i\phi}Z_2 | \theta, \phi \in \mathbb{R}\}$$

is the *Clifford torus* determined by the pair  $Z_1, Z_2$ . A Clifford torus is topologically a torus, and we have shown that each geodesic of  $H_{\mathbb{S}^3}$  lies on some Clifford torus. Every Clifford torus is an orbit of a maximal toral subgroup of  $U(2)$ .

The three-sphere  $S^3 \subset \mathbb{C}^2$  is fibred, by the Hopf fibration, over  $\mathbb{CP}^1 = S^2$ , which results by identifying  $Z$  with  $\lambda Z$  for  $\lambda \in U(1)$ . Thus, we can obtain the stereographic projection of the Hopf map by dividing the coordinates of a point of  $S^3$ :  $(z, w) \mapsto z/w$ . The image of the geodesic  $Z = e^{\lambda_1 t}Z_1 + e^{\lambda_2 t}Z_2$  is on a circle of the sphere. The circle is not a great circle unless  $N = 0$ , a special case to which we now turn.

## A.2 $N = 0$

The case  $N = 0$  is worthy of special consideration. In this case,  $M$  is constant and  $Z$  satisfies

$$\ddot{Z} = -M\bar{M}Z,$$

so the geodesic is a simple harmonic oscillator. In fact, we have  $\lambda_1 = -\lambda_2$ , and so

$$Z = e^{\lambda_1 t}Z_1 + e^{-\lambda_1 t}Z_2$$

is a great circle of the three-sphere. Under the Hopf map, this projects to a great circle of  $S^2$ . Conversely, any geodesic that projects to a great circle is of this kind.

### A.2.1 The Cayley transform

We consider a biholomorphism of the unit ball  $B_1(\mathbb{C}^2)$  in  $\mathbb{C}^2$ , defined by  $z\bar{z} + w\bar{w} < 1$ , onto the Siegel domain

$$\mathcal{S} = \{(Z, W) \in \mathbb{C}^2 | i(\bar{W} - W) > 2Z\bar{Z}\}.$$

The mapping  $\chi : B_1(\mathbb{C}^2) \rightarrow \mathcal{S}$  is given by the Cayley transform:

$$\chi : (z, w) \mapsto (Z, W) = \left( i \frac{z}{1-w}, i \frac{1+w}{1-w} \right).$$

Note that

$$\chi^{-1} : (Z, W) \mapsto (z, w) = \left( \frac{2Z}{W+i}, \frac{W-i}{W+i} \right).$$

Let  $\rho(Z, W) = 2Z\bar{Z} + i(W - \bar{W})$ . Then, with  $Z = i\frac{z}{1-w}$ ,  $W = i\frac{1+w}{1-w}$ , note that

$$\rho(Z, W) = 2 \frac{z\bar{z} + w\bar{w} - 1}{|1-w|^2}$$

which is negative if and only if  $(z, w) \in B_1(\mathbb{C}^2)$ . The transformation  $\chi$  has a continuous extension to  $\overline{B_1(\mathbb{C}^2)} \setminus \{(0, 1)\}$ , and maps bijectively to  $\overline{\mathcal{S}}$ . The contact one-form  $i\theta = (z d\bar{z} - \bar{z} dz) + (w d\bar{w} - \bar{w} dw)$  on the boundary becomes

$$i\theta = 2|w + i|^{-2} (2(Z d\bar{Z} - \bar{Z} dZ) - i(dW + d\bar{W})).$$

With

$$P = p_z \bar{w} - p_w \bar{z},$$

on the boundary (setting  $2Z\bar{Z} = I(\bar{W} - W)$ ):

$$P = \frac{W + i}{\bar{W} - i} ((\bar{W} + i)(p_Z - ip_W Z) + 2ip_W \bar{Z}).$$

Keeping only the terms of lowest homogeneity gives the Gromov tangent space:

$$\begin{aligned} \hat{P} &= p_Z + p_W (2\bar{Z} - iZ) \\ \hat{\bar{P}} &= p_{\bar{Z}} + p_{\bar{W}} (2Z - i\bar{Z}) \\ \{\hat{P}, \hat{\bar{P}}\} &= 2(p_W - p_{\bar{W}}). \end{aligned}$$

Thus we recover the Heisenberg group as the tangent space.

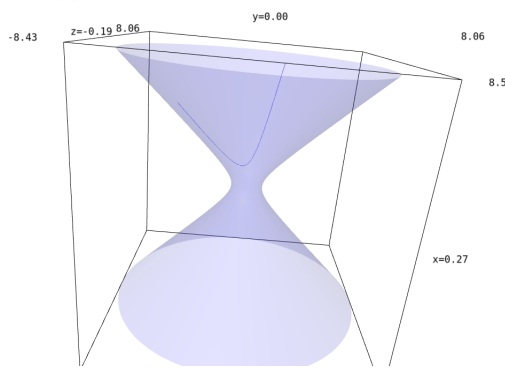


Figure 3: Typical geodesic, projected to the de Sitter space under the Hopf map

### A.3 $SL_2(\mathbb{R})$

We consider the spacetime as the three-dimensional Lie group  $SL_2(\mathbb{R}) \cong SU(1, 1) \cong Spin(1, 2)$ . Regarded as the spin group, this group admits a homogeneous action on the hyperboloid of one sheet in  $\mathbb{R}^3$  (two-dimensional de Sitter space). The corresponding anti-de Sitter space is one sheet of the hyperboloid of two sheets, which is just a model of the hyperbolic plane. As a spacetime, since the group is three-dimensional, this model will have one spatial one one time dimension, plus one small dimension analogous to the  $h, p_h$  direction of the Heisenberg model.

We describe the space using a complex model of  $SL_2(\mathbb{R})$ . For a vector  $Z \in \mathbb{C}^2$ ,  $Z = [z_1 \ z_2]$ , let

$$Z^\sigma = \begin{bmatrix} \bar{z}_2 \\ \bar{z}_1 \end{bmatrix}.$$

Note that

$$Z^\sigma = S \bar{Z}^T$$

$$\text{where } S = \begin{bmatrix} 0 & 1 \\ 1 & 0 \end{bmatrix}.$$

With  $\epsilon$  as before, we now have

$$\epsilon(\epsilon(Z^\sigma)^\sigma) = Z.$$

Let  $M = \epsilon(P \wedge Z^\sigma)$ ,  $\bar{M} = -\epsilon(P^\sigma \wedge Z)$ ,  $H = M \bar{M}$ ,  $N = \{M, \bar{M}\} \in i\mathbb{R}$ . Then  $\{N, H\} = \{Z \cdot Z^\sigma, H\} = \{P \cdot P^\sigma, H\} = 0$ .

We have  $M = MN$ ,

$$\begin{aligned} \dot{Z} &= \epsilon(Z^\sigma) \bar{M} \\ \dot{Z}^\sigma &= -\epsilon(Z) M \\ \ddot{Z} &= \epsilon(\dot{Z}^\sigma) \bar{M} + \epsilon(Z^\sigma) \dot{\bar{M}} \\ &= -\epsilon(\epsilon(Z) M) \bar{M} - \epsilon(Z^\sigma) \bar{M} N \\ &= Z M \bar{M} - \dot{Z} N, \end{aligned}$$

so

$$\ddot{Z} + \dot{Z}N - ZM\bar{M} = 0.$$

The characteristic polynomial is  $\lambda^2 + N\lambda - M\bar{M}$ , with roots  $\lambda_1, \lambda_2$  given by

$$\lambda = -\frac{N}{2} \pm \frac{1}{2}\sqrt{N^2 + 4M\bar{M}}.$$

We have  $N = -(\lambda_1 + \lambda_2)$  and  $H = -\lambda_1\lambda_2$ .

There are three possibilities, depending on the sign of the discriminant:

- $\lambda_1 - \lambda_2 \in \mathbb{R}$ :  $\lambda_1 = -\bar{\lambda}_2, \lambda_2 = -\bar{\lambda}_1$  (“timelike” case)
- $\lambda_1 - \lambda_2 \in i\mathbb{R}$ :  $\lambda_1 = -\bar{\lambda}_1, \lambda_2 = -\bar{\lambda}_2$  (“spacelike” case)
- $\lambda_1 = \lambda_2 = -\bar{\lambda}_1 = -\bar{\lambda}_2$  (“null” case)

We shall write

$$Z = e^{\lambda_1 t} Z_1 + e^{\lambda_2 t} Z_2$$

Let  $K = Z \cdot Z^\sigma$ , which is real, nonzero, and constant.

Note that on the one hand

$$\begin{aligned} \epsilon(Z \wedge \dot{Z}) &= \epsilon(Z \wedge \epsilon(Z^\sigma))\bar{M} \\ &= -Z \cdot Z^\sigma \bar{M} = -K\bar{M}. \end{aligned}$$

On the other hand,

$$\begin{aligned} \epsilon(Z \wedge \dot{Z}) &= \epsilon((e^{\lambda_1 t} Z_1 + e^{\lambda_2 t} Z_2) \wedge (\lambda_1 e^{\lambda_1 t} Z_1 + \lambda_2 e^{\lambda_2 t} Z_2)) \\ &= (\lambda_2 - \lambda_1) e^{(\lambda_1 + \lambda_2)t} \epsilon(Z_1 \wedge Z_2), \end{aligned}$$

so we get

$$\begin{aligned} K\bar{M} &= (\lambda_1 - \lambda_2) \epsilon(Z_1 \wedge Z_2) e^{-Nt} \\ KM &= -(\bar{\lambda}_1 - \bar{\lambda}_2) \epsilon(Z_1^\sigma \wedge Z_2^\sigma) e^{Nt}. \end{aligned} \tag{126}$$

#### A.4 Case $\lambda_1 - \lambda_2 \in \mathbb{R}$

Here  $\bar{\lambda}_1 = -\lambda_2$  and  $\bar{\lambda}_2 = -\lambda_1$ .

We have

$$\begin{aligned} \dot{Z} &= \lambda_1 e^{\lambda_1 t} Z_1 + \lambda_2 e^{\lambda_2 t} Z_2 \\ \epsilon(Z^\sigma) \bar{M} &= (e^{-\lambda_2 t} \epsilon(Z_1^\sigma) + e^{-\lambda_1 t} \epsilon(Z_2^\sigma))(\lambda_1 - \lambda_2) \epsilon(Z_1 \wedge Z_2) e^{-Nt} K^{-1}. \end{aligned}$$

Equating coefficients gives

$$\begin{aligned} \lambda_1 K Z_1 &= \epsilon(Z_1^\sigma)(\lambda_1 - \lambda_2) \epsilon(Z_1 \wedge Z_2) \\ \lambda_2 K Z_2 &= \epsilon(Z_2^\sigma)(\lambda_1 - \lambda_2) \epsilon(Z_1 \wedge Z_2). \end{aligned}$$

Equivalently,

$$\begin{aligned}\lambda_1 Z_1 &= \bar{M} e^{Nt} \epsilon(Z_1^\sigma) \\ \lambda_2 Z_2 &= \bar{M} e^{Nt} \epsilon(Z_2^\sigma) \\ \lambda_2 Z_1^\sigma &= M e^{-Nt} \epsilon(Z_1) \\ \lambda_1 Z_2^\sigma &= M e^{-Nt} \epsilon(Z_2).\end{aligned}\tag{127}$$

Taking the respective inner products with  $\epsilon(Z_2)$  and  $\epsilon(Z_1)$  gives

$$\begin{aligned}\lambda_1 K \epsilon(Z_1 \wedge Z_2) &= (\lambda_1 - \lambda_2) \epsilon(Z_1 \wedge Z_2) Z_2 \cdot Z_1^\sigma \\ \lambda_2 K \epsilon(Z_2 \wedge Z_1) &= (\lambda_1 - \lambda_2) \epsilon(Z_1 \wedge Z_2) Z_1 \cdot Z_2^\sigma.\end{aligned}$$

So we find

$$\begin{aligned}Z_2 \cdot Z_1^\sigma &= \frac{K \lambda_1}{\lambda_1 - \lambda_2} \\ Z_1 \cdot Z_2^\sigma &= \frac{K \lambda_2}{\lambda_2 - \lambda_1}.\end{aligned}$$

Now for the  $P$  variable, we have

$$\begin{aligned}\dot{P} &= \{P, M\} = -\epsilon(P^\sigma) M \\ \dot{P}^\sigma &= \{P^\sigma, M\} = \epsilon(P) \bar{M} \\ \ddot{P} &= -\epsilon(\dot{P}^\sigma) M - \epsilon(P^\sigma) \dot{M} \\ &= -\epsilon(\epsilon(P) \bar{M}) M - \epsilon(P^\sigma) M N \\ &= P M \bar{M} + \dot{P} N.\end{aligned}$$

So

$$\ddot{P} - \dot{P} N - P M \bar{M} = 0.$$

The characteristic polynomial is  $\mu^2 - N\mu - M\bar{M}$ , with roots  $\mu = \frac{N}{2} \pm \frac{1}{2}\sqrt{N^2 + 4M\bar{M}}$ , i.e.,  $\bar{\lambda}_1 = -\lambda_2$  and  $\bar{\lambda}_2 = -\lambda_1$ .

With  $P = e^{-\lambda_1 t} P_1 + e^{-\lambda_2 t} P_2$ , we have

$$\begin{aligned}M &= \epsilon(P \wedge Z^\sigma) \\ &= e^{-(\lambda_1 + \lambda_2)t} \epsilon(P_1 \wedge Z_1^\sigma + P_2 \wedge Z_2^\sigma) + e^{-2\lambda_1 t} \epsilon(P_1 \wedge Z_2^\sigma) + e^{-2\lambda_2 t} \epsilon(P_2 \wedge Z_1^\sigma).\end{aligned}\tag{128}$$

The last two terms must vanish identically, so we have  $P_1 = A_1 Z_2^\sigma$  and  $P_2 = A_2 Z_1^\sigma$  for some constants  $A_1, A_2$ .

Now we have

$$P^\sigma = \bar{A}_1 e^{\lambda_2 t} Z_2 + \bar{A}_2 e^{\lambda_1 t} Z_1$$

and so

$$\begin{aligned}\dot{P} &= -\epsilon(P^\sigma) M \\ &= -(\bar{A}_1 e^{\lambda_2 t} \epsilon(Z_2) + \bar{A}_2 e^{\lambda_1 t} \epsilon(Z_1)) M \\ \dot{P} &= -e^{-\lambda_1 t} A_1 \lambda_1 Z_2^\sigma - e^{-\lambda_2 t} \lambda_2 A_2 Z_1^\sigma.\end{aligned}$$

Equating coefficients,

$$\begin{aligned}-Me^{-Nt}\bar{A}_1\epsilon(Z_2) &= -A_1\lambda_1Z_2^\sigma \\ -Me^{-Nt}\bar{A}_2\epsilon(Z_1) &= -A_2\lambda_2Z_1^\sigma.\end{aligned}$$

Applying (127) to the left-hand sides gives:

$$\begin{aligned}-\bar{A}_1\lambda_1Z_2^\sigma &= -A_1\lambda_1Z_2^\sigma \\ -\bar{A}_2\lambda_2Z_1^\sigma &= -A_2\lambda_2Z_1^\sigma\end{aligned}$$

so that  $\bar{A}_1 = A_1$ ,  $\bar{A}_2 = A_2$ .

Now, using (128),

$$\begin{aligned}Me^{-Nt} &= \epsilon(P_1 \wedge Z_1^\sigma + P_2 \wedge Z_2^\sigma) \\ &= (A_2 - A_1)\epsilon(Z_1^\sigma \wedge Z_2^\sigma)\end{aligned}$$

But by (126),

$$KMe^{-Nt} = -(\bar{\lambda}_1 - \bar{\lambda}_2)\epsilon(Z_1^\sigma \wedge Z_2^\sigma) = (\lambda_2 - \lambda_1)\epsilon(Z_1^\sigma \wedge Z_2^\sigma).$$

So we have  $K(A_2 - A_1) = \lambda_2 - \lambda_1$ , and the general solution is

$$\begin{aligned}P &= A_1e^{-\lambda_1 t}Z_2^\sigma + A_2e^{-\lambda_2 t}Z_1^\sigma \\ A_1 &= \frac{\lambda_1 - \lambda_2}{2K} + c \\ A_2 &= \frac{\lambda_2 - \lambda_1}{2K} + c\end{aligned}$$

where  $c$  is real.

### A.5 Case $\lambda_1 - \lambda_2 \in i\mathbb{R}$

Here  $\bar{\lambda}_1 = -\lambda_1$  and  $\bar{\lambda}_2 = -\lambda_2$ .

We have

$$\begin{aligned}\dot{Z} &= \lambda_1 e^{\lambda_1 t}Z_1 + \lambda_2 e^{\lambda_2 t}Z_2 \\ \epsilon(Z^\sigma)\bar{M} &= (e^{-\lambda_1 t}\epsilon(Z_1^\sigma) + e^{-\lambda_2 t}\epsilon(Z_2^\sigma))(\lambda_1 - \lambda_2)\epsilon(Z_1 \wedge Z_2)e^{-Nt}K^{-1}.\end{aligned}$$

Equating coefficients gives

$$\begin{aligned}\lambda_1 K Z_1 &= \epsilon(Z_2^\sigma)(\lambda_1 - \lambda_2)\epsilon(Z_1 \wedge Z_2) \\ \lambda_2 K Z_2 &= \epsilon(Z_1^\sigma)(\lambda_1 - \lambda_2)\epsilon(Z_1 \wedge Z_2).\end{aligned}$$

Equivalently,

$$\begin{aligned}\lambda_1 Z_1 &= \bar{M}e^{Nt}\epsilon(Z_2^\sigma) \\ \lambda_2 Z_2 &= \bar{M}e^{Nt}\epsilon(Z_1^\sigma) \\ \lambda_2 Z_1^\sigma &= M e^{-Nt}\epsilon(Z_2) \\ \lambda_1 Z_2^\sigma &= M e^{-Nt}\epsilon(Z_1).\end{aligned}\tag{129}$$

Taking the respective inner products with  $\epsilon(Z_2)$  and  $\epsilon(Z_1)$  gives

$$\begin{aligned}\lambda_1 K \epsilon(Z_1 \wedge Z_2) &= (\lambda_1 - \lambda_2) \epsilon(Z_1 \wedge Z_2) Z_2 \cdot Z_2^\sigma \\ \lambda_2 K \epsilon(Z_2 \wedge Z_1) &= (\lambda_1 - \lambda_2) \epsilon(Z_1 \wedge Z_2) Z_1 \cdot Z_1^\sigma.\end{aligned}$$

So we find

$$\begin{aligned}Z_1 \cdot Z_1^\sigma &= \frac{K \lambda_2}{\lambda_1 - \lambda_2} \\ Z_2 \cdot Z_2^\sigma &= \frac{K \lambda_1}{\lambda_2 - \lambda_1}\end{aligned}$$

and (taking the opposite inner products)  $Z_1 \cdot Z_2^\sigma = 0$ .

Now for the  $P$  variable, we have

$$\begin{aligned}\dot{P} &= \{P, M\} = -\epsilon(P^\sigma)M \\ \dot{P}^\sigma &= \{P^\sigma, M\} = \epsilon(P)\bar{M} \\ \ddot{P} &= -\epsilon(\dot{P}^\sigma)M - \epsilon(P^\sigma)\dot{M} \\ &= -\epsilon(\epsilon(P)\bar{M})M - \epsilon(P^\sigma)MN \\ &= PM\bar{M} + \dot{P}N.\end{aligned}$$

So

$$\ddot{P} - \dot{P}N - PM\bar{M} = 0.$$

The characteristic polynomial is  $\mu^2 - N\mu - M\bar{M}$ , with roots  $\mu = \frac{N}{2} \pm \frac{1}{2}\sqrt{N^2 + 4M\bar{M}}$ , i.e.,  $\bar{\lambda}_1 = -\lambda_1$  and  $\bar{\lambda}_2 = -\lambda_2$ .

With  $P = e^{-\lambda_1 t}P_1 + e^{-\lambda_2 t}P_2$ , we have

$$\begin{aligned}M &= \epsilon(P \wedge Z^\sigma) \\ &= e^{-(\lambda_1 + \lambda_2)t} \epsilon(P_1 \wedge Z_2^\sigma + P_2 \wedge Z_1^\sigma) + e^{-2\lambda_1 t} \epsilon(P_1 \wedge Z_1^\sigma) + e^{-2\lambda_2 t} \epsilon(P_2 \wedge Z_2^\sigma).\end{aligned}\tag{130}$$

The last two terms must vanish identically, so we have  $P_1 = A_1 Z_1^\sigma$  and  $P_2 = A_2 Z_2^\sigma$  for some constants  $A_1, A_2$ .

Now we have

$$P^\sigma = \bar{A}_1 e^{\lambda_1 t} Z_1 + \bar{A}_2 e^{\lambda_2 t} Z_2$$

and so

$$\begin{aligned}\dot{P} &= -\epsilon(P^\sigma)M \\ &= -(\bar{A}_2 e^{\lambda_2 t} \epsilon(Z_2) + \bar{A}_1 e^{\lambda_1 t} \epsilon(Z_1))M \\ \dot{P} &= -e^{-\lambda_1 t} A_1 \lambda_1 Z_1^\sigma - e^{-\lambda_2 t} \lambda_2 A_2 Z_2^\sigma.\end{aligned}$$

Equating coefficients,

$$\begin{aligned}-M e^{-Nt} \bar{A}_2 \epsilon(Z_2) &= -A_1 \lambda_1 Z_1^\sigma \\ -M e^{-Nt} \bar{A}_1 \epsilon(Z_1) &= -A_2 \lambda_2 Z_2^\sigma.\end{aligned}$$

Applying (129) to the left-hand sides gives:

$$\begin{aligned}-\bar{A}_2\lambda_1Z_1^\sigma &= -A_1\lambda_1Z_1^\sigma \\ -\bar{A}_1\lambda_2Z_2^\sigma &= -A_2\lambda_2Z_2^\sigma\end{aligned}$$

so that  $\bar{A}_2 = A_1, \bar{A}_1 = A_2$ .

Now, using (130),

$$\begin{aligned}Me^{-Nt} &= \epsilon(P_1 \wedge Z_1^\sigma + P_2 \wedge Z_2^\sigma) \\ &= (A_2 - A_1)\epsilon(Z_1^\sigma \wedge Z_2^\sigma)\end{aligned}$$

But by (126),

$$KMe^{-Nt} = -(\bar{\lambda}_1 - \bar{\lambda}_2)\epsilon(Z_1^\sigma \wedge Z_2^\sigma) = (\lambda_1 - \lambda_2)\epsilon(Z_1^\sigma \wedge Z_2^\sigma).$$

So we have  $K(A_2 - A_1) = \lambda_1 - \lambda_2$ , and the general solution is

$$\begin{aligned}P &= A_1e^{-\lambda_1 t}Z_1^\sigma + A_2e^{-\lambda_2 t}Z_2^\sigma \\ A_1 &= \frac{\lambda_2 - \lambda_1}{2K} + c \\ A_2 &= \frac{\lambda_1 - \lambda_2}{2K} + c\end{aligned}$$

where  $c$  is real.

In summary, the trajectories in this case are similar to those in the case of  $SU(2)$ .

## A.6 $Sp(2)$

We next consider the structure group  $Sp(2) \cong Spin(5)$ , which is the Euclidean signature variant of the four-dimensional space-time model. This acts on the 4-sphere in the obvious way, and also on the 7-sphere. Our dynamical manifold will be the 7-sphere, regarded as the unit sphere of  $\mathbb{H}^2$ .

The reduced norm  $N(x)$  of an element of a central simple algebra  $A$  over  $k$  is defined as  $N_k(x) = \det_K(x)$ , where the determinant is computed in  $A \otimes_k K \cong M_n(A)$  where  $K|k$  is a splitting field of  $A$ . In the case of the real central simple algebra  $M_2(\mathbb{H})$ , we have  $K = \mathbb{C}$ . The isomorphism  $A \otimes_k K \cong M_n(K)$  is not compatible with the Galois group  $G(K|k)$ , but is twisted with a cocycle that cancels out when the determinant is taken, so the reduced norm is invariant and hence lies in  $k$ .

If  $t + xi + yj + zk$  is a quaternionic variable, then we define the associated momentum  $p_t - p_xi - p_yj - p_zk$  where  $p_t, p_x, p_y, p_z$  are the respective Poisson conjugates of  $t, x, y, z$ . For  $Z, P \in \mathbb{H}^2$ , define  $P \oplus Z^*$  to be the matrix in  $M_2(\mathbb{H})$  with columns  $P$  and  $Z^*$  (the quaternionic conjugate of  $Z^T$ ). Then define the Hamiltonian by

$$H = N(P \oplus Z^*).$$

Then  $H$  Poisson commutes with  $Z \cdot Z^*, P \cdot P^*$ . It is invariant under the group of symmetries  $\mathrm{Sp}(2)$ . The symplectic gradient of  $H$  is tangent to the codimension 3 contact structure  $\theta = Z \cdot dZ^* - Z^* \cdot dZ$ .

**Theorem 1.** *The generic geodesic for the Hamiltonian  $H$  is given by*

$$Z = e^{\mu_1 u t} Z_1 + e^{\mu_2 u t} Z_2$$

$$P = A_1 e^{-\mu_1 u t} Z_1^* + A_2 e^{-\mu_2 u t} Z_2^*$$

where  $u \in \mathrm{im} \mathbb{H}$ ,  $Z_1 u = u Z_1$ ,  $Z_2 u = u Z_2$ ,  $\mu_1, \mu_2 \in \mathbb{R}$ , and

$$Z_1 \cdot Z_1^* = \frac{\mu_2}{\mu_2 - \mu_1}, \quad Z_2 \cdot Z_2^* = \frac{\mu_1}{\mu_1 - \mu_2}, \quad Z_1 \cdot Z_2^* = Z_2 \cdot Z_1^* = 0$$

$$A_1 = \frac{\mu_1 - \mu_2}{2} u + c, \quad A_2 = \frac{\mu_2 - \mu_1}{2} u + c$$

where  $c$  is a real constant, and  $\mu_1, \mu_2, u$  are conserved along the geodesic.

The limiting geodesics are great circles on  $S^4$ .

*Proof.* We first count parameters. On the one hand, an initial point on the 7-sphere, and then a vector tangent to the all three contact distributions gets 11 dimensions, minus one dimension because each geodesic is counted overcounted, for a 10 dimensional family of geodesics. On the other hand, there is a 6-parameter family of totally geodesic 2-spheres on the 4-sphere. Each 2-sphere then has a 4-parameter family of geodesics on it for the corresponding copy of  $SU(2)$  inside  $SP(2)$ , again making 10 parameters.

To prove the theorem, we shall show that, for any geodesic  $Z$ , there exists an imaginary quaternion  $u$  such that  $uZ = Zu$ .

...

□

## A.7 $\mathrm{Sp}(1, 1)$

We come finally to the group  $\mathrm{Sp}(1, 1) \cong \mathrm{Spin}(1, 4)$ , which is a group of symmetries of the de Sitter spacetime (and a group of isometries of the four-dimensional hyperbolic space). We recall some generalities on this group. Let  $\mathbb{H}$  denote the space of quaternions, the degree four division algebra over  $\mathbb{R}$ , with conjugation denoted by  $z \mapsto \bar{z}$ . For a  $2 \times 2$  matrix  $A \in M_2(\mathbb{H})$  with entries in  $\mathbb{H}$ , let  $A^* = \bar{A}^T$ , where the bar denotes entrywise conjugation and the  $T$  denotes the transpose. Let

$$S = \begin{bmatrix} 0 & 1 \\ 1 & 0 \end{bmatrix}.$$

Define  $A^\sigma = SA^*S^{-1} = SA^*S$ .

**Definition 1.** *The group  $\mathrm{Sp}(1, 1)$  is the set of  $A \in M_2(\mathbb{H})$  such that  $A^\sigma A = I$ .*

For  $x \in M_2(\mathbb{H})$ , define the reduced trace  $T_{\mathbb{R}}(x) = T_{\mathbb{H}|\mathbb{R}} \mathrm{tr}(x)$ . Also define the  $\mathbb{R}$ -bilinear form  $k(x, y) = T_{\mathbb{R}}(xy)$ . The group  $\mathrm{Sp}(1, 1)$  acts on  $M_2(\mathbb{H})$  by conjugation:  $x \mapsto Ax A^\sigma$ , and this leaves the form  $k(x, y)$  invariant. The subspace

$\mathbb{X} = \{x \in M_2(\mathbb{H}) \mid x^\sigma = x, k(x, S) = 0\}$  is also invariant under the group. On this subspace,  $k$  is a quadratic form of signature  $(1, 4)$ , and this exhibits the two-to-one spin covering map  $\mathrm{Sp}(1, 1) \rightarrow SO_0(1, 4)$ .

We take as our phase space again pairs  $Z, P \in \mathbb{H}^2$ . The kinetic Hamiltonian is

$$H = N([P, Z^\sigma])$$

where  $Z^\sigma = Z^*S$ . Note that this can be calculated by using a representation of  $P$  and  $Z$  as  $4 \times 2$  matrices over  $\mathbb{C}$ , and computing a determinant.

**Theorem 2.**  $\{Z \cdot Z^\sigma, H\} = 0$

*Proof.* A brute force computation.  $\square$

**Theorem 3.** *The Gromov tangent space associated to the Hamiltonian  $H$  is the Poisson algebra generated by*

$$\begin{aligned} P_0 &= r_1 w_1 + r_2 w_2 + r_3 w_3 \\ P_1 &= q_1 + \frac{1}{2}(r_2 w_3 - r_3 w_2) \\ P_2 &= q_2 + \frac{1}{2}(r_3 w_1 - r_1 w_3) \\ P_3 &= q_3 + \frac{1}{2}(r_1 w_2 - r_2 w_1) \end{aligned}$$

where the variables  $q_i, r_i, w_i$  satisfy Poisson relations

$$\{w_i, q_j\} = 2\delta_{ij}, \quad \{q_i, q_j\} = \{q_i, r_j\} = \{w_i, w_j\} = \{r_i, r_j\} = 0.$$

In particular,  $P_0$  is central, and  $P_1, P_2, P_3$  generate the six dimensional Poisson algebra of §3.

*Proof.* The first step of the proof is to express  $H$  as a sum of four squares. We do this by taking its hessian in the  $p$ , and diagonalizing the resulting symmetric matrix. It is thus shown that

$$H = (Q_0^2 + Q_1^2 + Q_2^2 + Q_3^2)s$$

where

$$\begin{aligned}
s &= 2(z_{00}^2 + z_{01}^2 + z_{02}^2 + z_{03}^2)^{-1} \\
Q_0 &= p_{00}z_{00}^2 + p_{00}z_{01}^2 + p_{00}z_{02}^2 + p_{00}z_{03}^2 - (p_{10}z_{00} + p_{11}z_{01} + p_{12}z_{02} + p_{13}z_{03})z_{10} + \\
&\quad + (p_{11}z_{00} - p_{10}z_{01} + p_{13}z_{02} - p_{12}z_{03})z_{11} + (p_{12}z_{00} - p_{13}z_{01} - p_{10}z_{02} + p_{11}z_{03})z_{12} + \\
&\quad + (p_{13}z_{00} + p_{12}z_{01} - p_{11}z_{02} - p_{10}z_{03})z_{13} \\
Q_1 &= p_{01}z_{00}^2 + p_{01}z_{01}^2 + p_{01}z_{02}^2 + p_{01}z_{03}^2 - (p_{11}z_{00} - p_{10}z_{01} + p_{13}z_{02} - p_{12}z_{03})z_{10} - \\
&\quad - (p_{10}z_{00} + p_{11}z_{01} + p_{12}z_{02} + p_{13}z_{03})z_{11} + (p_{13}z_{00} + p_{12}z_{01} - p_{11}z_{02} - p_{10}z_{03})z_{12} - \\
&\quad - (p_{12}z_{00} - p_{13}z_{01} - p_{10}z_{02} + p_{11}z_{03})z_{13} \\
Q_2 &= p_{02}z_{00}^2 + p_{02}z_{01}^2 + p_{02}z_{02}^2 + p_{02}z_{03}^2 - (p_{12}z_{00} - p_{13}z_{01} - p_{10}z_{02} + p_{11}z_{03})z_{10} - \\
&\quad - (p_{13}z_{00} + p_{12}z_{01} - p_{11}z_{02} - p_{10}z_{03})z_{11} - (p_{10}z_{00} + p_{11}z_{01} + p_{12}z_{02} + p_{13}z_{03})z_{12} + \\
&\quad + (p_{11}z_{00} - p_{10}z_{01} + p_{13}z_{02} - p_{12}z_{03})z_{13} \\
Q_3 &= p_{03}z_{00}^2 + p_{03}z_{01}^2 + p_{03}z_{02}^2 + p_{03}z_{03}^2 - (p_{13}z_{00} + p_{12}z_{01} - p_{11}z_{02} - p_{10}z_{03})z_{10} + \\
&\quad + (p_{12}z_{00} - p_{13}z_{01} - p_{10}z_{02} + p_{11}z_{03})z_{11} - (p_{11}z_{00} - p_{10}z_{01} + p_{13}z_{02} - p_{12}z_{03})z_{12} - \\
&\quad - (p_{10}z_{00} + p_{11}z_{01} + p_{12}z_{02} + p_{13}z_{03})z_{13}.
\end{aligned}$$

We take the tangent space at the point  $Z = (1, 1)$ . We first find the privileged coordinates of degree 1 and  $-1$  at this point. To do so, we substitute  $Z = (1, 1)$  into the equations for  $Q$ , giving  $q_0 = \sqrt{s}Q_0 = p_{00} - p_{10}$ ,  $q_1 = \sqrt{s}Q_1 = p_{01} - p_{11}$ ,  $q_2 = \sqrt{s}Q_2 = p_{02} - p_{12}$ ,  $q_3 = \sqrt{s}Q_3 = p_{03} - p_{13}$ , so these quantities have degree  $-1$ . Next, the pairwise Poisson brackets of the  $Q_i$  show that  $r_1 = p_{01} + p_{11}$ ,  $r_2 = p_{02} + p_{12}$ ,  $r_3 = p_{03} + p_{13}$  are of degree  $-2$ . We dualize to obtain that  $w_1 = z_{01} - z_{11}$ ,  $w_2 = z_{02} - z_{12}$ ,  $w_3 = z_{03} - z_{13}$  are of degree 1. Now applying to  $\sqrt{s}Q_i$  the scalings  $q_i \mapsto q_i/t$ ,  $r_i \mapsto r_i/t^2$ ,  $w_i \mapsto tw_i$ , and keeping terms of order  $t^{-1}$  only, establishes the theorem.  $\square$

**Corollary 1.** *In the diagonalization  $H = (Q_0^2 + Q_1^2 + Q_2^2 + Q_3^2)s$ , the vector fields generated by  $Q_i\sqrt{s}$  generate a 7-dimensional Poisson algebra. In particular, they satisfy Chow's condition on the 7-dimensional space  $Z \cdot Z^\sigma = \text{constant}$ .*

*Proof.* The only part of the corollary that is not an immediate consequence of the theorem is the last statement. To show that  $Q_i\sqrt{s}$  Poisson commutes with  $Z \cdot Z^\sigma$  is again a brute force computation.  $\square$